ORNL/TM-2015/194

Superhydrophobic Powder Additives to Enhance Chemical Agent Resistant Coating Systems for Military Equipment for the US Marine Corps (USMC) Corrosion Prevention and Control (CPAC) Program

Approved for public release.
Distribution is unlimited.

S. J. Pawel
B. L. Armstrong
J. A. Haynes

May 2015

OAK RIDGE NATIONAL LABORATORY
MANAGED BY UT-BATTELLE FOR THE US DEPARTMENT OF ENERGY

DOCUMENT AVAILABILITY

Reports produced after January 1, 1996, are generally available free via US Department of Energy (DOE) SciTech Connect.

Website http://www.osti.gov/scitech/

Reports produced before January 1, 1996, may be purchased by members of the public from the following source:

National Technical Information Service
5285 Port Royal Road
Springfield, VA 22161
Telephone 703-605-6000 (1-800-553-6847)
TDD 703-487-4639
Fax 703-605-6900
E-mail info@ntis.gov
Website http://www.ntis.gov/help/ordermethods.aspx

Reports are available to DOE employees, DOE contractors, Energy Technology Data Exchange representatives, and International Nuclear Information System representatives from the following source:

Office of Scientific and Technical Information
PO Box 62
Oak Ridge, TN 37831
Telephone 865-576-8401
Fax 865-576-5728
E-mail reports@osti.gov
Website http://www.osti.gov/contact.html

This report was prepared as an account of work sponsored by an agency of the United States Government. Neither the United States Government nor any agency thereof, nor any of their employees, makes any warranty, express or implied, or assumes any legal liability or responsibility for the accuracy, completeness, or usefulness of any information, apparatus, product, or process disclosed, or represents that its use would not infringe privately owned rights. Reference herein to any specific commercial product, process, or service by trade name, trademark, manufacturer, or otherwise, does not necessarily constitute or imply its endorsement, recommendation, or favoring by the United States Government or any agency thereof. The views and opinions of authors expressed herein do not necessarily state or reflect those of the United States Government or any agency thereof.

ORNL/TM-2015/194

Materials Science and Technology Division

SUPERHYDROPHOBIC POWDER ADDITIVES TO ENHANCE CHEMICAL AGENT RESISTANT COATING SYSTEMS FOR MILITARY EQUIPMENT FOR THE US MARINE CORPS (USMC) CORROSION PREVENTION AND CONTROL (CPAC) PROGRAM

S. J. Pawel
B. L. Armstrong
J. A. Haynes

Date Published: May 2015

Prepared by
OAK RIDGE NATIONAL LABORATORY
Oak Ridge, TN 37831-6283
managed by
UT-BATTELLE, LLC
for the
US DEPARTMENT OF ENERGY
under contract DE-AC05-00OR22725

CONTENTS

LIST OF FIGURES v
LIST OF TABLES viii
ACRONYMS ix
ACKNOWLEDGMENTS xi
1. INTRODUCTION 1
1.1 REVIEW OF ORNL PROGRAM HISTORY 3
1.2 SUPERHYDROPHOBIC POWDER DEVELOPMENT 7
1.3 EVALUATION OF COATINGS 8
2. DEVELOPMENT AND CHARACTERIZATION ACTIVITIES IN YEAR 3 10
2.1 CONTACT AND ROLL-OFF ANGLE ASSESSMENTS 10
2.2 CALORIMETRY 13
2.3 SH POWDERS, TREATMENT, CHARACTERIZATION (SIZE, SHAPE, PROPERTIES), AND SCALE-UP OF PROCESS 16
2.4 POWDER COAT SYSTEMS WITH SH SILICA ADDITIONS 28
2.5 LIQUID SYSTEMS WITH SH SILICA ADDITIONS 41
2.5.1 Initial Attempts to Modify One-Component CARC Systems 42
2.5.2 Siloxane Coatings 43
2.5.3 One-Component Solvent-Borne CARC 48
2.5.4 Two-Component Urethane CARC 50
2.5.5 NCP Model Coatings with Siliceous Materials Removed 53
2.6 ARL MODEL COATINGS 65
2.7 TEMPORARY SURFACE MODIFICATIONS 71
3. KEY FINDINGS AND CONCLUSIONS 77
4. REFERENCES 78

LIST OF FIGURES

Fig. 1. An illustration (left) of the original objective for the ORNL program (Year 1), consisting of a thin film of superhydrophobic powders applied over a standard CARC surface to enhance water repellency and corrosion resistance. At right, the modified and elevated objective (Year 2) of developing a bulk, single-step SH CARC system as a direct drop-in replacement for existing CARCs. 4
Fig. 2. Schematic representations of a hydrophilic liquid droplet (A) and a hydrophobic liquid droplet (B) on a solid surface. 11
Fig. 3. Liquid droplet on an inclined plane where "t" is the roll-off angle. 11
Fig. 4. Influence of surface roughness on water droplet wetting. 13
Fig. 5. Paint additive powder nanostructure with surface roughness due to powder morphology, whereas the powder surface modification mimics the chemistry link. 13
Fig. 6. TGA data for SHS powders. 18
Fig. 7. Contact and rolling angles of SHS loaded 53039C Type II CARC sprayed onto steel coupons. 19
Fig. 8. SEM secondary electron images of a steel panel with CARC 53039C Type II topcoat, sprayed using military-standard specifications, at various magnifications. 20
Fig. 9. SEM secondary electron images of a steel panel with CARC 53039C Type II topcoat containing 7.8% SH powder synthesized with 10% surface treatment and 2% of the dispersant, at various magnifications. 20
Fig. 10. SEM secondary electron images of a steel panel with CARC 53039C Type II topcoat containing 8.6% SH powder synthesized with 20% surface treatment and 2% of the dispersant, at various magnifications. 20
Fig. 11. SEM secondary electron images of a steel panel with CARC 53039C Type II topcoat containing 8.6% SHS powder synthesized with 20% surface treatment and no dispersant, at various magnifications. 21
Fig. 12. TGA data for SHS powders modified at different batch sizes. 22
Fig. 13. TGA weight loss curves of crystalline silica starting material and the powders modified with 20% chlorosilane through the previously established standard method. 23
Fig. 14. Surface areas of silica-based powders. 24
Fig. 15. Surface coverage of fluorocarbon on powders. 25
Fig. 16. TGA weight-loss curves for SHDE particles. 26
Fig. 17. SHDE in NCP Type II developmental coatings at increasing particle size, from left to right (A, no Diafil addition; B, 2 µm; C, 6 µm; D, 10 µm; E, 15 µm). 27
Fig. 18. SHDE in Type IV at increasing particle size, from left to right (A, no Diafil addition; B, 2 µm; C, 6 µm; D, 10 µm; E, 15 µm). 27
Fig. 19. Water droplets on the surface of urethane (top two rows) and epoxy (bottom row) powder coat panels as a function of SHS additions to the powder coat formulation. 30
Fig. 20. Contact and roll-off angle measurements for pure water droplets on the surface of powder coat panels as a function of SHS addition. 31
Fig. 21. Urethane powder coat panels following two weeks of exposure in B117 conditions. 32
Fig. 22. Urethane powder coat with 1.5% SHS addition after a total exposure time of 10 weeks in B117. 33
Fig. 23. Powder coat panels prepared at Albany following 28 days of standard B117 salt fog exposure. 34
Fig. 24. Powder coated panels with and without a trapped air layer on the submerged surface after 48 hours of immersion in deionized water. 35
Fig. 25. Epoxy powder coat specimens with (left) and without (right) 1% SHS additions following immersion in DI water and then 5% salt water for one week each. 36

Fig. 26. Keyence optical microscope views of the surface of cured powder coat specimens of epoxy (left column) and urethane (right column) comparing relative surface roughness with and without SHS additions. 37
Fig. 27. Scanning electron microscope images of urethane powder coat surfaces as a function of SHS addition. 37
Fig. 28. A cross section of the urethane powder coat containing 1% SHS addition (top) showing a number of cracks/voids penetrating much of the coating thickness. 38
Fig. 29. Appearance (left) and water drop contact angle (right) of urethane powder coat panels as a function of SHDE addition to the powder material. 39
Fig. 30. Appearance of urethane powder coat specimens (prepared identically to the small specimens shown in Fig. 29) following 1 week of exposure in B117 salt fog. 40
Fig. 31. Backscattered electron images of urethane powder coat surfaces as a function of SHDE addition to the original powder material. 40
Fig. 32. Steel panels with variable primer and topcoat combinations following 28 d in standard B117 salt fog conditions. 43
Fig. 33. Siloxane panels as exposed in B117 salt fog chamber after 2 and 8 d. 45
Fig. 34. Siloxane panels as exposed in B117 salt fog chamber after 16 d. 45
Fig. 35. Backscattered electron images of unexposed surfaces of siloxane coatings relatively high in added silica (top series) and relatively low in added silica (bottom series). 46
Fig. 36. Scanning electron microscope element maps for oxygen (O), silicon (Si), and chromium (Cr) from the surfaces of siloxane coatings relatively high in added silica (top series) and relatively low in added silica (bottom series). 47
Fig. 37. Secondary electron images on an unexposed surface of a siloxane coating with no SHS addition and solids other than color pigments removed. 47
Fig. 38. Summary of relationship among SHS additions, coating structure, and water droplet contact angle for experimental siloxane coatings. 48
Fig. 39. Panels with 1K solvent-borne CARC and identical panels with 1K solvent-borne CARC modified with 8% SHS following 8 d of exposure in B117 salt fog. 49
Fig. 40. Secondary electron images of the 1K solvent-borne CARC with and without modification to include 8% SHS. 50
Fig. 41. Salt fog exposure comparison of urethane topcoats with 0, 4, and 8% SHS additions. 51
Fig. 42. Surface structure and silicon maps for the 0% and 8% SHS versions of the experimental urethane topcoat. 51
Fig. 43. Metallographic cross sections (left column) and element maps for silicon in the corresponding region (right column) for the 0% and 8% SHS versions of the experimental urethane coating. 52
Fig. 44. Representative surface structure of an experimental 2K urethane topcoat with 15% SHS addition (all other siliceous material removed). 53
Fig. 45. Arrangement of NCP model coatings in the B117 salt fog chamber before exposure. 55
Fig. 46. NCP model coatings exposed y d in the B117 salt fog chamber. 56
Fig. 47. Immersion testing arrangement and representative rust bloom results. 56
Fig. 48. Scanning electron microscopy (backscattered electrons) of the surface structure and distribution of chromium and silicon for panels 72-D (left) and 72-E (right). 58
Fig. 49. Scanning electron microscopy (backscattered electrons) of the surface structure and distribution of chromium and silicon for panel 72-B. 58
Fig. 50. Surface structures of representative 80-x series (water-borne CARC) coatings. 59
Fig. 51. SEM backscattered electron images comparing structural details within the coating matrix for no siliceous loading and the highest silicon loading for Diafil 525 and nanosilica forms. 60
Fig. 52. Comparison of pigment distribution (chromium maps) and silica distribution (silicon maps) for representative coatings in the 80-x series of water-borne CARC. 61

Fig. 53. Series of backscattered electron images of the surface of the NCP 72-x series coatings as a function of relative composition of silica type. 62
Fig. 54. Cross-sectional analysis of the 72-B coating (100% untreated Diafil addition). 63
Fig. 55. Comparison of through-thickness metallographic sections (top image) and element mapping results for coatings 72-D (left) and 72-E (right). 64
Fig. 56. Backscattered electron images with associated element maps for the immediate vicinity of through-thickness cracks in coating types D (left) and E (right). 64
Fig. 57. Backscattered electron images (left column), associated silicon maps (center column), and surface topology comparison as a function of coating composition. 65
Fig. 58. Backscattered electron images of the surfaces of water dispersible coatings as a function of flattening agent and projected gloss. 67
Fig. 59. Secondary electron images of the surfaces of water dispersible coatings as a function of flattening agent and projected gloss. 67
Fig. 60. Backscattered (top row) and secondary electron (bottom row) images of solvent-borne coating materials under evaluation for ARL. 68
Fig. 61. Metallographic cross section of ARL panel 316, showing substrate steel, primer, and the full topcoat thickness. 69
Fig. 62. Backscattered electron image of the analysis area (top left) along with corresponding element maps for the indicated constituents for ARL coating panel #16. 70
Fig. 63. Backscattered electron image of the analysis area (left) and element maps for carbon, chromium, and molybdenum for ARL panel coating #4 (solvent-borne, polymer bead flattened, gloss 1.0°). 71
Fig. 64. Backscattered electron image of the analysis area (left) and element maps for carbon, chromium, and molybdenum for ARL panel coating #1 (water-dispersible, polymer bead flattened, gloss 1.0°). 71
Fig. 65. Development of rust bloom and corrosion associated with an “x” scratch as a function of salt fog exposure time for Products A and B. 73
Fig. 66. Products C and D, with and without the addition of 15% treated silica, with brief salt fog exposure. 74
Fig. 67. Product D with and without 10% treated silica following immersion testing in deionized water for 48 hours. 75
Fig. 68. Lifting a treated panel from the water immersion tank as portion of film subjected to immersion lifts from the panel surface. 75
Fig. 69. Salt fog result (5 d) for baseline Product E (no silica additions) and surface structures showing 0 and 9% silica additions. 76
Fig. 70. Water droplet contact angle as a function of Taber test abrasion cycles for different temporary surface products. 77

LIST OF TABLES

Table 1. Contact angles of powders with water as calculated from h_i data based on Equation (1) 15
Table 2. Water drop contact and roll-off angle data for modified silica additions to CARC. 22
Table 3. Contact angle and roll-off angle data with water for NCP developmental coatings with various SHDE modifications. 26
Table 4. Contact and rolling angle data for SHDE/SHS mixing study 28
Table 5. Summary of siloxane coating formulations 44
Table 6. Matrix of model coating compositions based on two-component solvent borne urethane CARC (NCP N1433A) 54
Table 7. Matrix of model coating compositions based on two-component water borne urethane CARC (NCP N8066A/B)..... 54
Table 8. Identity codes and information associated with coating specimens provided to ORNL from ARL..... 66

ACRONYMS

ΔH_i	heat of immersion
ARL	US Army Research Lab
BET	Branauer-Emmett-Teller
CARC	chemical agent–resistant coating
CPAC	Corrosion Prevention and Control
CPC	corrosion protection compound
DE	diatomaceous earth
DI	deionized (pertaining to water)
DOD	US Department of Defense
DOE	US Department of Energy
ITC	isothermal calorimetry
NCP	NCP Coatings, Inc. (Niles, Michigan-based business)
ORNL	Oak Ridge National Laboratory
PVC	pigment volume concentration
SEM	scanning electron microscopy
SH	superhydrophobic
SHDE	superhydrophobic diatomaceous earth
SHS	superhydrophobic silica
TGA	thermogravimetric analysis
USMC	US Marine Corps
VOC	volatile organic compounds

ACKNOWLEDGMENTS

The authors of this document functioned as principal investigators and task leads with responsibility for all activities and documentation requirements. However, the authors gratefully acknowledge the support efforts of a substantial team of people whose expertise and effort made a project of this huge scope possible.

At ORNL, the following individuals made significant contributions to this report:

- Z. Burns—coupon preparation, including surface preparation, coating, and testing; operation and maintenance of test equipment
- K. Cooley—laboratory operations associated with silica handling and treatments, thermogravimetric analysis measurements
- D. Counce, W. Hames, and K. Jones—technical editing and formatting of the final document
- D. Hillesheim—silica characterization and treatment; scale-up experimentation
- S. Hunter—initial program development activities; scanning electron microscopy (SEM) examinations, Taber measurements, contact angle measurements
- T. Jordan—metallographic preparation of coating specimens for analysis
- M. Lance—Keyence microscope profile measurements
- T. Lowe—SEM examinations of coating surface and cross sections; elemental mapping
- D. Schaeffer—contact angle measurements
- J. Simpson—initial development activities and development of some of the intellectual property associated with superhydrophobic treatments
- T. Strader—team leadership for laboratory health and safety protocols
- B. Tobler—activities at maintenance depots and corrosion rehabilitation facilities in support of panel preparation and failure analysis
- T. Vane—initial program development activities
- D. Wilson and T. Aytug—review of the manuscript

Representing the USMC/CPAC team:

M. Koch, F. Pilgrim, A. Sheetz, and G. Jolley—These individuals provided funding and technically managed the effort, including substantial technical guidance, routine participation in regular project reviews, and provision of access to Marine Corps facilities, including corrosion rehabilitation facilities, maintenance depots, and the Star4D program training.

Collaborations with NCP Coatings in Niles, Michigan, were spearheaded by R. Terrill.

Insights and specimens for examination from the Army Research Laboratory were provided by J. Escarsega.

1. INTRODUCTION

The US Marine Corps (USMC) Systems Command established the Corrosion Prevention and Control Program (CPAC) to extend the useful life of USMC tactical ground and ground support equipment, as well as to reduce maintenance requirements and associated costs through the identification, implementation, and, if necessary, development of corrosion prevention and control products, materials, technologies, and processes. The use of these technologies and processes is intended to repair existing corrosion damage and prevent, or at least significantly retard, future corrosion damage on Marine Corps vehicles and equipment.

Oak Ridge National Laboratory (ORNL) is a US Department of Energy (DOE) multi-program science, technology, and energy laboratory with distinctive scientific and specialized technical assistance capabilities in materials science and engineering, including corrosion prevention technologies. In 2010, the USMC entered into an agreement with ORNL to support the CPAC program office in its efforts to provide the USMC the best equipment and protection technologies available to enable its worldwide mission requirements.

The primary goal of the CPAC program at ORNL was to explore the feasibility of introducing various silica-based superhydrophobic (SH) powder additives as a way to improve the corrosion resistance of US Department of Defense (DOD) military-grade chemical agent resistant coating (CARC) systems. ORNL had previously developed and patented several SH technologies of interest to the USMC, and one of the objectives of this program was to identify methods to incorporate these technologies into the USMC's corrosion-resistance strategy.

USMC corrosion problems are the most challenging among the armed forces because of the harsh exposure conditions (often including seawater) of combat and support vehicles. The USMC CPAC program has extensively implemented most of the more traditional methods of corrosion prevention and support, and it has shown the most improvement in corrosion prevention of any US armed service over the past decade. However, significant and costly corrosion challenges remain because of the inherent severity of most USMC operating environments.

USMC CPAC made the strategic decision to partner with a national laboratory (ORNL) for exploration and development of more specialized and higher-risk technologies, with the goal of eventually identifying and developing new practical solutions to its corrosion challenges. The SH powder technologies developed by ORNL were of particular interest to USMC CPAC for the development of one or more water-repellent thin film or paint systems.

ORNL CPAC research began in December 2010 with the following primary tasks and subtasks:

- Task 1: Development of Superhydrophobic (SH) Coating Systems
  1.1: SH Powder Development
  1.2: Exploration of SH Corrosion Protection Compounds (CPCs)
  1.3: Development of SH Surface Treatments (Development of SH CARC Year 2)
  1.4: Development of Transparent Permanently Bonded SH Coatings for Glass

- Task 2: Development of Advanced Infrared Corrosion and Crack Detection
- Task 3: Coating Deposition and Standardized Corrosion Testing

The first year of the program included substantial time and cost invested in purchasing and installing the new laboratory capabilities specified by USMC CPAC, familiarizing ORNL staff with USMC combat platforms and corrosion prevention and repair strategies, educating ORNL staff on USMC maintenance depots and maintenance procedures, exposing ORNL staff to common USMC corrosion problems, and developing SH thin-film overlayer surface treatments in Subtask 1.3. Details of Year 1 research activities are available through the annual report previously submitted to CPAC.

Task 2 was eliminated during Year 2 because of a lack of demonstrated feasibility of using infrared thermography and/or ultrasonic detection methods as a practical large-scale method for evaluating subsurface corrosion attack or cracking of armor on USMC platforms. Details of Task 2 activities can be found in the ORNL annual reports to CPAC and are not included in this report.

As is discussed in more detail in the next section, the objectives of Task 1 were modified by CPAC in Year 2 to replace development of SH surface treatments with the development of a bulk SH CARC system that could be a drop-in replacement for current CARC systems. It was agreed that this modification of goals was much more challenging, and would necessitate an additional three years of R&D activity, beyond the original three year program schedule. Further, an additional subtask under Task 1 was added in Year 3 to evaluate the feasibility of developing SH powder coatings. However, because of federal budget sequestration in FY13, CPAC was not able to secure the second half of the required funding and was prematurely concluded after Year 3 at 50% completion.

This final report discusses the research activities, primarily from Year 2 and Year 3, related to Tasks 1 and 3. It includes the development, testing, and characterization of (1) a highly consistent manufacturing process for DOD-quality SH powder additives for CARC, (2) various experimental CARC-type coatings (most with polyurethane resins) with SH powder additives, and (3) SH powder coatings.

Transparent Superhydrophobic Coatings: A second report, complementary to the present report, has been submitted to USMC CPAC describing ORNL's activities related to Subtask 1.4, development of transparent, permanently bonded SH coatings for glass. This subtask, which included fabrication of highly durable, transparent, SH thin-film coatings on glass (using commercial-scale processes), was brought to completion in 3 years with extremely successful outcomes [1]. The resultant coating technologies have application for water- and ice-repellent transparent thin films for transparent armor, windshields, sensors, antennae, and other applications.

University of Hawaii Pacific Rim Corrosion Subcontracts: In years 2, 3 and 4, at the request of USMC CPAC, ORNL established and monitored two consecutive one-year subcontracts with the University of Hawaii primarily to measure corrosion rates at specific Pacific Rim locations of interest to the USMC. The results of the work conducted in those two subcontracts will not be discussed in this report, but they are detailed in a final report from the University of Hawaii delivered to ORNL and USMC CPAC in January 2015 [2].

1.1 REVIEW OF ORNL PROGRAM HISTORY

The October 2010 launch of the ORNL CPAC Program was followed by a visit from USMC CPAC management to ORNL in November 2010 for the first planning meeting. During the subsequent 3 years of the program, it experienced several shifts of primary focus, as directed by the USMC, all of which fit the scope of the original statement of work.

Initially, a 3 year program with the primary objective of developing SH thin films to overlay existing USMC CARC systems was proposed and approved by the USMC, and the first 9 months of powder and coatings research was invested toward achieving that goal. However, after a very positive review of first-year ORNL progress in a meeting with USMC CPAC and the US Army Research Lab (ARL) in June 2011, CPAC requested that the ORNL program goals be elevated to development of SH paint systems with drop-in capability (i.e., direct replacement of current paint systems while using current painting hardware) for the USMC.

In the June 2011 meeting at ARL, it was agreed that an additional 3 years of activity and funding would be necessary to achieve the higher goal of a new SH bulk paint system, creating a 6 year total proposed activity. It was also agreed that the second 3 years of the program would be funded in late 2013, if funds were available. Subsequently, it was also determined that the initial funding received by ORNL would also support subcontract activity with the University of Hawaii for Pacific Rim corrosion research in Years 2 and 3.

Progress and performance highlights for ORNL associated with Tasks 1 and 3 included the following:

1. meeting the proposed primary objectives (determined in collaboration with both CPAC and ARL) for developing highly consistent, scalable SH powders as paint additives in Years 2 and 3;

2. connecting the SH CARC research and development with a major USMC paint vendor (NCP Coatings, Niles, Michigan) in FY 2013;

3. demonstrating the feasibility of several SH coating systems for further development; and

4. receiving three very positive annual reviews from USMC CPAC management.

However, owing to a combination of budget sequestration funding limits and policy changes associated with end-of-year DOD funds, the ORNL CPAC effort did not receive the anticipated funding for the second half of the program in September 2013. Thus, the program completed existing activities, including the second University of Hawaii subcontract, and began closeout in 2014.

Year 1 Summary: In Year 1, ORNL began the process of familiarization with USMC platforms, corrosion protection materials, manufacturing processes, and CPAC's maintenance processes. Visits were made to the Maintenance Center at Albany (Georgia) and to the Corrosion Rehabilitation Facilities (CRFs) at USMC bases in Hawaii (Kaneohe) and North Carolina (Lejeune) to begin to develop a practical understanding of what would be required to actually deploy a thin-film coating at a depot. A coating deposition and accelerated weathering laboratory, with equipment purchased in accordance with USMC CPAC specifications, was assembled at ORNL following a visit by ORNL staff to the Carderock Naval

Surface Warfare Center to examine test protocols and specimen handling. ORNL staff attended Star4D training to be educated in specific techniques and quality control expectations for depositing CARCs via military-approved methods and equipment. ORNL also initiated the process of establishing a large subcontract with the University of Hawaii for Pacific Rim corrosion testing in Year 2 (which was followed by a second subcontract in Year 3). Development of a parallel smaller activity to develop transparent SH coatings was also initiated at ORNL (Subtask 1.4, discussed in a separate report).

Change of Program Direction: Approximately 9 months into the project, in the summer of 2011, the CPAC program manager and ORNL staff met with John Escarsega (team lead for the Army's Organic Coatings Team) at ARL to review ORNL's Year 1 progress. The degree of progress made by ORNL in Year 1 resulted in ARL's recommending that the ORNL program goals be elevated to development of a new SH CARC system.

Thus, CPAC made the decision, based on the ARL recommendation, to change the direction of the ORNL program. **The original goal of pursuing development of a SH thin film (for deposition over existing CARC topcoats) using ORNL's existing SH powders was superseded by a new goal of developing a *bulk* SH CARC polyurethane topcoat that could be applied in a single step using existing USMC depot painting equipment and processes**. The basic concept of each approach is illustrated in Fig. 1.

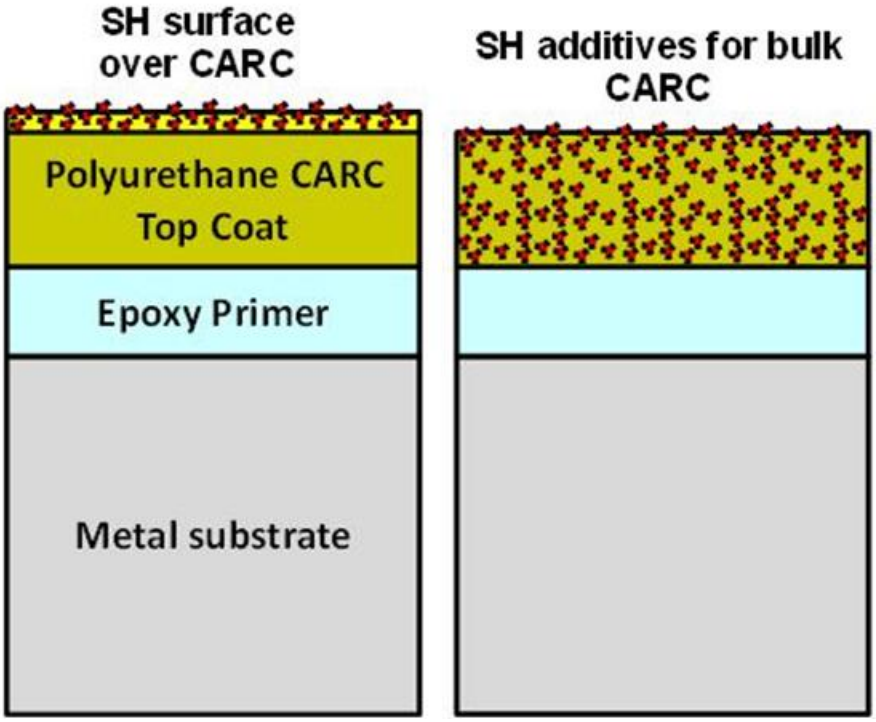

Fig. 1. An illustration (left) of the original objective for the ORNL program (Year 1), consisting of a thin film of superhydrophobic powders applied over a standard CARC surface to enhance water repellency and corrosion resistance. At right, the modified and elevated objective (Year 2) of developing a bulk, single-step SH CARC system as a direct drop-in replacement for existing CARCs.

In the June 2011 meeting, it was agreed by all parties that development of a bulk SH CARC system was a much more challenging objective than the original goal of developing an SH thin film, and would require

at least 5 more years of effort (totaling 6 years) and approximately twice the original funding. It was also agreed that such an effort would require substantial CARC/paint reformulation expertise, a skill set that ORNL did not possess. The primary objective of the program was thus changed with the understanding that (1) ARL would provide paint chemistry reformulation support to ORNL, and (2) CPAC would attempt to secure additional funds to cover the additional time and expense of developing a bulk, drop-in SH CARC. Note that CPAC secured additional "sweep-up" funding for the ORNL program in September 2011, but other intergovernmental issues developed (unrelated to the CPAC program) that prevented DOE's acceptance of the extended effort at that time.

Year 2: Before any CARC paint reformulation efforts, ARL required ORNL to establish a very tightly controlled process for manufacturing extremely consistent SH powders for paint additives. In response, a powder processing and colloids specialist was added to the ORNL program in the latter portion of Year 1 who subsequently directed the successful development of a series of tightly controlled and scalable SH powder additive manufacturing processes using both sub-micron silica and various types of low-cost diatomaceous earth (DE). Once the new paint and corrosion testing labs were installed and qualified, ORNL also began to develop expertise with deposition, characterization, and ASTM B117 salt fog [3] corrosion testing (and a suite of related protocols) of various types of solvent-borne and water-borne polyurethane CARC topcoatings.

ORNL conducted a large matrix of post-addition (meaning additions to the coating system *after* original formulation) experiments by systematically incorporating various types, sizes, and loadings of SH powders to off-the-shelf varieties of CARCs. It was demonstrated in the spring of 2012 that it was possible to deposit an SH CARC (with water droplet contact angles of up to 170°) using standard USMC materials and processes. However, results also clearly showed that post-formulation addition of SH powders overloaded the off-the-shelf CARC resin, resulting in cracking of the coating matrix. In particular, topcoats modified by post-addition of SH powders were substantially faulted (cracked and porous), and salt fog readily penetrated coatings to cause extensive rust on an unprimed steel substrate. Thus, none of the post-addition SH CARCs showed improved resistance to B117 salt-fog testing. **Results clearly showed that CARC reformulation was an absolute necessity if SH powders were to be added to bulk CARC without overloading and cracking the resin.**

Note that salt fog testing is not an ideal scenario for SH surfaces, because such a surface is designed to repel liquid water (which has significant surface tension) as opposed to condensing water vapor. Condensation of salt fog vapor is the driving force for B117 tests, which are a reluctantly accepted test standard throughout the corrosion community. However, the question of whether salt fog exposure provides an accurate discrimination of the protective capability of an SH surface in a typical environment that is not primarily condensation-driven is open to debate. Thus, it is possible that the salt fog test results in this study provide one or more false negatives associated with the performance of various SH coating configurations. Unfortunately, an acceptable, affordable, accelerated test alternative was not identified; and the atmospheric testing scheduled for year 4 in Hawaii did not occur because of the premature conclusion of this program.

In Year 2, ORNL successfully demonstrated permanently bonded transparent SH coatings for windshields and transparent armor, and conversations were initiated between ORNL, CPAC, and Program Executive Officer Land Systems to consider steps toward additional work under Land Systems to enable

deployment. However, Land Systems was ultimately unable to fund this activity in FY 2013 because of budget sequestration funding limits.

ORNL also demonstrated the potential for SH powder coatings in late Year 2 and was directed by CPAC to begin a parallel effort to develop SH powder coatings in Year 3. After a very successful annual program review in August 2012, CPAC again attempted to secure additional sweep-up funding for the ORNL program in September 2012 but was unsuccessful.

A key barrier in Year 2 was related to fiscal and staff limits at ARL, which prevented them from providing the anticipated CARC formulation support to ORNL. Additionally, at the end of Year 2, it was concluded that existing infrared thermography methods were not appropriate for the USMC's practical field corrosion and crack detection needs, so Task 2 was ended.

Year 3: Development of SH powder coatings was initiated in Year 3, at the direction of CPAC, after a review of preliminary ORNL experiments. This new effort was pursued in collaboration with both the University of Northern Iowa and the Albany Maintenance Center. Very high water drop contact angles, as well as excellent durability in B117 testing for powder coatings (without any underlying primer), were demonstrated for some types of SH polyurethane powder coatings. **Although ORNL delivered several batches of highly consistent SH powder additives to ARL in Year 2 as requested, ARL continued to be unable to provide CARC reformulation support to ORNL due to limited availability of staff.**

Thus, in the later portion of Year 2 and first quarter of Year 3, ORNL searched for a CARC manufacturer willing to collaborate on the development of SH CARC. Several months were spent exploring that possibility with two large CARC manufacturers, but neither proved fruitful. In January 2013, ARL introduced ORNL to NCP Coatings of Niles, Michigan; in February 2013, ORNL visited the company, which had been founded in 1948 as Niles Chemical Paint Company. NCP expressed significant interest in collaborating to develop SH CARC, and experimental work began in March 2013. By summer 2013, a number of promising preliminary results had been demonstrated with various types of reformulated NCP CARC, including both solvent- and water-borne polyurethanes and a siloxane composition. The first successful B117 tests of non-cracked SH CARC (wherein SH CARC topcoats performed better than standard CARC topcoats) were demonstrated in late July 2013. Various siloxane coating chemistries showed substantial improvements over polyurethane, and a number of very promising new directions for SH coating development were identified. Further, preliminary results of testing of chemical agent surrogates suggested potential for SH CARC to resist some types of chemical agents. After the successful annual review in August 2013, USMC CPAC management again attempted to secure new sweep-up funds in September 2013 to continue the program, but they were unable to do so. Research activities at ORNL shifted to closeout mode in October 2013. ORNL concluded some obvious high-value activities during FY 2014 while continuing to also manage the University of Hawaii subcontract. Research with NCP was halted in September 2013, unfortunately during the peak period of productive discovery and momentum.

Year 4: The ORNL CPAC became minimally active in 2014, with the small amount of remaining funding used to support activities primarily consisting of completing data evaluation; disassembling and returning equipment to USMC CPAC; compiling the final report; and overseeing the University of Hawaii subcontract, which was completed in November 2014 except for finalizing the documentation.

1.2 SUPERHYDROPHOBIC POWDER DEVELOPMENT

The development and evaluation of durable, low-cost SH silica powder additives is a key part of CPAC's mission to develop multifunctional protective coating systems to provide improved corrosion protection as well as increased durability and availability for military vehicles and equipment. To use these new silica powder materials effectively within either a CARC or a corrosion protection compound (CPC) system, the powders must be reproducible and scalable and the final product must be easily deployable at both the original equipment manufacturer and maintenance depot level. To provide consistent, reproducible properties, the SH powders must be (1) chemically and physically consistent from batch to batch; (2) dispersible (or exhibiting controlled dispersion, i.e., floating to the surface); (3) adherent to the coating system resin; and (4) stable over long processing, transport, and storage periods. To meet these demanding and diverse requirements, the basic material properties of the powder additive before, during, and after processing must be understood and controlled. With these goals in mind, ORNL selected two raw materials for evaluation as potential silica powder additives: (1) DE and 2) chemically pure silica. These powder additions to CARC topcoats were examined with and without chemical treatment (discussed later in this report) to render the silica SH in its interaction with water droplets. The morphology (shape and size) and surface characteristics (physical and chemical) of the powders as a function of powder treatment were evaluated for various quality and reproducibility parameters critical to bulk processing.

Throughout the course of this project, the focus of the powder development effort (Task 1) was to establish the processing–property interrelationships influencing the ultimate qualities desired by the USMC CPAC mission. All of the silica-based materials were characterized in order to facilitate the establishment of the necessary physical and chemical treatment protocols to achieve multifunctional coating systems for the USMC. Characterization was designed so that the critical parameters that influence consistent powder incorporation into coating systems could be defined. Initially, DE powders were selected based on experience obtained from previous research, as well as related intellectual property developed on DE powders at ORNL and the fact that DE powders are significantly more cost-effective than silica equivalents. Thus, the first efforts evaluated the function of milling parameters on architectures and chemical modifications of DE powders. However, because of concerns about the structure (range of size and shape distribution) and chemistry (purity) variation associated with a naturally derived material such as DE, the focus in the second year of the research shifted to chemical silica, a more chemically and physically homogeneous starting material.

Early in the effort, familiarity with the various CARC systems and coating deposition processes used by the USMC and DOD was established, and a working relationship with the Organic Coatings Team at ARL (led by John Escarsega) was developed. Research related to developing methods for manufacturing consistent, reliable SH powders was undertaken to enable systematic and reproducible production of SH powders, which was defined by ARL (and supported by CPAC) as a first priority. Extensive scientific research was conducted to systematically identify key SH powder variables—such as raw materials, size, shape, milling conditions, water content, silanation conditions, thermal processing, surface charge and charge modification, dispersion strategies, and SH quality—and methods to control these factors.

Ultimately, after a variety of systematic studies (and a modest incorporation of trial-and-error evaluations), nanocrystalline silicon oxide (99.9%) from American Elements and Diafil from World

Minerals (Celite Corp.) were selected as primary materials for silica powder and DE, respectively. A specific silanation process was developed for large batch processing of silica powders to yield consistent properties. In this process, a 0.19 M stock solution of (tridecafluoro-1,1,2,2-tetrahydrooctyl)-1-trichlorosilane in 100 mL of dry hexane was used to silylate the samples. In instances where a fluorinating dispersant was used, silica powder was added to a stirring solution of dispersant in hexane. Varying levels of stock solution, calculated to produce the desired addition of the chlorosilane by weight of silica, were added; and subsequently the vessel was closed and stirred for 1 hour at room temperature. The reaction was filtered on a medium-porosity glass frit and the resulting powder washed with 100 mL each of hexane and tetrahydrofuran, followed by a vacuum cure step at 70°C (600 torr).

The silica powders prepared in this program were characterized using a variety of analytical methods. This nanocrystalline silica powder was determined to be amorphous by x-ray diffraction analysis using Cu kα radiation (Panalytic Xpert diffractometer). Surface area was determined using Brunauer-Emmett-Teller BET analysis on a Quantachrome Autosorb-1 instrument. Optical microscopy and scanning electron microscopy (SEM) were used to examine particle size distribution and morphology. Thermogravimetric analysis (TGA) coupled with mass spectroscopy was used to determine the weight change of the SHDE and/or SH silica (SHS) at varying temperatures and times as a function of a variety of processing conditions.

Experiments were conducted to add—post-formulation—SH powders to various types of epoxy and polyurethane coating systems to develop deposition and characterization practices. These experiments laid the groundwork for activities in the final year of the effort. Although some SH functionality was demonstrated within existing CARC systems via post-formulation additions of high concentrations of SH powders and solvent to form prototype coatings, it was determined that doing so often resulted in a highly flawed structure due to encroachment on a critical pigment content. As a result, further development also examined powder additions to the CARC system in the formulation stage, via informal collaboration with NCP Coatings. (These collaborations are discussed in more detail in various sections that follow).

1.3 EVALUATION OF COATINGS

The primary purpose of the corrosion portion of the coating development effort (Task 3) was to establish and operate laboratory facilities to compare standardized performance evaluations of coating systems being developed (in Task 1, Powder Development) to extend the lifetimes of USMC corrosion protection systems and reduce coating system maintenance requirements. The accelerated weathering resistance of baseline coating systems (e.g., standard CARC) was compared with the resistance of similar coating systems modified to incorporate SH powders of several varieties/sizes. The goal was to identify critical composition and formulation/application parameters that improve and potentially maximize long-term protection of the substrate (pointing to a direction for future efforts/improvements) while retaining all the other performance characteristics required of CARCs.

At the beginning of the project, CPAC personnel directed the acquisition of specific laboratory equipment at ORNL to support the preparation of appropriate standardized test panels, as well as environmental chambers for corrosion testing. The painting equipment included a high-ventilation paint booth, a drying dock, and a variety of approved articles of spray equipment consistent with that used at USMC depots around the globe. Further, ORNL personnel took part in a weeklong education session to become

officially trained/certified in Star4D military-approved techniques and practices associated with application of CARC-style coatings.

Primarily because it is standardized, condensing salt fog exposure according to ASTM B117 [3] is a commonly employed accelerated weathering test to evaluate the corrosion protection characteristics of coating systems. It has been known for some time that the results generated in B117 tests do not always correlate with performance observed in outdoor weathering stations or in actual service conditions. However, the test remains in common use because it is relatively easy to perform/operate, it is consistently reproducible among various laboratories, and it makes relative comparisons of performance results among coating systems reasonably straightforward. At the outset of this program, USMC/CPAC determined that salt fog exposures were to be the primary evaluation technique used at ORNL in the coating development efforts, and it specified the particular chambers to be purchased in support of the effort.

Very early in this program, salt fog tests of standard CARC topcoat materials applied directly to bare steel revealed that, as a generality, CARC provides little or no corrosion protection as a stand-alone coating. That is, because it is a heavily loaded material and intended to impart characteristics other than corrosion resistance, it tends to cure with the formation of cracks and/or pores so that salt and moisture quickly (in as little as 48 hours) penetrate. This situation leads to rust bloom, blistering, and, via substrate corrosion, complete loss of coating adhesion. The use of a commercial-grade primer—inexpensive and only marginally protective compared with military primer standards—before CARC application was not found to change this result appreciably. In contrast, the same CARC coatings applied over the usual robust military-grade primer (for example, MIL-DTL-53022D type II epoxy) were exposed to the same condensing salt fog routinely for at least 1000 hours with no hint of degradation (no rust bloom, scribe creep, or blistering and no change in pull-off adhesion strength). Although the absolute durability of the epoxy primer was not examined in any detail, exposures of the primer as a stand-alone coating system for steel in excess of 2,500 hours were completed with no measureable degradation in the B117 chamber.

Although the primary performance characteristic of CARC is ***not*** enhancement of overall coating system corrosion resistance, the minimization of cracks and pores in the CARC structure as an intended consequence of incorporation of SH powders could result in overall corrosion protection improvements as well as a surface much easier to decontaminate in the event of chemical agent exposure. However, attempting to use screening tests (e.g., salt fog) that incorporate a robust primer in concert with each new topcoat modification of interest relegates the program to very slow (at least 1,000 hours per evaluation cycle) discrimination between developmental variants and thus seriously impedes the decision-making process that is directed by progressive results. Therefore, it was decided that developmental coatings would be exposed to salt fog testing via application to bare steel (no primer at all) or, in some cases, by application over a commercially available primer (inexpensive and marginally protective compared with military primer standards). With screening tests performed in this way, more timely performance results could be generated and progress could be more rapidly accomplished with concomitant lower costs.

Another observation from early in this test program was that, despite the “consuming fog” environment within a B117 chamber, the underside of panels exposed to salt fog responded differently from topside exposure surfaces. For example, the underside of various coated panels commonly exhibited reduced (or even no) changes in pull-off adhesion strength, much less rust bloom and blister development, less oil

displacement (used in an attempt to fill pores), and condensate that was observed to "bead" for extended periods compared with the topside exposure result. While these differences are not new to the technical community, they highlight the concept that the actual failure mechanism(s) of USMC vehicle coating systems must be understood thoroughly to design and implement a "defense" against those failures. For example, these observations raise questions about the physical and chemical differences between exposures in

- immersion conditions;
- active condensation conditions, with a continuous but relatively thinner film of moisture compared with immersion conditions;
- high humidity conditions, with a continuous or semi-continuous film thinner than that produced by active condensation;
- moisture accumulations driven by the presence of hygroscopic salts or other contaminants; and
- relative movement of the moisture present (for example, hose application vs. rainwater vs. dew accumulation).

Other factors, such as the potential for wet/dry cycles and temperature or oxygen gradients across the affected surface also impart physical and chemical stresses on a coating. Highlighted by the interest in superhydrophobicity developments for coatings, another potentially significant factor is the surface tension difference between moisture arriving as liquid/droplets and moisture arriving as a vapor. In particular, changes in coatings to incorporate SH powders are not expected to resist all of these liquid conditions equally, suggesting the potential for specific solutions tailored to specific problems. In this program, however, no attempt was made to distinguish among these various mechanical and chemical factors in a service environment for coatings; instead, B117 exposures were simply used as a screening method to discriminate among potential coating formulation improvements. Ultimately, more extensive testing—including field exposures—would be required to advance any particular modification among those discussed here.

2. DEVELOPMENT AND CHARACTERIZATION ACTIVITIES IN YEAR 3

2.1 CONTACT AND ROLL-OFF ANGLE ASSESSMENTS

Whereas water contact angle measurements were used periodically throughout the test program as a simple indicator of wetting and thus potential SH behavior, the third year of the effort yielded the realization that contact angle and bulk coating structure often could be correlated to influence developmental goals for both properties. For example, efforts to maximize contact angle often resulted in coatings so overloaded with solids that other performance characteristics were compromised by cracking or porosity. As a result, contact angle details were revisited to improve that capability as a screening test concept.

When a liquid is deposited on a solid surface, the angle formed at the interface of the liquid and solid is the contact angle. Contact angle is among the most common methods to assess wetting behavior, or the

interaction capacity, of a liquid on a solid surface. The intermolecular forces (for example, surface tension) within the liquid and the solid, and the interaction of the two, govern this wetting behavior and the resulting liquid droplet contact angle. The environment surrounding the liquid/solid interface—for example, ambient air or perhaps a vacuum—also potentially contributes to the interactions that determine contact angle. If the contact angle is less than 90°, the surface is considered wettable or hydrophilic (Fig. 2a); in such a case, the adhesive forces (solid–liquid) are stronger than the competing cohesive forces (liquid–liquid), and the liquid tends to interact more with the solid than with itself. If the contact angle is between 90° and 180°, it is considered non-wetting (Fig. 2b). In this case, the cohesive forces are relatively stronger, and the liquid interacts more with itself than the solid. Contact angles in the range of 90–150° are generally described as indicative of hydrophobic character, while even greater contact angles (> 150°) are often referred to as superhydrophobic character and indicate very limited interaction between the solid and liquid.

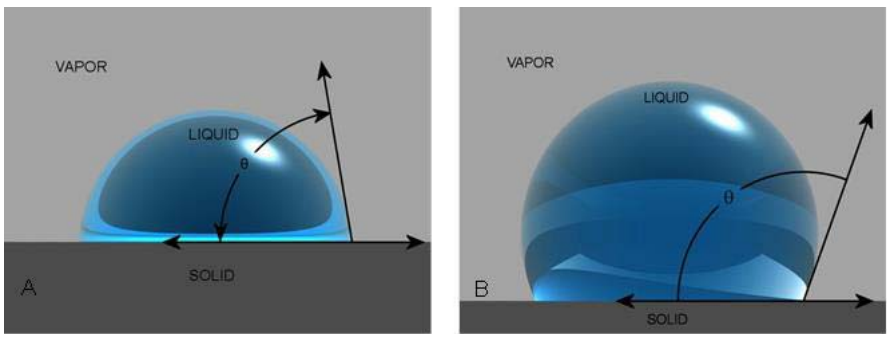

Fig. 2. Schematic representations of a hydrophilic liquid droplet (A) and a hydrophobic liquid droplet (B) on a solid surface.

A related measurement, frequently termed the roll-off angle (or dynamic contact angle), determines the amount of inclination of the measurement surface required to cause the liquid droplet to move/roll on the previously horizontal substrate (see Fig. 3). At low levels of interaction/wetting, low roll-off angles (say, < 10°) are often determined, although relative surface roughness of the substrate is an obvious variable. Higher rolling angles indicate greater interaction between the liquid and the solid substrate.

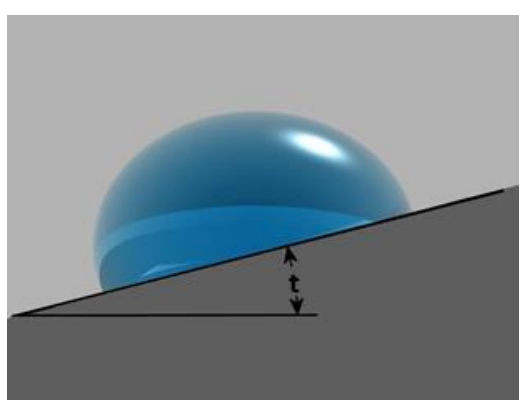

Fig. 3. Liquid droplet on an inclined plane where "t" is the roll-off angle.

Contact angles were measured with an optical tensiometer (KVS Instruments/Biolin Scientific Attension Theta 2) that measures static water droplet contact angles using a semi-automated sessile drop method with a resolution of 0.1°. Roll-off angles were assessed somewhat more crudely, using a wedge-shaped pair of flat steel panels—one affixed to horizontal and one that can be inclined at an angle to be measured (Smart Tool M–D 92346 inclinometer) with a resolution of 0.1°.

For evaluating contact angles, the procedure incorporated making five measurements with reagent grade water (average droplet size is 6 μL) on the substrate of interest at 20 mm increments across the surface with a delay of 5–10 s before taking each measurement. The surfaces to be measured were "cleaned" with compressed air to remove lint and other non-attached contaminants before loading on the platform. Typically, the measured areas were selected randomly, starting at one end of the plate and working in 20 mm increments across the surface. The droplets were dispensed from the needle at the selected locations by manually raising the platform holding the substrate of interest to just barely create contact between the droplet at the needle tip and the measurement substrate. Slow withdrawal of the substrate from this position usually resulted in the droplet adhering to the coating at the intended location, but there was some variability, particularly when the coating was relatively hydrophobic. In addition, other significant factors were found to include the camera settings to create a baseline contrast for droplet photos, the water drop delivery details including the time between drop placement and photography, size/volume of the droplet, and perhaps most importantly, the localized surface roughness at the measurement location. The authors expect the combination of factors listed here will result routinely in contact angles with a variability of approximately 5°.

In nature, both surface architecture (e.g., roughness, special regularity) and chemistry (e.g., bonding sites, relative polarity) can contribute to relative wetting phenomenon. Typically, the highest contact angles (lowest degree of wetting) are generated by regularly spaced angular nanoscale surface features. The lotus leaf is a well-known example of this behavior, and Fig. 4 is a schematic representation of a high contact angle developed on such a surface. In this project, both surface roughness and chemistry of silica paint additives were manipulated to create superhydrophobic effects on the resulting coating surfaces. The silica powder was engineered with nanosized surface features and was chemically modified to help reduce intermolecular forces creating the low energy "surface" (Fig. 5). The silica powder is an agglomerate of multiple smaller nanoparticles. The surface roughness resulting from these agglomerates exposed at the coating surface creates the nanosized features necessary to limit wetting. The silica nanostructure naturally mimics plant architecture due to surface roughness and morphology, whereas the powder surface modification mimics the chemistry link.

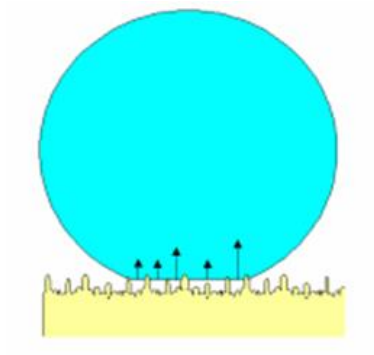

Fig. 4. Influence of surface roughness on water droplet wetting. The angular surface roughness on a very fine (nano) scale contributes to the lack of wetting by the droplet.

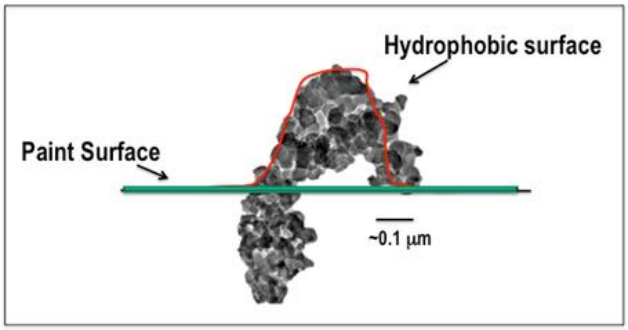

Fig. 5. Paint additive powder nanostructure with surface roughness due to powder morphology, whereas the powder surface modification mimics the chemistry link. Silica powder clusters that break the surface of the coating mimic the angular surface roughness required to minimize wetting.

The initial working theory for this project was that if high contact angles and low rolling angles were achieved, the surfaces would be resistant to interaction with water and would exhibit improved performance and corrosion protection qualities. Thus, at least initially, contact angle (and sometimes roll-off angle) was used as a rapid screening metric to assess the efficacy of various powder modifications and related developmental variables. However, as the program progressed, it became evident that reaching for the highest possible contact angle was not necessarily the best metric, as other concomitant factors were sometimes detrimental to coating integrity. These factors are discussed in detail in the relevant discussions regarding results.

2.2 CALORIMETRY

Because of the uncertainties associated with contact angle measurements, there is a strong driver for the development of a technique to quantify the potential hydrophobicity of silica powder additives prior to incorporation into a paint system or other matrix/resin. Thus, another technique called isothermal calorimetry (ITC) was pursued. Although ITC analysis more commonly is used for the analysis of proteins in pharmaceuticals and biological applications, the viability of the technique for characterizing inorganic powders was evaluated. Typical ITC data reports the heat of immersion (ΔH_i) of a material in a solvent, and this data is correlated directly with the extent to which a surface interacts with a solvent. Stronger interactions will release energy, yielding negative ΔH_i values, whereas non-wetting interactions

will produce positive values of ΔH_i. These ΔH_i values may be used to predict a contact angle suggesting an independent metric for the powder surface and its potential wettability.

To evaluate this technique, the TAM III Isothermal Micro Calorimeter from TA Instruments was used. The TAM III measures changes in heat generated from a chemical reaction, change of state, or formation of a solution. The liquid bath temperature can be controlled meticulously and can be operated in isothermal, step-isothermal, or temperature-scanning mode.

Three model samples were evaluated: an as-received silica currently being used as the starting material for ORNL SHS powders (silica 518), a commercially available silica reported to have hydrophobic properties (AeroSil 8200), and an ORNL SHS (produced from the as-received silica). These three samples were selected because they have widely different surface chemistries, spanning the range from hydrophilic to superhydrophobic. Further, these powders have been well characterized at ORNL and have been incorporated previously in the 43039 CARC system, enabling a correlation between contact and roll-off angle data with values suggested by heat of immersion data. The solvents used for the study were reagent grade water and reagent grade toluene. Water and toluene similarly span a range of potential solvents of interest to the development of paint-compatible superhydrophobic powders.

To measure ΔH_i, selected powders were loaded into glass ampules that were degassed at 80°C for 1 hour to remove residual surface moisture. Subsequently, the ampules were placed into the solvent of interest and broken or crushed while immersed in the solvent to eliminate exposure to other environments (e.g., lab air). The ΔH_i was measured immediately upon breaking the powder container. Calibration of the instrument occurred several times before and after breaking of the ampule to maintain a precise/consistent baseline temperature/energy reading so the change in enthalpy could be measured. Each powder sample was measured twice for reproducibility.

A literature search generated several mathematical formulas for calculating the contact angle for a powder/solvent/air interface from the enthalpy of immersion (h_i). The value of h_i in J/m^2 can be calculated by dividing the ΔH_i (J/g) by the surface area (m^2/g) of the powder being analyzed. Yan et al. [4] derived the following formula for calculating contact angles for fumed silica nanoparticles using h_i data:

$$\cos\theta = \frac{-KT - h_i}{\gamma_{lv}} \tag{1}$$

where K is the difference between the temperature dependence of solid–liquid interfacial tension and that of solid surface tension, T is absolute temperature in kelvin, and γ_{lv} is liquid surface tension. Whereas T is reported experimentally and tabulated values of γ_{lv} are reported in the literature for a number of solvents, K is a variable dependent on the temperature, the solid–liquid interface (γ_{sl}) and the surface tension (γ_s) of the solid in question.

$$K = \frac{d\gamma_{sl}}{dT} - \frac{d\gamma_s}{dT} \tag{2}$$

Therefore, to calculate accurate contact angles, *K* must be determined experimentally for each powder, solvent, and surface/liquid system analyzed at multiple temperatures. Calculating *K* for powders is difficult because of inconsistencies in powder uniformity, uncertain capillary effects, unstable powder beds, surface compression, variable powder surface morphology, porosity, and solvent incompatibility. Based on the data provided by the instrument manufacturer, contact angle was calculated using Equation (1), assuming an approximate value for *K* of 7×10^{-5} J/m^2; it is reported in Table 1. This value of K was reported in reference 4. This value is assumed to be relatively accurate for certain low energy surfaces but is derived from assumptions of an idealized silica surface, not a powder.

Table 1. Contact angles of powders with water as calculated from h_i data based on Equation (1)

Powder type	Heat of immersion (J/gm)	Contact angle (°)
Silica 518	-11.3	16
	-13.1	Off scale (<0°)
AeroSil 8200	0.087	107
	-0.294	105
ORNL SHS	0.821	113
	0.852	113

Note: SHS = superhydrophobic silica

Despite the number of assumptions made in deriving Equation (1), the calculated contact angles nevertheless reflect the general trend expected for the selected samples. The as-received silica has a low contact angle, reflective of the material's hydrophilic nature. AeroSil and ORNL SHS are both significantly more hydrophobic than silica because of the hydrophobic surface groups (methyl in the case of AeroSil and fluorocarbon in the case of ORNL SHS). Unfortunately, the difference in magnitude of the calculated contact angles of AeroSil and ORNL SHS is not reflective of the previously observed characteristics of these powders in the CARC systems. Incorporation of the powders and their resulting hydrophobicity into a complex paint system is a function of particle wetting and reorganization upon drying, so differences in the contact angles may be observed. The ORNL SHS yielded greater improvement in contact angles than the AeroSil 8200 when introduced at equivalent concentrations into CARC 53039 Type IIC.

Because of the number of assumptions that must be made to calculate contact angle data, directly comparing enthalpy of immersion as normalized for surface areas of powders may lead to a characterization metric somewhat superior to simple contact angle. It should be possible to use the heat of immersion as the measured variable while changing any number of powder modification conditions and, therefore, quantify the effects of the different treatment parameters and processing conditions.

The data in Table 1 mirrors the expected trend in the relative values of heat of immersion in the water affinity of the samples. The as-received silica powder has a polar hydrophilic surface and absorbs water while releasing heat. Because AeroSil powder has a methylated surface, and the powder surface is hydrophobic, it should not interact strongly with water. The surface modification technique used to

produce ORNL SHS powder results in fluorocarbons on the surface of the silica that have been shown to strongly repel water, and therefore, additional energy is required to cause the two materials to interact. This energy requirement is measured as a positive enthalpy of mixing.

Potential contact angles were also estimated for toluene–powder interactions which, based on heat of immersion measurements, suggest reactions generally less energetic than those with water. As expected, the methylated surface of AeroSil interacts strongly with the similarly non-polar toluene. Despite its strong hydrophilic tendencies, the pure silica exhibits some energy release upon mixing with toluene. ORNL SHS powder requires energy to mix with toluene. This result lends quantification to the observed difficulties in integrating ORNL SHS powders with solvent-based CARC. Although SHS/CARC mixtures that display SH tendencies have been produced, these enthalpy results could assist in explaining the migration of the ORNL SHS powder to the paint surface; such behavior may be attributed to this energy requirement. TA Inc. has confirmed that it is possible to analyze paint in the instrument, opening the possibility to probe the effects of powder surface treatments and dispersants on the interaction energy of powders with CARC or other paint systems. These results are encouraging and indicate the feasibility of using this technique to define further and model powder surfaces and their relationship to final paint properties. However, the program was terminated before researchers could explore this avenue of assessment further.

2.3 SH POWDERS, TREATMENT, CHARACTERIZATION (SIZE, SHAPE, PROPERTIES), AND SCALE-UP OF PROCESS

The use of SHS in a CARC topcoat has the potential to generate water repellent surfaces as long as the nanostructure and chemistry of the SHS powder is available at or near the exposed surface of the coating, while also maintaining good adhesion of the uniformly distributed powder particles with the polyurethane surface matrix. The first step toward uniformly introducing any powder into a coating system is to ensure resin/solvent compatibility and uniform dispersion to prevent uncontrolled flocculation of the silica additives. If the additive is incompatible, it will either agglomerate and/or change the flow behavior of the coating, thus preventing it from being sprayed consistently. Dispersion, or the controlled agglomeration of the powders within the binder solution (paint), can be manipulated at multiple stages of paint formulation. A dispersant is typically used with the addition of powders to any suspension to control surface tension of the powder, thereby controlling the agglomeration and homogeneity of the mixture. The dispersant assists in wetting the powder and matching the surface tension of the powder to the binder solution. When using a powder that has a SH surface and that resists wetting by the binder solution, a viable dispersant strategy must be developed. In particular, because integration of hydrophobic particles into a water-borne CARC system would theoretically prove problematic (SH particles by definition resist interaction with and incorporation by water), researchers focused on creating powders suitable for addition in a solvent-based CARC system.

The goal in adding SHS to a coating system is to homogeneously distribute the SH powder throughout (at least) the surface of the outermost coating layer in a manner that allows the powder to remain surface active. If this architecture can be maintained, the surface structure necessary to produce superhydrophobicity can be achieved. A finely divided (high surface area) powder perhaps offers the best opportunity for homogeneous dispersion in the coating material, but high surface area also introduces additional complexity for the incorporation of the powder into the paint.

Before learning to disperse SH powders in CARC formulations, dispersion of silica powders was required to properly receive the silanation treatment that develops the SHS properties. Part of this effort to define the powder treatment process (discussed in Section 1.2 focused on the impact of dispersants added during the silanation process. The use of a dispersant in the solvent for the silanation process before incorporation into the paint system should assist in achieving a less agglomerated powder structure and encourage a more even and chemically efficient distribution of chlorosilane on the surface of the starting silica powder.

To evaluate the role of the dispersant and the resulting extent of silanation of the powder surface, thermal gravimetric analysis (TGA) was used. Thermal decomposition of organic components of a modified silica powder is reflected in TGA via proportional weight losses at a specific temperature (or temperature range). When more material is bound to the silica particles, more weight loss is observed with TGA once the appropriate reaction temperature of the compound is reached or exceeded. By examining the effect of weight loss as a function of temperature and differing surface modification conditions, correlations between the powder chemistry and surface-substrate corrosion protection properties can be drawn. Additionally, the impact of these various powder processing conditions (including the use of a dispersant during powder surface conversion) on the incorporation of varying quantities of SH silica powders into existing CARC topcoats was investigated.

Mass spectrometry of the gases evolved during TGA of the as-received silica powders showed only water adsorbed to the powder surface being released with a completion temperature of approx. 110°C. Water is commonly found adhered to surfaces of all kinds because of simple contact with moist air, and the amount of water is typically a function of structure/roughness, surface area, and relative substrate purity. A series of SHS powders, modified with either 10% or 20% fluorination compound and with or without the dispersant DS06, were subsequently synthesized and analyzed. After the chemical surface modification treatment, an additional weight loss event (over and above the loss of water completed at ~ 100°C) with onset temperature near 400°C was observed, corresponding to the release of thermally induced decomposition products of $(CH_2)_2(CF_2)_5CF_3$ groups chemically bound to the surface of the silica particles. The magnitude of the weight losses is indicative of the amounts of various compounds bound to the surface of silica particles. Representative results of these analyses, shown in Fig. 6, indicate that the different surface modification methods indeed resulted in different powder surface modification percentages and properties. Two batches of each type of material were characterized, with a different part of the procedure varied each time (i.e., with and without dispersant DS06 in 10% or 20% fluorination compound by weight of silane compound).

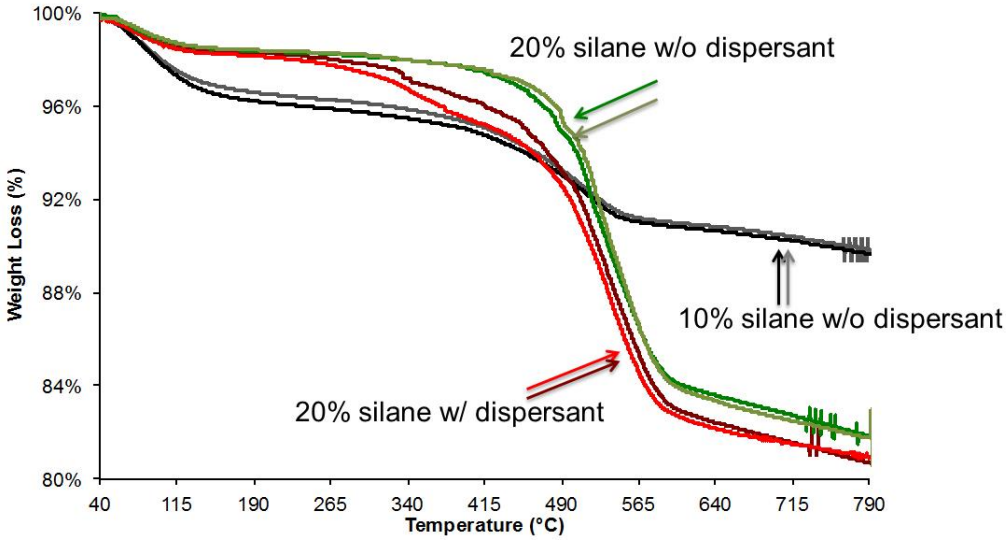

Fig. 6. TGA data for SHS powders. Based on mass spectrum analysis (not shown), the weight loss event, with an onset temperature of approximately 400°C, reflects the amount of surface modification by fluorination compound, whereas the losses below 120°C are primarily due to surface-bound water.

The weight loss event initiated at ~400°C was substantially larger when 20% by powder weight of silylating agent was employed. This indicates that more material was deposited on the powder surfaces during fluorination at 20% compared with 10%. There was also less water adsorbed on the 20% powder surface, as indicated by the reduced weight loss at temperatures below 120°C. The dispersant used in this experiment did not appreciably change the amount of material deposited on the powder surfaces. Overall, this comparison indicates that the 20% modified powder is likely to be more hydrophobic than the 10% modified material at the molecular/surface level. Note that the dispersant and non-dispersant powder groups are reproducible and have consistent weight losses as a function of temperature. To evaluate whether or not this particle hydrophobicity would translate to the CARC topcoat, a series of powder loading experiments was performed.

The modified SHS powders were incorporated into the CARC topcoat to determine if the changes in powder surface modification could be realized in the water-repellency characteristics of the coating surface produced by spraying. In all cases, it was necessary to add thinner to the resulting mixtures of topcoat and SHS to achieve a sprayable consistency. These paint mixtures were sprayed onto plates, and the contact and rolling angles were measured after curing. Figure 7 shows the effect of the solids loading on the contact and rolling angles as a function of the surface treatment. The data suggest that the use of the dispersant during powder surface modification does not show any benefit in contact angle at equivalent surface treatment conditions. However, doubling the concentration of the surface treatment from 10% to 20% increased the contact angle at similar levels of modified powder solids loadings with or without the use of a dispersant in the powder fluorination processing step. The importance of the amount of surface treatment is further emphasized in the rolling angle results shown in Fig. 7. Rolling angles were greatly reduced by doubling the surface treatment concentration whether or not a dispersant was used. From these three material conditions, the following conclusions were drawn: (1) the current dispersant, when used during the powder treatment step, is not effective for improving contact or rolling angles on

the coating; and (2) the powder surface treatment concentration is a critical variable in the reduction of the rolling angle and in the increase in contact angle at powder loads < 20%.

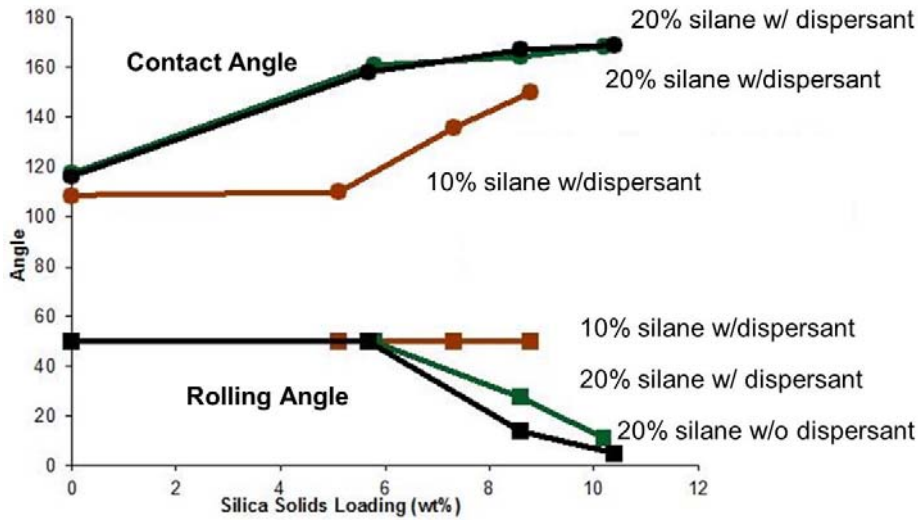

Fig. 7. Contact and rolling angles of SHS loaded 53039C Type II CARC sprayed onto steel coupons. The hydrophobic characteristics are dependent on both the amount of surface modification of the silica particles and the loading concentration.

Figure 8 shows scanning electron microscopy images of the surface of a standard 53039C Type II CARC topcoat surface without the addition of SHS powder. The images increase in magnification from left to right to show the overall perspective of the surface topology of the CARC system in a highly magnified view revealing the presence and topology of various organic and inorganic additives in the base resin system. The surface is rough and porous, but no micro-cracking of the topcoat matrix is evident for this unmodified CARC.

Figures 9 to 11 show a series of surface coatings composed of an approximately 8 wt % mixture of the SHS in the same type of CARC topcoat. A panel sprayed using 7.8% SH powder (synthesis conditions: 10% surface treatment, 2% dispersant) mixed into the CARC is shown in Fig. 9. Small amounts of micro-cracking are evident in this coating (Fig. 9a). SHS is just visible in Figs. 9b and 9c as very fine agglomerated spheroids. The presence of SHS on the coating surface indicates that the modified SH powders are able to break the surface of the topcoat, but this behavior has not yet been optimized as confirmed by the contact and rolling angles reported in Fig. 7. It is likely that the already highly loaded CARC resin is overloaded by the addition of approximately 8% SHS, as indicated by cracking of the topcoat matrix.

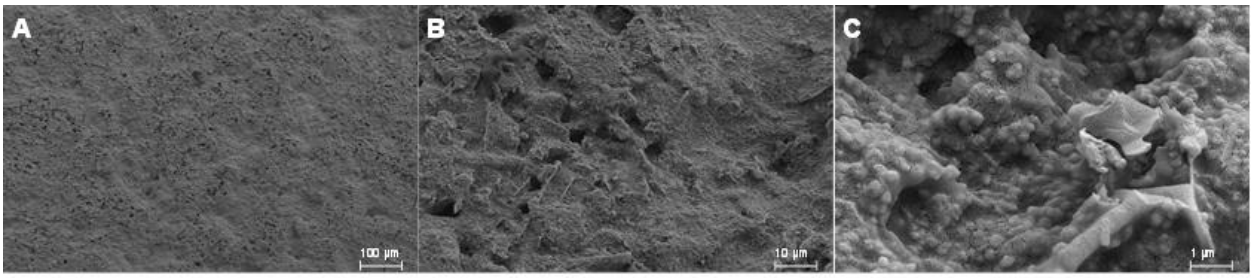

Fig. 8. SEM secondary electron images of a steel panel with CARC 53039C Type II topcoat, sprayed using military-standard specifications, at various magnifications.

Fig. 9. SEM secondary electron images of a steel panel with CARC 53039C Type II topcoat containing 7.8% SH powder synthesized with 10% surface treatment and 2% of the dispersant, at various magnifications. Image A highlights representative micro-cracking, and Image C shows particles of SHS (brighter white; two agglomerates are noted by red arrows) penetrating the surface of the paint.

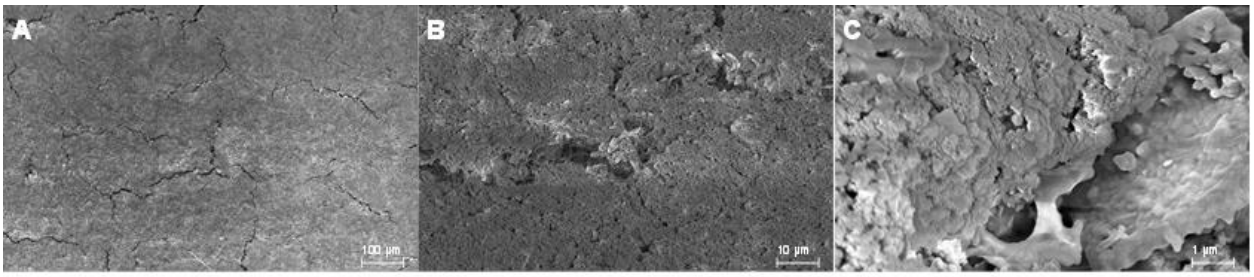

Fig. 10. SEM secondary electron images of a steel panel with CARC 53039C Type II topcoat containing 8.6% SH powder synthesized with 20% surface treatment and 2% of the dispersant, at various magnifications. Note the significant increase in quantity of the silica particles on top of the polymer in the CARC topcoat compared with Fig. 9.

Fig. 11. SEM secondary electron images of a steel panel with CARC 53039C Type II topcoat containing 8.6% SHS powder synthesized with 20% surface treatment and no dispersant, at various magnifications. Note the micron sized cracks in the surface in image B and the higher density of agglomerated silica particles in image C.

Panels made with equivalent solids loadings of 8.6% SHS powder with 20% surface treatment, with and without dispersant, are shown in Figs. 10 and 11, respectively. The levels of micro-cracks in these coatings appeared to be equal to or greater than those in Fig. 9. There appeared to be a significant increase in particles at the surface of the CARC topcoat for the 20% surface treatment condition, compared with the 10% surface modification coating in Fig. 9. This suggests that higher levels of powder hydrophobicity may drive more of the particles to the surface and indicates the importance of understanding and controlling powder properties to enable tailoring of the coating surface characteristics. Specific conclusions regarding the differences in surface structure of panels prepared with and without dispersant used in the silica treatment (Figs. 10 and 11) were not pursued because of the limited number of images and the alternate research direction that was chosen.

Efforts to incorporate SHS powder additions to existing CARC paint systems resulted in a material that was sprayable using coating standard deposition methods. The resulting coatings demonstrated SH contact angles with water. While the rolling angles resulting from SHS additions showed marked improvement over standard CARC, additional work is required to improve the powders and/or modify the CARC system to minimize flaws within the polyurethane matrix caused by exceeding critical pigment volumes. Most importantly, these results demonstrated that the properties of SHS powders can be translated to a sprayable CARC system to produce coatings with varying degrees of SH properties. Perhaps the most significant observation of the CARC loading study was the ability of SHS powders to break through the surface of the CARC resin and impose their SH properties on the bulk polyurethane surface.

The initial powders for study of powder properties and as resulting paint additions were prepared from small (< 30 grams) batch sizes. However, as directed by CPAC and ARL, larger reproducible quantities of SH powders were necessary to demonstrate feasibility of an additive to be used at the depot level. This powder modification process was successfully scaled up to > 150 gram batch sizes in response to that requirement. The reproducibility of the process was demonstrated by the representative TGA weight loss curve shown in Fig. 12. The weight loss magnitudes and event temperatures are equivalent across the profile for both the small and large batch sizes, indicating equivalent loading of water and $(CH_2)_2(CF_2)_5CF_3$ groups independent of batch size.

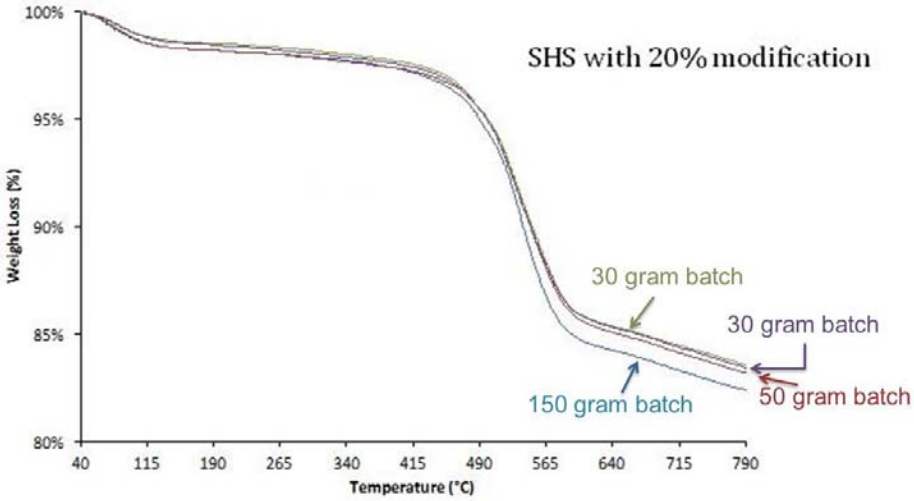

Fig. 12. TGA data for SHS powders modified at different batch sizes. Reproducibility of the process at varying scales was demonstrated.

Once larger scale powder modification protocols were established, work then began on the evaluation of dispersion behavior, contact and rolling angles, and surface topology as a function of silica surface area and/or particle size. Although high contact angles (greater than 150°) were achieved previously with the addition of modified amorphous silica powders to CARC, the ability to simultaneously reduce the rolling angle (aimed for an arbitrarily selected value of ≤ 10°) was adversely affected by the concomitant formation of defects in the fully cured coating. Despite the very high solids loading (probably responsible for crack formation), it was anticipated that the distressed structure could be mitigated through control of the particle size and particle size distribution of the additive powder. To test this hypothesis, two crystalline silica powders (Min-U-Silica and JM Silica) as well as one amorphous DE form of silica (Celtix) powder were modified using (tridecafluoro-1,1,2,2-tetrahydrooctyl) trichlorosilane at 20% by weight. The powders were incorporated as post-formulation additions into 53039C—Type II CARC, spray-applied, and the resulting water drop contact, rolling angles, and surface microstructures were characterized.

The results shown in Table 2 reveal that contact angles greater than 150° can be achieved with starting materials that are not amorphous; that is, crystallinity does not prevent surface modification via chlorosiliane chemistry. Clearly, at a loading of ~ 10% additional silica solids, particle size is not a strong factor influencing contact angle. Despite high contact angles, low rolling angles were not observed for any powder addition with the exception of the silica 518 (ORNL standard).

Table 2. Water drop contact and roll-off angle data for modified silica additions to CARC. For comparison, a standard CARC (53039C Type II) without additions exhibited a contact angle of about 110° (± 5) and a roll-off angle greater than 50°.

Powder type	Average particle size (µm)	Structure	Surface area (m^2/g)	% Solids loading	Contact angle (°)	Roll-off angle (°)
Min-U-Silica	1.7	crystalline	5.7	9.1	159 ± 2	> 50
JM Silica	3.7	crystalline	5.8	9.1	158 ± 2	> 50
Celtex	16.0	amorphous	37.8	9.1	158 ± 1	> 50
Silica 518	9.7	amorphous	47.4	9.2	170 ± 2	8–11

Figure 13 shows the TGA weight-loss curves for the modified silica powders evaluated. Although all the powders were modified under identical conditions, and a weight loss event corresponding to surface fluorination was observed for each silica powder, the amount of the fluorocarbon material present on the crystalline silica powders was far less than that on the amorphous silica counterparts. The lack of surface fluorination is a possible explanation for the lack of change in roll-off angle in CARC that was loaded with modified crystalline silica. However, despite the low surface concentrations of fluorocarbon, CARC containing modified crystalline powder displayed contact angles well into the superhydrophobic range (loosely defined as >150°). To better understand the role of percent surface modification and particle size on rolling angle, a study of the effect of percent surface modification on silica-based powder as a function of surface area/morphology was performed.

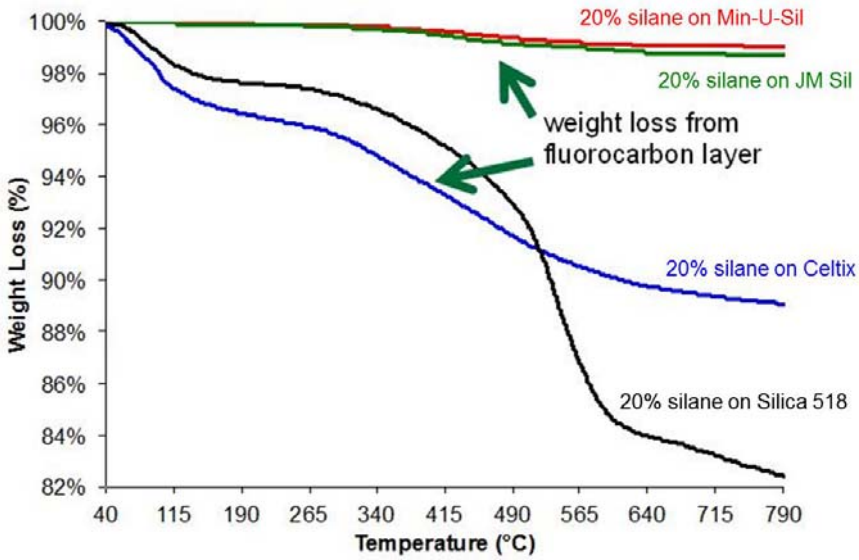

Fig. 13. TGA weight loss curves of crystalline silica starting material and the powders modified with 20% chlorosilane through the previously established standard method.

The surface area and morphology of a powder affect the chemical modification step, the integration of the modified powder into a resin matrix, and the structural effects that powder can produce in a fully cured coating. Thus, the amount of surface area available to participate in the above-mentioned processes is valuable to the design of a robust process. The surface areas of the powders were measured by BET analysis on a Quantachrome Autosorb-1 instrument with nitrogen as the sorbtion gas. The surface area of the powder is plotted against the wt/wt % of chlorosilane to powder used for the modification step in Fig. 14. The DE materials (Celtix and Diafil) were found to have lower surface area than the amorphous silica powders, primarily due to the larger particle sizes of the DE materials when compared with silica. In general, all the powders revealed a nominal decrease in surface area as the amount of chlorosilane used in the fluorination step increased (for every 1% increase in wt % chlorosilane, the surface area decreased by ~1 m^2/g). Based on the amount of surface area decrease observed, it is likely that multiple layers of fluorocarbon are being bonded to the powder surface. Particularly in the case of DE materials, excess chlorosilane may be blocking certain pores and structures internal to the individual particles. The decrease in surface area and/or the formation of multiple layers of fluorocarbon may not be disadvantageous for

producing SH surfaces, but minimizing the amount of chlorosilane needed will be of utmost importance to keeping costs low, maximizing dispersion, and optimizing binding.

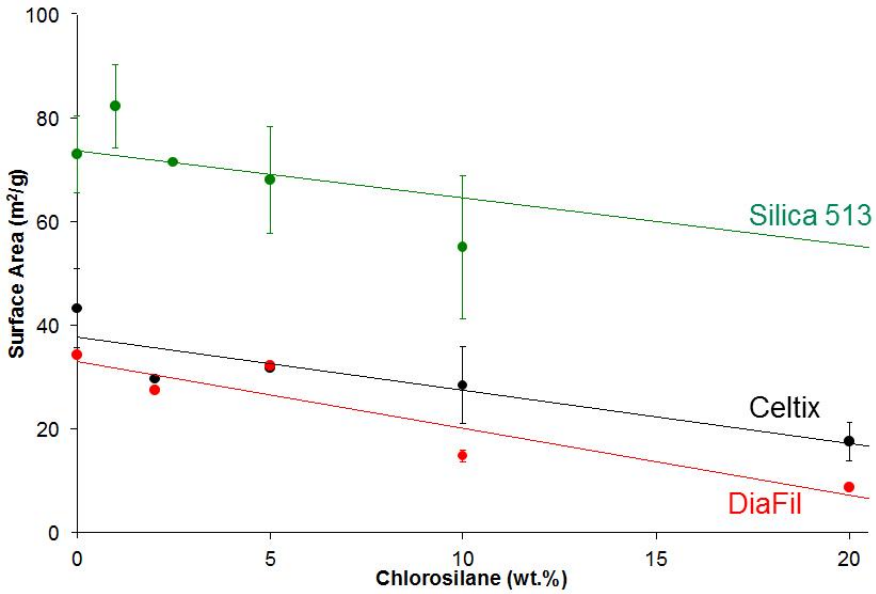

Fig. 14. Surface areas of silica-based powders. If multiple points for a single wt % were available, that data was averaged, and the error bar was plotted at one standard deviation. A larger number of measurements contributes to larger error bars for the Silica 513 material.

To better understand the trend of decreasing powder surface area with increasing surface modification, the surface coverage was determined. The surface coverage is defined as the amount of labile material on a powder relative to its surface area. This metric normalizes the surface modification of various powders by combining the weight loss data from thermogravimetric analysis (previously reported) with the surface area measurements obtained from BET. Weight losses above ~200°C were used to calculate the deposition quantities of fluorocarbon on the powder surface, and the surface area of the unmodified starting material was used to calculate the surface coverage. The data is plotted in Fig. 15. Diafil has the highest percentage of its surface covered by a fluorocarbon layer of the evaluated materials, which suggests the Diafil morphology and surface chemistry is more compatible with the fluorocarbon. Also, the powders with lower surface areas will have even less non-wetting surface available than higher surface area powders, potentially making incorporation into a paint system more reliable. In contrast, powders with high surface areas may need large quantities of fluorocarbon to achieve comparable surface coverage to their lower surface area equivalents.

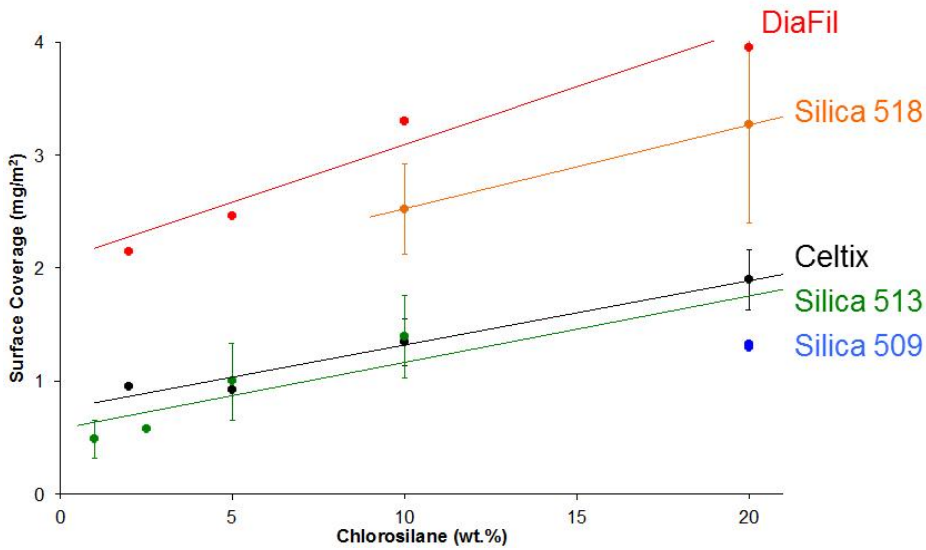

Fig. 15. Surface coverage of fluorocarbon on powders. If multiple data points for a single wt % were available, that data was averaged, and the error bar was plotted at one standard deviation. A larger number of measurements contributes to larger error bars for the Silica 513 and 518 materials.

The effect of particle size on the paint surface was observed when SHS was added to an NCP paint formulation under high shear conditions. This produced well-dispersed small agglomerates of SHS and a coating surface that was relatively defect-free. In contrast, when similarly sized SHS powder was introduced into the NCP coatings under low-shear conditions, the resulting agglomerate size and the coating surface were severely compromised, despite having large contact angles.

To investigate the effect of SH particle size, four samples of the DE silica (Diafil) were prepared. Initially, milling studies were carried out to determine the correct conditions needed to achieve various reproducible particle sizes of DE. Once the milling curve was established, batches of DE were milled from the as-received mean particle size of 15 µm to produce powders with approximate mean particle sizes of 10 µm, 6 µm, and 2 µm. The powder surfaces were then modified at 10% by weight under previously discussed conditions to produce superhydrophobic diatomaceous earth SHDE of differing average particle sizes. Thermogravimetric analysis (see Fig. 16) and surface area determination allowed for the calculation of average surface coverage in milligrams of fluorocarbon per square meter of powder surface. The inset table in Fig. 16 shows the results of that analysis. The relative similarities in the surface coverage numbers were encouraging because this meant that any performance/structure effects observed in CARC surfaces clearly would be caused by the particle size, not by the amount of low-energy material (fluorination) on the particle surface. Furthermore, the highly reproducible TGA curves and limited "spread" in surface coverage numbers indicated that, at least for this set of DE powders, the modification process that results in SHDE also was reproducible.

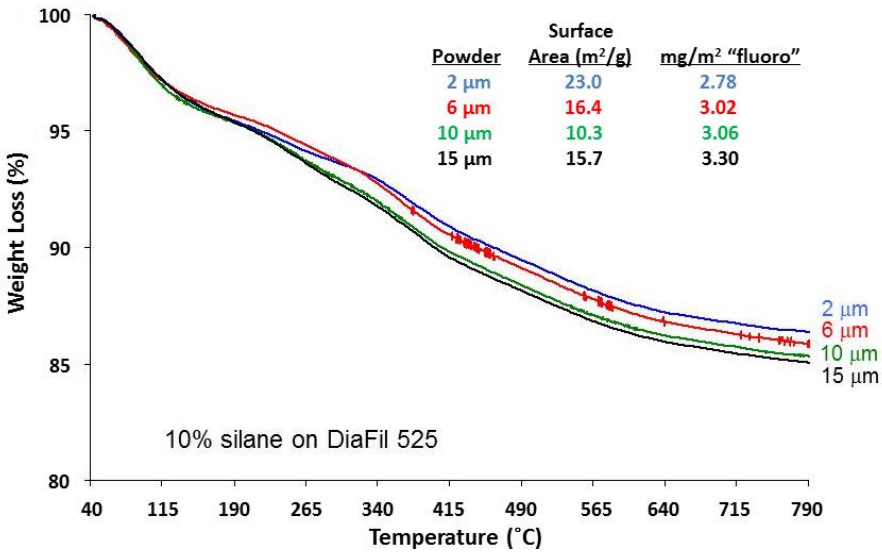

Fig. 16. TGA weight-loss curves for SHDE particles. The surface coverage was calculated using the total weight loss above 150°C in the TGA assessments.

The powders analyzed in Fig. 16 were post-added (that is, as an addition to the otherwise final product) into NCP Type II and Type IV CARC systems using the standard method of pre-wetting the powder before manually mixing the powder into the resin. These modified systems were sprayed using Star4D (Northern Iowa University training academy) procedures, and the resulting panels were tested for hydrophobicity (Table 3) and SEM imaged (Figs. 17 and 18).

Table 3. Contact angle and roll-off angle data with water for NCP developmental coatings with various SHDE modifications. Optimum values are achieved in both resins with 6 µm average particle size Diafil that has been modified with 10% chlorosilane. All angles given in degrees.

Type II	Diafil size	% SHS	Contact angle	Roll-off angle (static)	Roll-off angle (dynamic)
A	n/a	0%	129 ± 2	>90	>90
B	2 µm	9.2%	143 ± 4	>90	10
C	5.7 µm	9.1%	159 ± 2	>90	13
D	10 µm	9.2%	155 ± 2	>90	14
E	15 µm	9.2%	154 ± 1	>90	≈20
Type IV	**Diafil size**	**% SHS**	**Contact angle**	**Roll-off angle (static)**	**Roll-off angle (dynamic)**
A	n/a	0%	107 ± 3	>90	>90
B	2 µm	9.2%	154 ± 3	>90	13
C	5.7 µm	9.2%	160 ± 1	>90	6
D	10 µm	9.2%	157 ± 2	>90	10
E	15 µm	9.2%	153 ± 2	>90	21

Notes: SHS = superhydrophobic silica; n/a = not applicable.

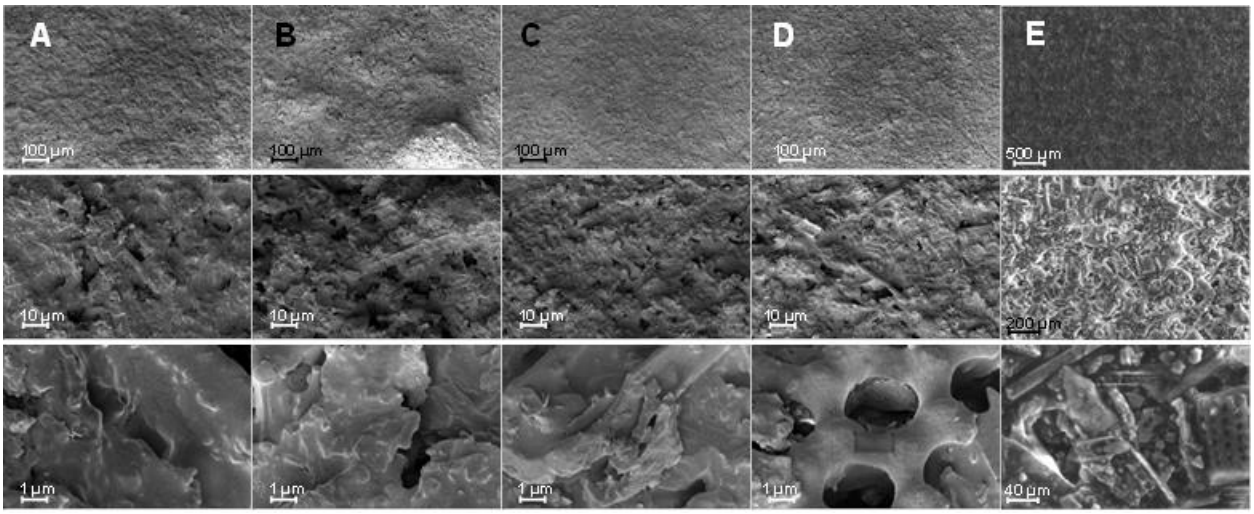

Fig. 17. SHDE in NCP Type II developmental coatings at increasing particle size, from left to right (A, no Diafil addition; B, 2 µm; C, 6 µm; D, 10 µm; E, 15 µm). Data for particle size and percent loading is given in Table 3.

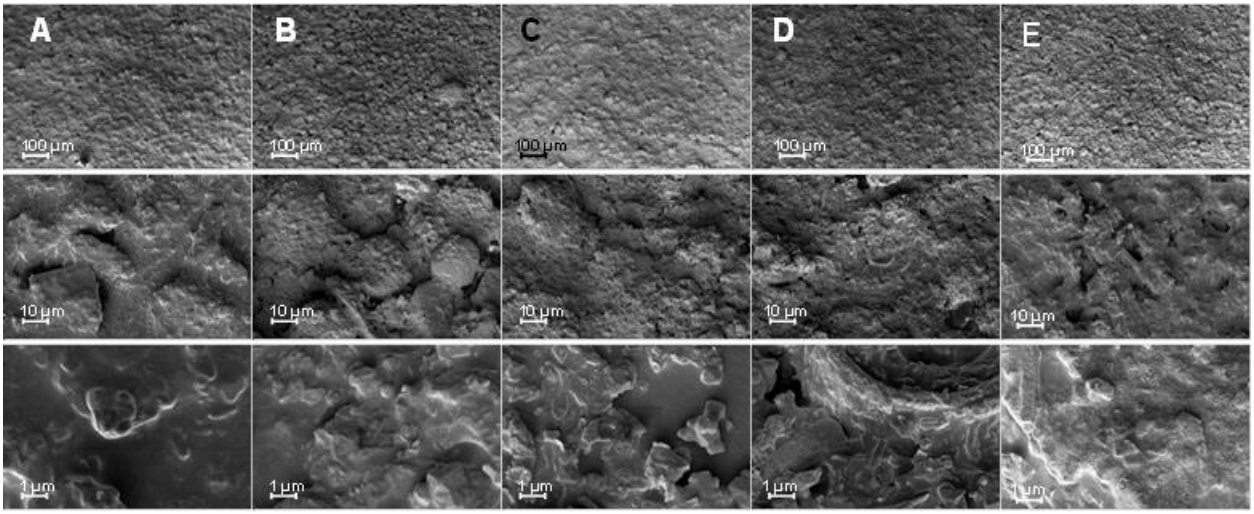

Fig. 18. SHDE in Type IV at increasing particle size, from left to right (A, no Diafil addition; B, 2 µm; C, 6 µm; D, 10 µm; E, 15 µm). Data for particle size and percent loading is given in Table 3.

The results from the integration of milled SHDE into CARC coatings were encouraging. The coatings generally were uniform and defect-free at SH particle sizes under 10 µm. At the 10 and 15 µm average particle size, surface cracking and defects were detected in the coatings although contact angles were >150°. The SHDE modified surfaces were more adherent and uniform in appearance than the high-shear mixed SHS in either coating system while maintaining the defect free surface. Based on the optical and scanning electron microscopy images collected for the resulting coatings, the presence of SHDE at the surface of the CARC coatings seemed well dispersed. Particle size and DE surface texture could be targets for modification to influence the resulting surface characteristics.

With the encouraging results obtained by integrating SHDE into CARC resins, the ratio of SHDE to SHS was varied during a mixing study. The goals of this set of experiments were (1) to ascertain the viability

of using SH powders to minimize critical pigment loading in a CARC resin and (2) determine if a bimodal size distribution of SH powder would produce defect-free coatings with higher contact and lower roll-off angles. The NCP Type II solvent-borne resin was selected for the study, and the results are summarized in Table 4. The two powders that were used for this study were 10% modified 15 µm Diafil (SHDE) and 20% modified submicron SHS. The 50/50 mixture of the two powders provided highest contact angles and lowest roll-off angles with minimal or no surface cracking.

Table 4. Contact and rolling angle data for SHDE/SHS mixing study. All angles given in degrees.

SHDE/SH	% Additive	Contact angle	Roll-off angle (static)	Roll-off angle (dynamic)
n/a	0%	120 ± 3	>90	>90
100/0	9.2%	154 ± 1	>90	≈20
75/25	9.3%	159 ± 2	>90	≈10
50/50	9.4%	163 ± 3	>90	≈5
25/75	9.2%	162 ± 3	>90	≈5
0/100	9.1%	171 ± 3	18–45	n/a

Notes: SHDE = superhydrophobic diatomaceous earth; SH = superhydrophobic; n/a = not applicable;

2.4 POWDER COAT SYSTEMS WITH SH SILICA ADDITIONS

Powder coat technology has gained favor recently for applications involving military assets. Therefore, in the final year of this program, SHS additions to powder coat materials were included in a preliminary evaluation process. The primary driving force for the recent foothold gained by powder coat technology is the elimination of a large fraction of the hazardous materials associated with standard liquid coating processes, such as all of the heavy metals associated with primary surface treatments and most of the volatile organic compounds (VOCs) from solvents necessary to formulate and/or spray most liquid systems. In addition, for specific service duties, powder coating can offer increased through-put and highly reproducible coating quality compared with more traditional coating processes, particularly for components within size/geometry limits amenable to somewhat specialized handling and curing within a furnace. Of particular interest to this development program, however, is that powder coats tend to be more uniformly dense than coatings generated by liquid spray (especially for solvent-borne systems), and thus there is potential for improved chemical agent and/or corrosion resistance.

Further, modification of liquid CARC systems with SH powder additions requires careful balancing of total solids content as well as critical selection of chronology and amount(s) of specialized solvents to achieve complete mixing and proper application. In comparison, however, it was expected that addition of dry SH powders to powder coat materials would offer far fewer complications in proper dispersion (solubility/wetting) and uniform incorporation of the SH component. Therefore, an attempt to integrate SH powders into standard military powder coat materials/processes was included in the coating development efforts. The performance (corrosion protection qualities) of steel panels prepared with standard powder coating processes and materials was compared with that for panels prepared with

identical coating processes including SH materials. In selected cases, structures and coating composition were analyzed.

Representative of best laboratory practice, powder coats for this study were prepared initially at the Northern Iowa University (Star4D) facility, which included training of ORNL staff members as part of the effort. Subsequently, a limited number of sample powder coat panels was produced at the USMC Albany Maintenance Depot as representative of best industrial practice. Powder coated panels for testing also were prepared at ORNL to manipulate key variables, including post-application heat treatment requirements. Local industrial shops providing powder coat capability also were investigated briefly, but processing at these facilities typically incorporates "Vulcan black" polyester resin (or comparable material), which routinely performed poorly in B117 exposures; therefore, this option was not pursued further.

In the most detailed study supporting this portion of the effort—performed by ORNL staff at Northern Iowa—two commercial powder coat products were examined with and without variable amounts of SHS powder added to the coating:

- EGS2-90007, seafoam green 24533, epoxy (MIL-PRF-32348, Type II, interior)
- UHS2-20025, desert tan 595-33446, Type III) urethane polyester (Type III, CARC finish)

Thin gage mild steel panels (about 0.03 in. thick) were prepared for coating with surface processing in a series of chemical cleaning steps (an alkaline degreasing step followed by two water rinses) and finished with a non-phosphate conversion coating; neither grit blasting nor primer application was employed. Urethane powders with 0, 0.5, 0.7, 0.85, 1.0, and 1.5% SHS (20% surface-treated with chlorosilane at ORNL) added to the commercial powder were then sprayed and furnace-cured in standard fashion. In addition, identically cleaned steel panels were coated with the commercial epoxy powder over a smaller range of formulations (0 and 1.0% SHS addition). All powders were mixed for 15–20 min in a tumbler rotating at ~ 80 rpm and containing a mixture of ceramic beads (1–2 mm diameter) with the powders to enhance dispersion/mixing.

During the initial trials of these powder coat experiments, it was observed that somewhat higher curing temperatures and/or longer curing times were required for powder mixes that incorporated SHS. Based on visual assessment by the experts at Northern Iowa and their best judgment for adjustment of curing conditions, some attempt was made to modify the standard curing practice recommended for the baseline products in this experiment. However, it is recognized that optimized curing for each different powder mix likely was not achieved.

In all cases, fusion/curing of coated panels was achieved in a conveyor type furnace (ambient air fed). Precise times and temperatures for any particular coated panel within the furnace are not known, but these critical factors were tracked via "dummy" steel panels with thermocouples attached, which sent information to a data logger. Thus, both curing times and temperatures for panels varied over a modest range, but as a generality, all panels were heated to about 400–410°F for 10–12 min to achieve curing. The average coating thickness achieved was 2.9 ± 0.5 mils for the polyurethane panels and 2.4 ± 0.3 mils for the epoxy panels.

Following curing, all of these panels were similarly macroscopically uniform, without mud cracking, pinholes, or similar defects. Among the panels coated with urethane, no obvious color gradient resulted from the small but variable additions of SHS to the coating formulation. However, a modest color change toward paler green was observed for the increase from 0% to 1% SHS addition in the epoxy coating system. Figure 19 shows a representative portion of each panel in the test matrix. The photos of each panel were taken with the same camera in the same light stand with identical exposures, so the colors are relatively true among the photos. Another feature of the panels—also evident in Fig. 19—is the variable tendency toward relative wetting of water droplets as a function of SHS content. The water droplets for these photos were created with a standard medicinal dropper. For the urethane series of coatings, the droplets tend to be relatively flat with a large contact area on the coating surface for 0 and 0.5% SHS additions, but for the 0.85, 1.0, and 1.5% SHS added surfaces, the droplets are much more rounded. The 0.7% SHS panel appears to represent something of a "transition" between these two behaviors. Furthermore, for the highest three levels of SHS addition to urethane, it was quite difficult to get droplets to remain on the surface as they readily rolled (even "bounced" on occasion) across the surface at the slightest vibration or tilt. Similarly, the epoxy surface containing 1% SHS addition shows more rounded droplets than the corresponding panel with no silica addition.

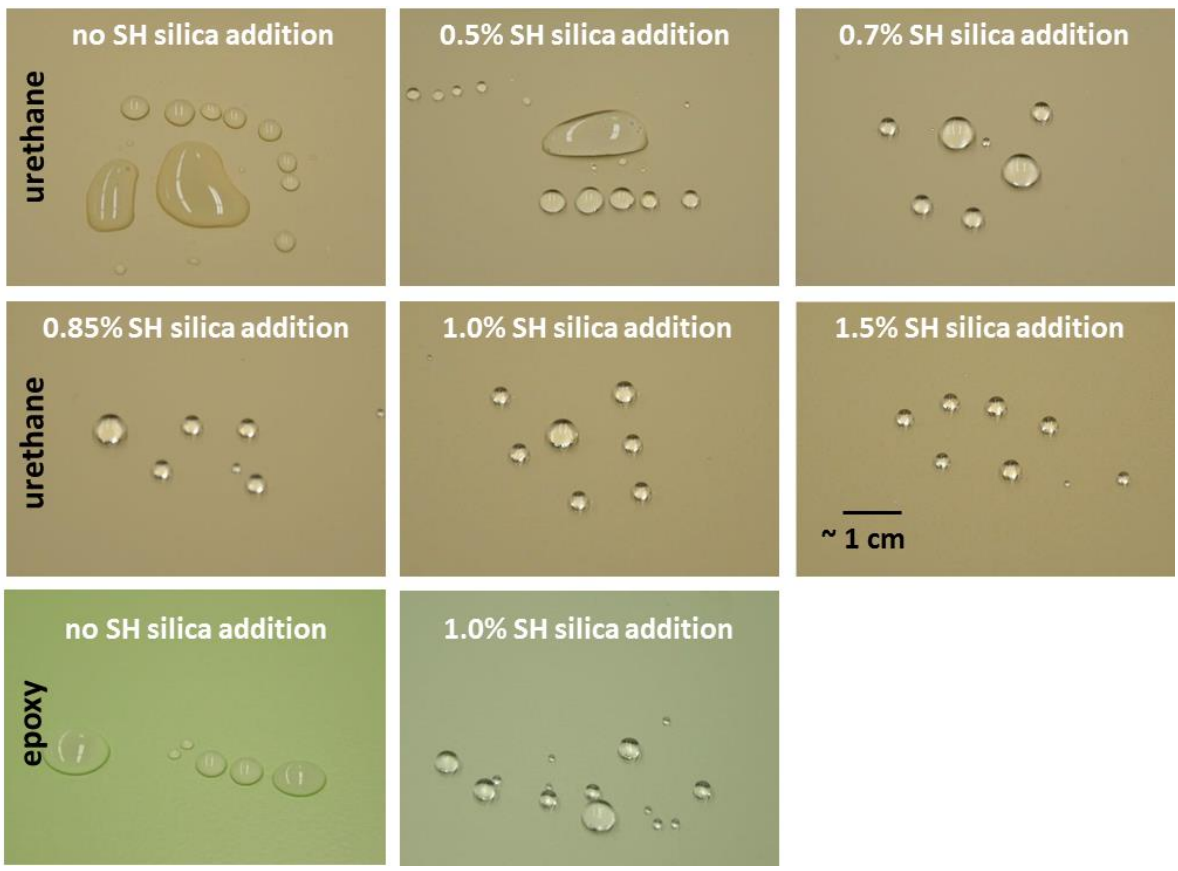

Fig. 19. Water droplets on the surface of urethane (top two rows) and epoxy (bottom row) powder coat panels as a function of SHS additions to the powder coat formulation.

However, a surface roughness gradient was readily detected among the powder coat panels by light stroking with a fingertip—for example, as the SHS loading in urethane increased from zero (very smooth

to the touch) to 1.5%, the surface roughness uniformly increased not unlike that of increasing coarseness of fine grit sandpaper surfaces. This observation revealed that at least some of the SHS powder is present at the surface of the coating.

In an attempt to quantify these observations, contact and roll-off angles for standardized water droplets were measured for an average of five locations on each panel as a function of SHS addition. The results are plotted in Fig. 20. The contact angle possibly changed similarly for the urethane and epoxy systems (although only two data points obviously compromises detailed assessment of the epoxy system). Compared to the unmodified coating, as little as 0.5% SHS addition dramatically changed the contact angle observed on the urethane surface; however, the contact angle increased only modestly with further additions of silica. In contrast, consistent with the behavior noted in trying to create the photographs in Fig. 20, the roll-off angle on the urethane surfaces exhibited a sharp decrease between 0.7 and 0.85% SHS additions (and this behavior will be considered again in subsequent paragraphs), while the roll-off angle of the epoxy panels was insensitive to added silica at these amounts.

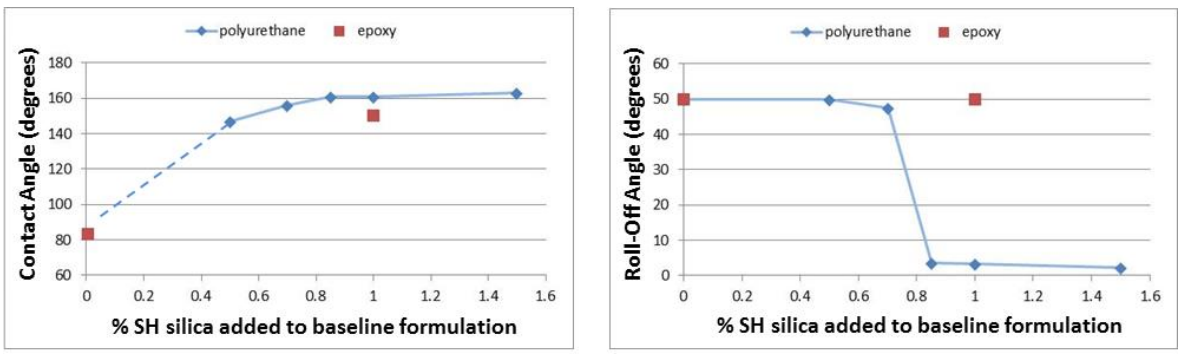

Fig. 20. Contact and roll-off angle measurements for pure water droplets on the surface of powder coat panels as a function of SHS addition.

Standardized pull-off adhesion tests (ASTM D-4541) were performed on the as-prepared powder coat panels. The results varied substantially among the panels, with a recorded range of 50–1,000 psi; most results were in the 50–150 psi range. Only panels with no SHS additions to the coating yielded results at the high end. Although this result was not examined in detail, it is believed that presentation of SHS at the free surface of the coating interfered with the ability to develop good adhesion between the aluminum test dolly and the bulk coating surface. Almost without exception, the low strength pull-off results were characterized by a dolly surface retaining only adhesive but rarely more than a trace of coating material. This result suggests that the modified powder coats may be improved if the SHS additions were more uniformly distributed throughout the coating (as opposed to possibly concentrating at the surface) or, alternatively, were more strongly bound to the coating matrix.

Powder coated panels from this campaign were also exposed to standard condensing salt fog conditions (ASTM B117) as one technique to assess the utility of the SHS additions to the coating. The photograph in Fig. 21 shows the generalized result, which compares polyurethane coatings with a range of SHS additions after two weeks exposure in B117 testing. All of the powder coats examined were similarly effective for protection of the substrate, with coating failure and streams of oxide limited to the edges of each panel, whereas the main surfaces of each were nearly free of corrosion. However, beads of condensate were observed to form very readily on all urethane panels with at least 0.85% SHS addition,

while essentially none formed on urethane panels with ≤ 0.7% SHS addition. This demarcation—a change in wetting behavior between 0.7 and 0.85% SHS added—is consistent with the step function change in roll-off angle measurements shown in Fig. 20.

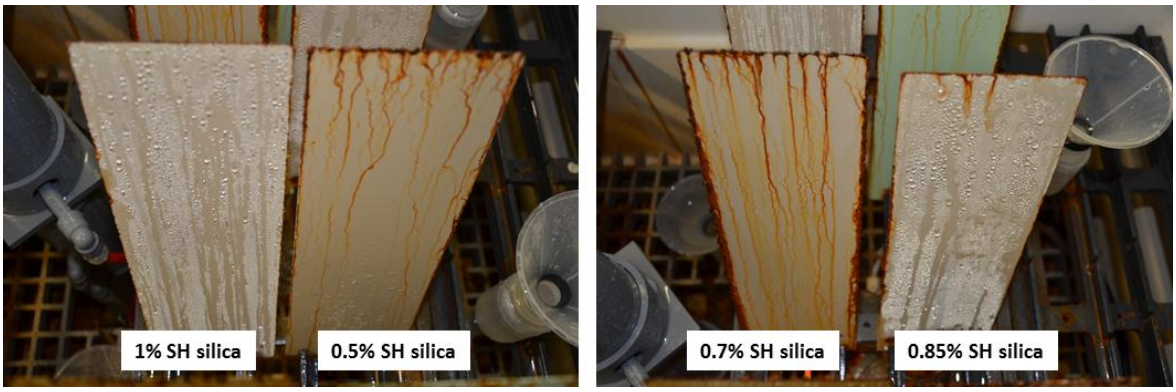

Fig. 21. Urethane powder coat panels following two weeks of exposure in B117 conditions. The panels shown here were photographed within the B117 exposure chamber. Note that the urethane surfaces wetted by moisture in the fog chamber also have taken on a darker coloration not observed on the original (unexposed) panels.

This result suggests that above a minimum concentration, the presence of SHS can impart SH properties to the coating material. That such a relatively small amount of silica (~ 0.85%) is capable of producing this effect indicates a potential concentrating mechanism—that is, a driving force causing silica to come to the free surface in amounts disproportionately higher than the small weight percentage addition to the baseline material would suggest. Condensate that beads up and rolls from the panel surface—that is, does not wet the surface—does not interact efficiently in terms of penetration or permeation and therefore cannot effectively corrode the substrate. For panels wetted by condensate, the panels tended to remain wet for extended periods (even when removed from the exposure chamber), thus indicating penetration of moisture into the coating structure and (eventual) onset of substrate corrosion. Further, it is significant that even the streams of iron oxide emanating from the edges of the panel (coupon edges are most difficult to adequately coat with a powder technique) do not appear to adhere to the main surface during the exposure. This indicates that the majority of the oxide debris is also "washed" from the surface as the condensate beads roll off and suggests the potential for relatively easy surface cleaning long-term for powder coats containing SHS in excess of the minimum required. It is interesting, however, that any beading of condensate was observed on these panels, given that the moisture arriving at the coating surface is primarily a vapor with no surface tension; generally speaking, the primary mechanism by which superhydrophobic surfaces repel moisture requires the resident liquid to have surface tension. This observation suggests further evaluation of the topography and physics of SH surfaces, as well as further evaluation of the screening tests used to evaluate and compare performance, is necessary to understand and predict performance of these SH surfaces and coating systems.

Beading of condensate appeared consistent and persistent among multiple urethane panels prepared in this campaign. Undisturbed urethane panels were exposed for over 3,000 hours in B117 conditions, and continuous condensate beading was observed throughout the exposure period for all panels with ≥ 0.85% SHS added, as well as limited encroachment of rust stains onto the main surfaces of the panel.

After about 6 weeks (1,000 hours) of exposure in B117 conditions, some urethane panels were lightly abraded with a standard kitchen scrub pad (finger pressure only) on one half of the panel "topside" and were returned to the B117 chamber. A representative result is shown in Fig. 22. In this case, the left half of the panel remained undisturbed and continued to bead condensate. The right side of the panel, which was lightly abraded, largely ceased to bead condensate; oxide stains from streaming associated with the panel edges and active corrosion on the main panel surface are evident. The cessation of condensate beading was observed almost immediately (within a few hours) after returning the partially abraded panels to the fog chamber, but the appearance of active corrosion required several hundred more hours to develop to the state shown in Fig. 22.

Fig. 22. Urethane powder coat with 1.5% SHS addition after a total exposure time of 10 weeks in B117. For the first 6 weeks, the panel was undisturbed, after which the right half of the panel was lightly abraded with a scrub pad. Note that there was no primer beneath the urethane coating.

Beading of condensate—at least to the degree observed on some polyurethane panels—was not observed among the more limited set of epoxy powder coated panels. More modest beading—far fewer droplets, but not an absence of droplets, was observed for the first few weeks of exposure in B117 fog, but extended exposure was associated with the absence of condensate beading on the epoxy panels and substantial rust streams (mostly from active corrosion at the panel edges) accumulating on the test surface. Apparently, 1% addition of SHS is below the critical threshold for superhydrophobic behavior in epoxy (consistent with the roll-off angle data in Fig. 21), and/or a different concentrating mechanism operates so that more silica is required to get the same condensate behavior observed for ≥ 0.85% silica additions to urethane.

In the powder coat trials at Albany, the baseline powder materials were somewhat different from those at Star4D. (The common products in service at Albany included Seafoam Green epoxy [2GS2-9000-C-50] and Air Force Green urethane [PGS4-99021-SC].) At Albany, researchers attempted to produce epoxy powder coats at 2% addition of SHS (the silica used in Star4D trials) to improve condensate beading, but the coating appeared similar to a "dry spray" result in that the surface was brittle (it crumbled and rubbed off on contact) and contained a high fraction of voids and regions with poor coverage. This will be

discussed further in a subsequent paragraph on powder coat structure, but there appears to be a physical limit to the amount of silica that can be added without dramatic effects on powder application and distribution—silica negatively affects electrostatic application—as well as the curing process and final coating structure. Other results of note from the Albany trials include the fact that both of the baseline materials—epoxy and urethane—beaded condensate for an extended B117 exposure period, which was somewhat different from theStar4D panels' behavior. Potential reasons for the different behavior include different baseline product characteristics and a different curing procedure. Panels prepared at Albany were cured 16 min at 365–385°F compared with the manufacturer's recommendation of 10–15 min at 400°F; this potential under-curing may improve plasticity and positively alter surface characteristics. The 1% SHS modification of urethane prepared at Albany performed unusually in that the panel appeared completely dry for at least 40 days of B117 exposure. It showed no apparent condensate or wetness at all and no rust bloom at any non-edge location for almost 50 days before minor spots appeared. Finally, the 2% SHS modification of epoxy exhibited simultaneous extensive beading of condensate and widespread rust bloom, indicating some positive features of the silica addition but disruption of the coating continuity. A representative view of each of the Albany panels appears in Fig. 23 following 28 days of B117 exposure. This comparison indicates that the powder coat panels from Star4D and Albany performed substantially differently, suggesting there are poorly understood process variables (composition, curing, silica mixing, etc.) in need of further development.

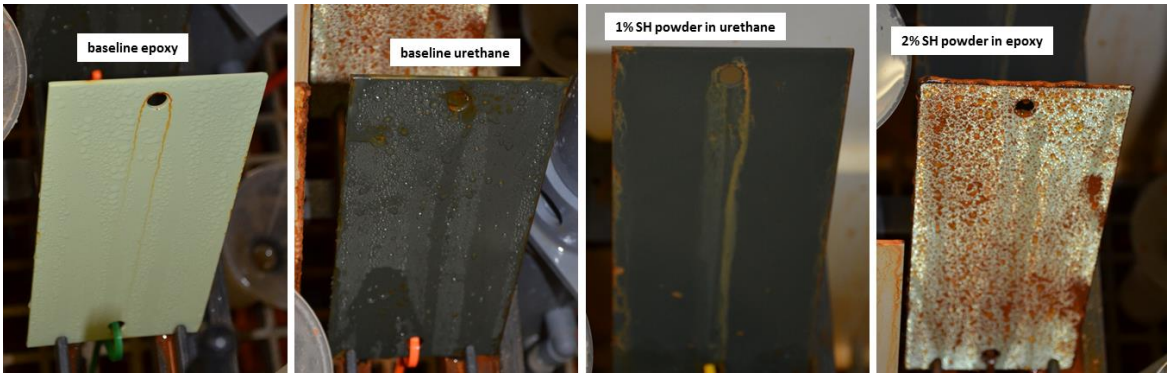

Fig. 23. Powder coat panels prepared at Albany following 28 days of standard B117 salt fog exposure. Panels here remain within the chamber for the photograph, only seconds after opening the fog enclosure. Note that compared with the other panels, the 1% SHS panel appears essentially dry (no condensate beads or any discoloration due to moisture).

To distinguish details of the powder coat surfaces further, another potentially discriminating test was incorporated. A duplicate of each of the above powder coated panels (Star4D and Albany preparations) was immersed in deionized (DI) water for one week—similar to the "water resistance" test called out by MIL-PRF-32348 for powder coat materials. Consistent with the original roll-off angle measurements of the as-prepared panels, the urethane formulations with 0.85, 1.0, and 1.5% SHS (Star4D and Albany panels) appeared to resist wetting completely upon immersion—a thin layer of air apparently was trapped between the panel surface and the water, and each of these panels remained completely dry during the entire immersion period. One of these panels (1% SHS sprayed at Star4D) was removed for a few hours each morning to encourage "dry-out" before re-immersion, but this alternating wet/dry cycling did not appear to adversely affect the superhydrophobic behavior of the coating surface in this brief exposure

period. All the other panels (urethane with lower amounts of SHS additions as well as both epoxy panels) exhibited wetting by the deionized water immediately upon immersion.

Interestingly, after a few minutes to an hour, the wetted panels also displayed a uniform array of fine/small gas bubbles across the immersed surface. The identity of the gas in the bubbles was not assessed, but it seems likely that entrained air within the water nucleated as discrete bubbles at surface irregularities (flaws, active corrosion sites, etc.) that are otherwise "masked" by a superhydrophobic surface. The bubbles returned at various rates after the panels were disturbed to shake the bubbles free from the surface. For comparison, a bare steel surface was also covered in bubbles almost immediately upon immersion in DI water, and the panel was quickly covered with oxide. A standard CARC panel similarly immersed was wetted but revealed only a few gas bubbles across the surface.) At the end of one week's immersion, however, none of the panels exhibiting superhydrophobic behavior or those with nominal wetting revealed any corrosion or rust bloom except along the edges, which were protected only marginally by brushed-on epoxy to minimize corrosion at this location. Figure 24 shows representative photographs of panels partially immersed in deionized water for 48 hours.

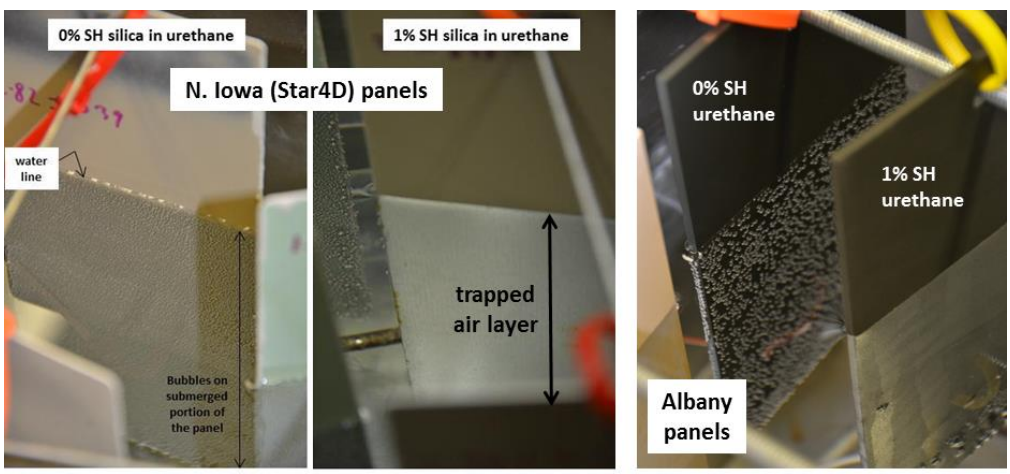

Fig. 24. Powder coated panels with and without a trapped air layer on the submerged surface after 48 hours of immersion in deionized water.

Subsequently, sufficient salt (as NaCl) was added to the immersion tank to transform the deionized water to a 5% salt solution, and the panels were again immersed for one week. Panels exhibiting superhydrophobic behavior (≥ 0.85% SHS addition in urethane) were again quite resistant to corrosion, with trapped air apparently protecting all but the extreme edges of the panel surface and a very few "flaws" in the coating at which steel corrosion was observed to initiate. Although the epoxy powder coats did not exhibit superhydrophobic behavior in these immersions via a trapped air layer (in DI or 5% salt water), the epoxy was nevertheless quite protective of the substrate with a 1% SHS addition. Figure 25 is representative of this observation, which compares performance of epoxy with and without a 1% SHS addition following immersion for one week in DI water followed by one week in 5% salt water.

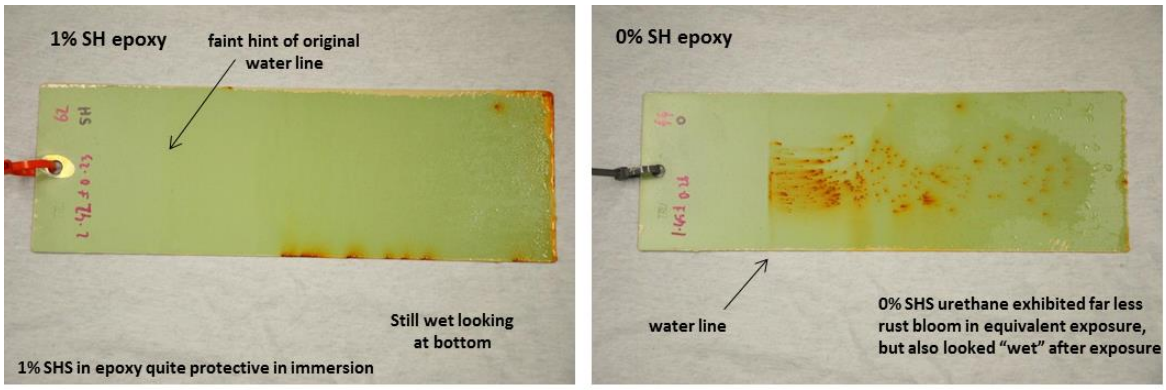

Fig. 25. Epoxy powder coat specimens with (left) and without (right) 1% SHS additions following immersion in DI water and then 5% salt water for one week each.

The structure of the powder coat materials was studied using several different techniques. A Keyence VH-Z100UR optical profiler and digital microscope was used to quantify the surface relief changes that result from SHS additions to the baseline material. Figure 26 is representative of the results, which suggest that additions of silica tend to increase the roughness associated with the cured powder coat surface. In the particular analysis areas shown (each about 300 × 300 µm, selected at random), the addition of sufficient silica to epoxy to generate condensate beading (~ 2%) increased the roughness by a factor of about 10. A smaller addition of silica to the urethane material (similarly led to condensate beading) increased the apparent roughness by a factor of only about three. Curiously, the roll-off angle for water droplets was observed to *decrease* with increased silica additions (which increased surface roughness), suggesting the change in surface tension for water interaction with the surface is a much greater factor than overcoming the height of bumps and valleys for a bead to roll from the surface. Clearly, reduced surface roughness is not a necessary feature of merit for development of a superhydrophobic surface.

Examination of the powder coat surfaces with the scanning electron microscope yielded results represented by the images in Fig. 27. As the amount of SHS addition increased, the surface roughness tended to increase. At a concentration similar to that predicted by Fig. 20 for a sudden decrease in roll-off angle (between 0.7 and 0.85% silica), the surface character tends to change dramatically toward rougher morphologies and an increased number of pores and cracks resulting from poor or incomplete fusion in the curing process.

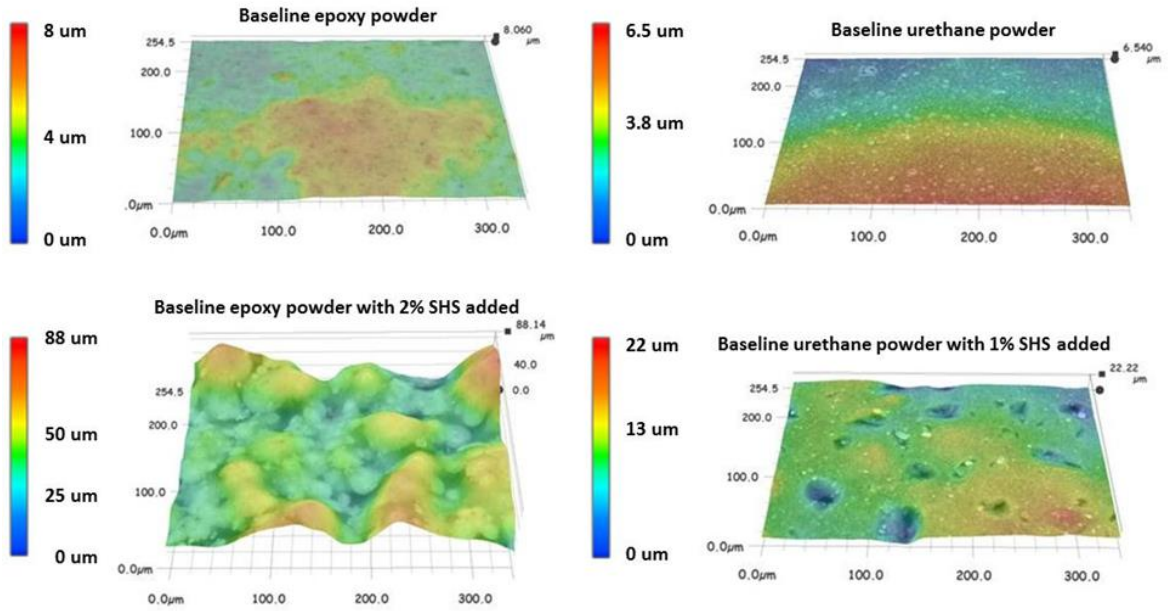

Fig. 26. Keyence optical microscope views of the surface of cured powder coat specimens of epoxy (left column) and urethane (right column) comparing relative surface roughness with and without SHS additions.

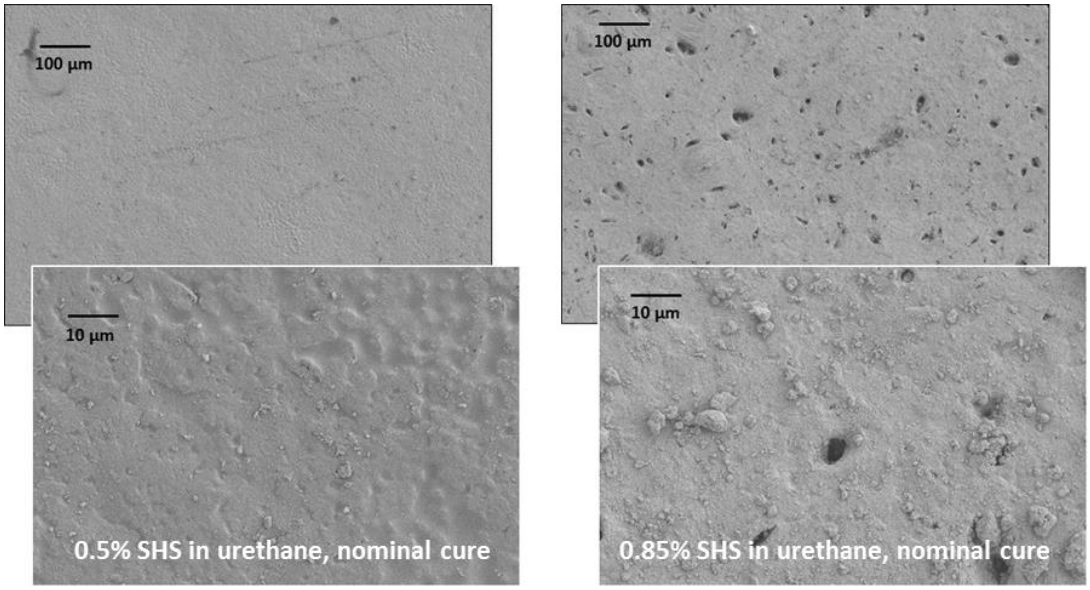

Fig. 27. Scanning electron microscope images of urethane powder coat surfaces as a function of SHS addition.

Further examination of representative powder coat panels revealed a potential explanation for the unexpected result of the performance tests —the higher SHS loads seemed more protective in a salt fog environment and water immersion despite a higher incidence of cracks and pores in the structure. Figure 28 shows a cross section of a urethane panel from Star4D containing 1% SHS addition. The coating integrity is somewhat poor, as indicated by the photo at the top of the collage showing a number of cracks, several of which penetrate to (or very nearly to) the steel substrate. Such a coating might be

expected to provide poor corrosion protection for the substrate in salt fog or immersion in water but, as the above results have shown, superior corrosion resistance with very low roll-off angles was observed. At the bottom left in Fig. 28 is a scanning electron microscope image of the coating cross section, showing it to be less than fully dense (lots of rounded pores) and showing one partially-penetrating "crack" at the right side. The silicon map (bottom right) highlights the location of the SHS addition within the coating matrix (relatively higher concentrations appear as more intense/concentrated areas of "white" in the photograph). It is clear that much of the silica present in the powder coat has managed to accumulate on the free surfaces, including pores and cracks, perhaps yielding corrosion resistance at the surface similar to what might be expected from much higher bulk silica content. Similar behavior was observed in the epoxy powder coats.

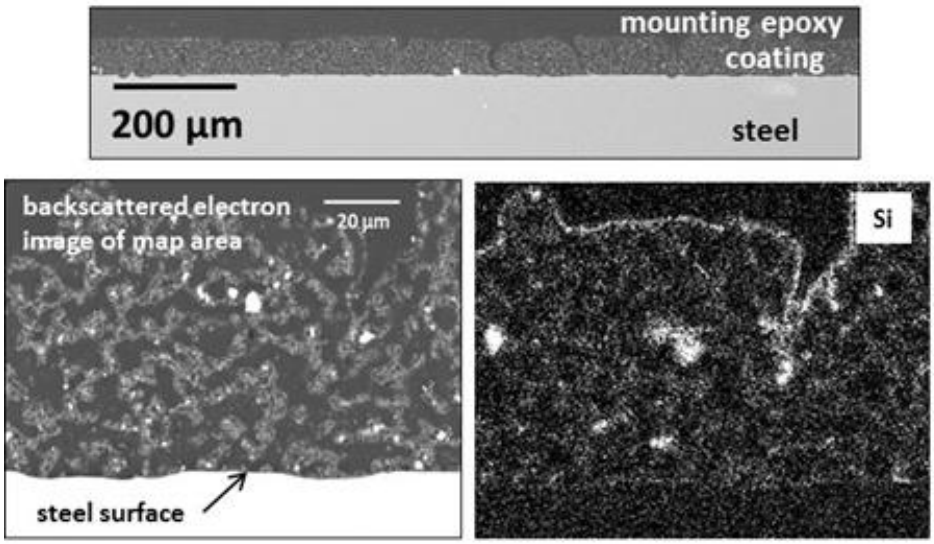

Fig. 28. A cross section of the urethane powder coat containing 1% SHS addition (top) showing a number of cracks/voids penetrating much of the coating thickness. Bottom row shows, at left, a SEM image at high magnification of the same coating and, at right, an element map of the same area showing the presence of silicon.

It appears that the accumulation of silica on the free surface is beneficial for reducing wetting by water (generating high contact angles) and decreasing roll-off angles, but it may suggest poor surface durability. For example, only a modest amount of erosion or other physical damage of the coating surface would be expected to remove (or compromise) a substantial fraction of the original silica addition. Taber testing (ASTM D-4060) of a limited number of coated panels indicated this seems likely—following only 5–50 abrasion cycles, contact angles for powder coats with silica additions decreased dramatically, approaching values consistent with no additions of silica. Further development of powder coat materials and additives to incorporate silica additions will need to address durability issues.

At ORNL, additional experiments were performed in an attempt to modify urethane powder coat materials with the DE form of silica (Diafil; 20% treated with silane) rather than the identically silane-treated but more compositionally refined and physically uniform (and thus more expensive) SHS.

The primary purposes of these experiments were

- to examine composition limits—that is, determine an upper bound on the amount of SHDE that could be added without detriment to coating performance;
- to examine the influence of composition on the time-at-temperature curing requirements for the powder; and
- to determine whether the type of silica added to the powder coat materials was important to the wettability, structural characteristics, and corrosion performance of the coating.

Figure 29 is representative of a number of experimental results. It shows a series of panels produced by spraying urethane powder (Sherwin Williams desert tan urethane; UHS2-20005 595-33446) with increasing amounts of SHDE additive premixed into the dry powder. Note that as the amount of SHDE was increased in sequence (from 0% to 1% to 2% to 5% to 10%), the contact angle measured for water droplets on each surface increased sharply following the addition of 1% SHDE but much more slowly for greater additions of silica. Curiously, the contact angles continued to increase with increasing silica additions (roll-off angles remained near 90° and unchanged) despite the fact that coating coverage became increasingly irregular with higher silica additions, which is also evident in Fig. 29. While the cause of the irregular coating was not examined in any significant detail, it seems likely that the electrostatic spray character of the powder (particle distribution, component coverage) was degraded with increasing additions of silica because of the electrically insulating nature of the silica disrupting the electrostatic potential gradient for powder application.

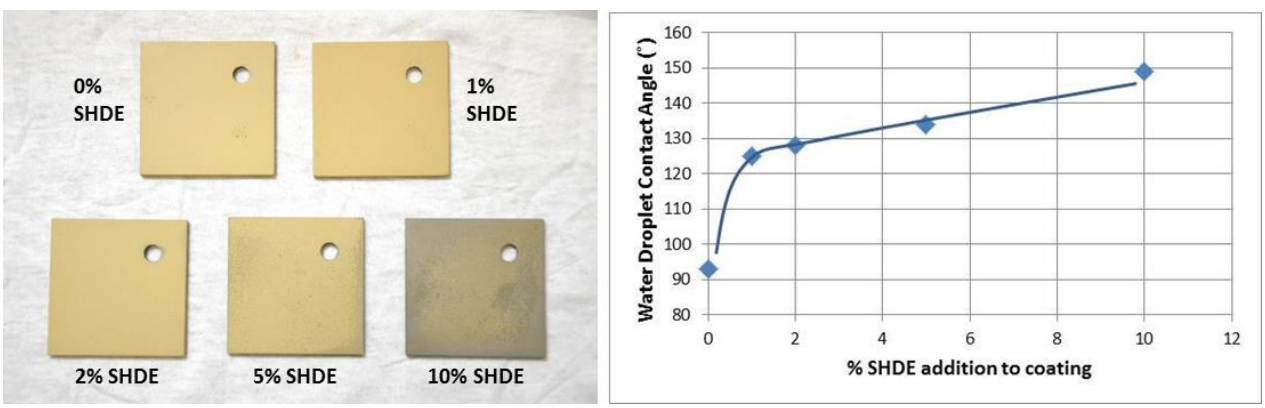

Fig. 29. Appearance (left) and water drop contact angle (right) of urethane powder coat panels as a function of SHDE addition to the powder material. Average contact angles given represent at typical spread of ± 3°. Average roll-off angles were all ~ 90° and unaffected by percent of SHDE addition.

Performance of these powder coated panels in B117 salt fog generally was distinguished in 1 week of exposure. Figure 30 shows a representative result, which indicates that urethanes with 1–2% SHDE addition tended to bead condensate and were relatively protective of the steel substrate, whereas larger additions of SHDE disrupted the structure sufficiently to destroy corrosion protection properties. Curiously, all of the powder coat structures for the panels shown in Figs. 29 and 30, independent of percent of SHDE addition, exhibit somewhat irregular surface features indicating perhaps only partially

melted polymer beads (the surface would be smoother with more uniform melting). An example set of photographs showing the surface of these panels appears in Fig. 31.

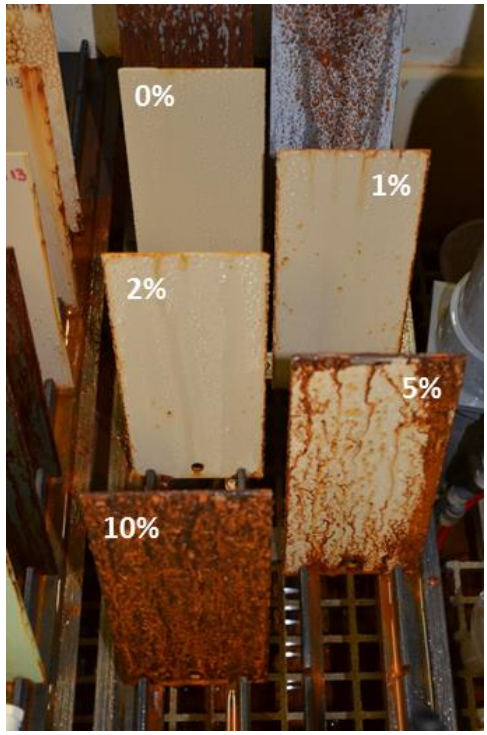

Fig. 30. Appearance of urethane powder coat specimens (prepared identically to the small specimens shown in Fig. 29) following 1 week of exposure in B117 salt fog. The percent of SHDE addition in each case is given on an upper corner of each panel.

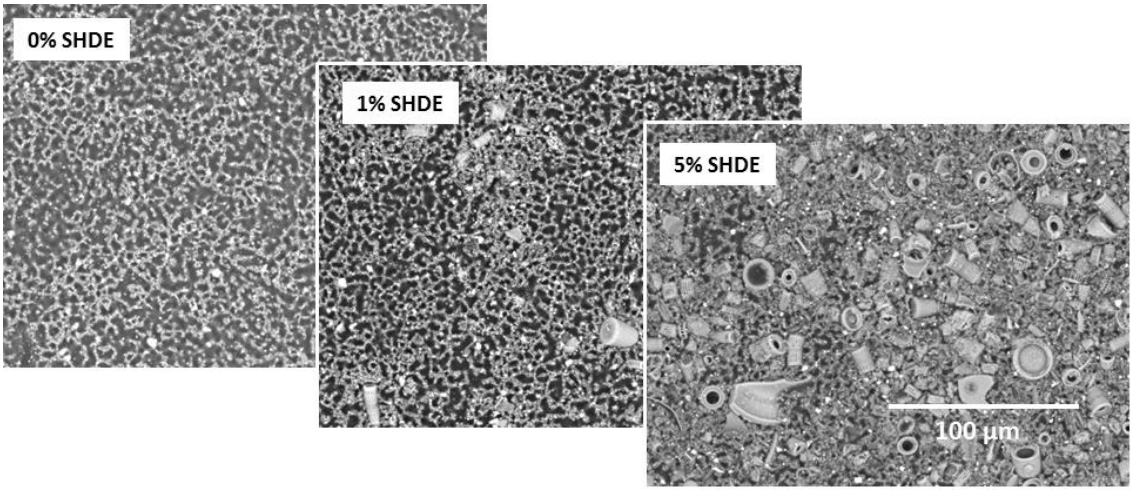

Fig. 31. Backscattered electron images of urethane powder coat surfaces as a function of SHDE addition to the original powder material. Note the similarly irregular surface features and voids in all specimens.

Within the capability of B117 salt fog exposures to distinguish, very little difference in corrosion performance was observed for increasing curing times of panels from 15 to 20 or 25 minutes after panels reached curing temperature, nor for increasing the curing temperature across the range of 195 to 215°C (383 to 419°F). However, a few details of the curing procedure stand out as potentially significant. For a wide range of powder coat materials, including those used for this experiment, curing for ~ 15 minutes at 204°C (400°F) is recommended by the manufacturer. In the experiments performed at ORNL, panel temperature in a curing furnace was monitored in several ways. One method included using high-temperature tape to hold a thermocouple against a bare steel panel of a size and shape identical to those being coated. In another technique, the high temperature tape and thermocouple junction was in place before powder coating, so that the coating covered this joint. Finally, a thermocouple was taped directly to a steel support fixture centrally located within the cluster of panels being cured within the box furnace. The results suggest that even for very small components—panels as small as 2 × 2 × 0.125 in.—placed into a furnace already at the desired curing temperature, there is a 30–40 min rise time for the surface of the panel to approach the desired curing temperature, after which there should be 10–15 min at curing temperature to complete curing. This result stands in obvious contrast to industrial powder coat procedures observed by ORNL staff members at several locations (including USMC depot practice) in which only a total of ~10–15 min of furnace time was afforded powder coated components on a constant speed conveyor. While it is recognized that coated panels perhaps heat somewhat faster than a bare counterpart because of the emissivity difference between bare steel and the coating surface, the coating itself also provides some amount of thermal insulation for the substrate steel, thus contributing to a thermal "balance" associated with the coating. Ultimately, the point is not to denigrate any particular curing practice (all of which have no doubt been "calibrated" to performance expectations) but to highlight the observation that powder coat performance appears to have room for development with incorporation of (thermally insulating) silica powders and adjusting curing temperatures appropriately.

In any case, the fact that as little as 1% silica—whether very uniform chemical grade silica or somewhat variable diatomaceous earth—is capable of dramatically altering urethane (and epoxy) powder coat wettability, and corrosion performance is worthy of extended study, including the refinement of curing time-at-temperature parameters.

2.5 LIQUID SYSTEMS WITH SH SILICA ADDITIONS

The initial attempts at ORNL to design additions of silica powders to standard varieties of CARC provided by commercial suppliers were potentially hampered by inadequate knowledge of bulk coating chemistry and solvent interactions. Further, until near the end of the project, ORNL was able to make only post-production additions to already formulated coatings; that is, adding SH powder additives to existing coatings without the ability to optimize suitable solvents and addition/mixing sequences to encourage improved incorporation (solubility, wetting, distribution, etc.) of the powder additions. The inclusion of NCP Coatings as an informal project collaborator late in the final fiscal year helped generate some success because they were able to help create new coatings via incorporation of ORNL-treated silica within existing paint formulations and, critically, manipulate the total solids content and solvent selections to aid powder incorporation. This section summarizes initial efforts at ORNL as well as several systems exhibiting some success through the collaboration.

2.5.1 Initial Attempts to Modify One-Component CARC Systems

ORNL attempts to modify one-component CARC systems originally targeted SH powder additions on the order of 10 wt % based on laboratory experiments suggesting this level of addition tended to maximize contact angle (~ 170°) and minimize roll-off angle (< 5°) for water droplets. Typically, CARC system experiments—meaning evaluation of the topcoat portion of the overall paint system for ground vehicles—included additions of different types of silica (diatomaceous earth or reagent grade chemical silica) at different average particle sizes and particle size mixes, with and without silane treatments. The usual test matrix of panel preparation for screening test exposures in B117 salt fog included preparation of two sets of panels. In one set, the coating was applied to grit-blasted steel primed with a standard (inexpensive, readily available) commercial product. The set included (1) topcoating the commercial primer with the unmodified CARC coating, (2) topcoating the commercial primer with CARC coating modified with additional thinner to examine the role of extra solvent as a stand-alone consideration, and (3) topcoating the commercial primer with CARC material modified with additional thinner and the SHS addition. In a duplicate set of panels, the same series of coatings was applied over grit-blasted steel primed with military grade epoxy primer (as specified for all CARC systems).

However, it quickly became obvious *none* of the CARC systems—even the standard specified topcoat system with no solvent or silica additions—were capable of providing corrosion protection of the substrate as evaluated in B117 salt fog without the military grade primer beneath the topcoat. Brief salt fog exposures demonstrated, and SEM examinations of selected coating cross sections confirmed, that fully loaded CARC topcoats (especially solvent-borne versions) were extensively cracked and/or quite porous after curing. Furthermore, additions of SH components simply exacerbated the cracking and porosity. The cracks/pores commonly penetrated the entire coating thickness, so salt fog exposures were quite corrosive to the substrate when less-than-superior primer materials were used in panel preparation. Unfortunately, the very effective corrosion protection afforded by the military grade primer also rendered it impossible to distinguish performance between the various experimental topcoats in a timely fashion.

A representative example result from salt fog exposures of experimental coating systems is shown in Fig. 32. In this case, 53039D type III CARC was examined (1) as-received, meaning no modifications to the standard product; (2) modified with an addition of thinner but no SHS powder: and (3) modified with thinner and ~ 10% SHS (silane-treated) as diatomaceous earth. The results routinely indicated that even the unmodified standard CARC material (front left in Fig. 32) is so porous and cracked that it is not capable of providing more than trivial corrosion protection for a steel panel that has only a modestly performing primer material. Additions of thinner and/or thinner with SH powder to the topcoat perhaps aggravated the cracking and porosity in the topcoat, but the B117 result is not changed appreciably. However, with the military grade primer beneath the topcoat, performance of the different topcoats is essentially indistinguishable. In the case of the fully-modified topcoat applied over military grade primer (at back right in Fig. 32), the topcoat is mud-cracked so that the oxide streams—the corrosion product entrained in the condensate that trickles down the front of the panel—emanating from the poorly coated hole at the top of the panel (where there is exposed substrate) filled the cracks in the topcoat. However, the bulk of the panel substrate is protected fully from corrosion by the military grade primer. This condition developed quickly during the B117 exposure and was essentially unchanged from this appearance following 4,000 hours of exposure, when the evaluation was terminated.

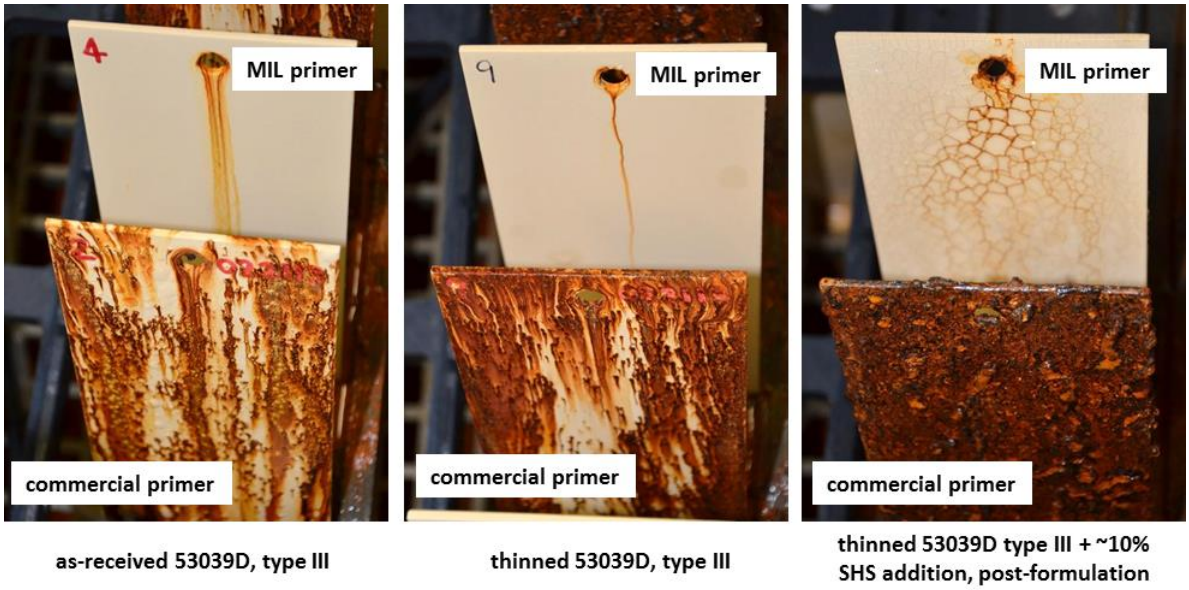

Fig. 32. Steel panels with variable primer and topcoat combinations following 28 d in standard B117 salt fog conditions.

This result, and many others like it, was significant to the overall screening test strategy applied in this investigation. That is, topcoat modifications that would minimize or eliminate cracks and pores in the coating (thus inhibiting penetration of chemical agents and adding a component of corrosion protection via shedding of water) were evaluated primarily via application to bare or intentionally poorly primed steel to accelerate comparison of the relative protective (structural) coating properties for experimental systems. Improvements in coating structure and performance then could be distinguished more readily for further development.

2.5.2 Siloxane Coatings

In discussions with collaborators at NCP Coatings, the potential for improved compatibility of siloxane coating chemistry (already rich in Si-O components) with manipulations via silica powder additions appeared promising. SH powders treated with silane at ORNL were added in the early stages of formulation to siloxanes of interest to NCP. In the most comprehensive experiment, a series of siloxane coatings (using an experimental 383 green CARC system) was formulated as follows. The baseline siloxane material containing color pigments only (all other solids removed) was prepared with a residual pigment volume concentration (PVC) of 11.6. A similar batch of coating material was prepared (PVC = 11.6) to which about 20 wt % of SHS was added, creating an estimated PVC value of 33.0. Blends of these two materials—with and without the SHS addition, but other solids removed—were used to create intermediate loading levels of SHS in the resulting siloxane. In addition to this simplified siloxane chemistry, versions of each coating (with and without SHS additions) also were examined after incorporation of a “flex” additive at two concentrations to examine potential effects on film qualities and hydrophobicity. Table 5 summarizes the different siloxane coating formulations examined.

Table 5. Summary of siloxane coating formulations

Lab code for coating	Description	PVC[a]	Water droplet contact angle
9-66-C	Color pigments only	11.6	92–120°
9-66-H	"C" with flex additive	11.2	
9-66-M	"C" with 2× flex additive	10.9	
9-66-G	25% "D" + 75% "C"	17.0	116–122°
9-66-L	"G" with flex additive	16.4	
9-66-P	"G" with 2× flex additive	16.0	
9-66-F	50% "D" + 50% "C"	22.3	142–147°
9-66-K	"F" with flex additive	21.7	
9-66-O	"F" with 2× flex additive	21.2	
9-66-D	SHS[b] added to "C"	33.0	151–157°
9-66-E	75% "D" + 25% "C"	27.6	
9-66-J	"E" with flex additive	27.0	
9-66-N	"E" with 2× flex additive	26.3	

Note: Organized in this way, there were essentially four "groups" of coatings at approximately constant PVC values, as follows:

- no SHS addition PVC = 10.9–11.6
- low SHS addition PVC = 16.0–17.0
- intermediate SHS addition PVC = 21.2–22.3
- high SHS addition PVC = 26.3–33.0

Performance comparisons (B117 salt fog) and interpretations of results (structure, composition) are described as consistent with these groupings.

[a]PVC = pigment concentration volume; this is an estimate for all except the baseline materials C, H, and M.

[b]SHS = superhydrophobic silica.

Panels representing each formulation in Table 5, with coatings applied at NCP to bare steel (no primer or other surface preparation), were exposed to B117 salt fog conditions at ORNL. Figures 33 and 34 show the appearance of these panels as a function of exposure time in B117 salt fog. In Fig. 33, after 2 d, panels with coatings containing high and intermediate additions of SHS revealed significant rust bloom. After 8 d, substrate corrosion advanced on the panels with high silica additions, but panels with the lowest levels of silica addition remained more resistant to substrate corrosion. In Fig. 34, after 16 d of exposure, the coatings with intermediate levels of silica addition revealed clear signs of failure (advancement of rust bloom and even a few blisters), while the coatings with the lowest levels of silica addition continued to bead condensate and substantially resist rust bloom. As exposure time was extended in the B117 chamber, the more readily corrosion protection performance was distinguished among these coatings, with best performance after 30 d of exposure very clearly associated with coatings bearing either no SHS or low SHS additions.

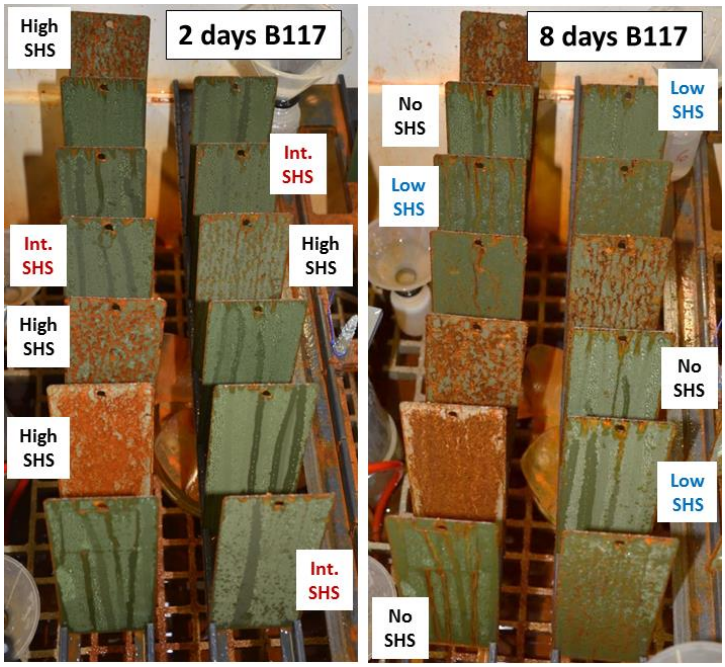

Fig. 33. Siloxane panels as exposed in B117 salt fog chamber after 2 and 8 d.

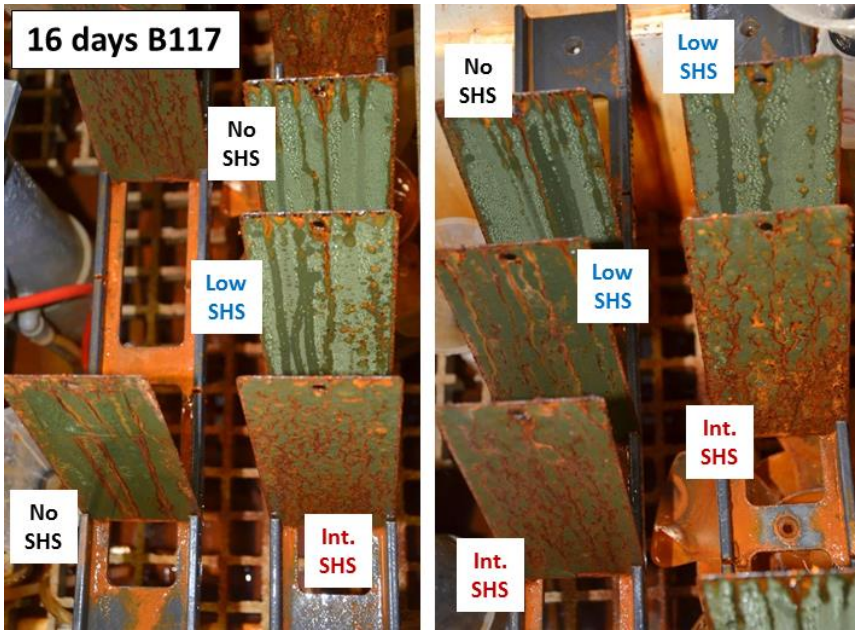

Fig. 34. Siloxane panels as exposed in B117 salt fog chamber after 16 d. The most heavily rusted panels shown in the previous figure have been removed from the chamber.

Examination of the surface of these coatings in the scanning electron microscope indicated that cracking tendency of the coating (and thus corrosion protection of the substrate) was a function of the solids loading. Figure 35 shows a series of images of unexposed coating surfaces representing the highest (PVC = 26.3–33.0) and lowest (PVC = 16.0–17.0) SHS additions to the coating. In the coating with the highest

solids loading, a network of large cracks is readily detectable even at only modest magnification. At higher magnification, fine cracks were observed throughout the coating matrix. In contrast, for the coating with the lowest SHS addition, no cracking is evident at all within the coating structure, even at quite high magnification. This is of course consistent with the B117 results on duplicate panels in that the cracked coatings (high and intermediate silica additions) were unable to protect the substrate from corrosion, but the relatively crack-free coatings (no silica addition and the low silica addition) were much more protective.

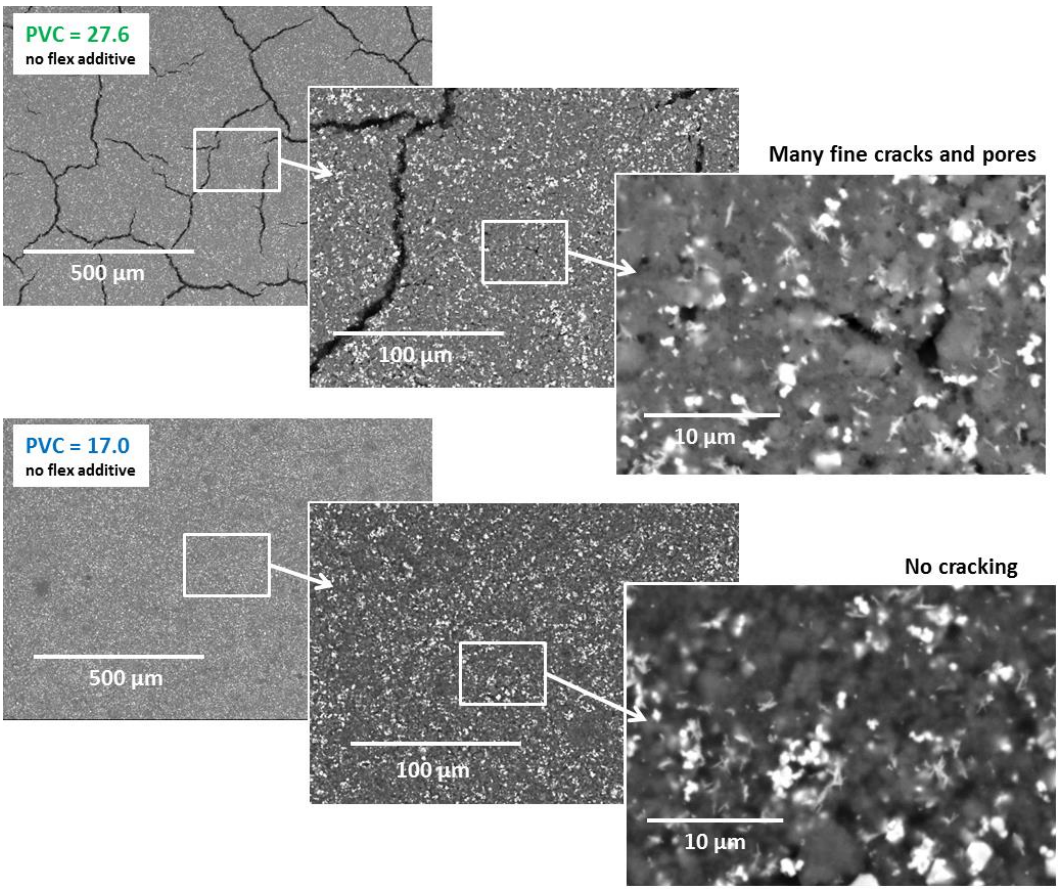

Fig. 35. Backscattered electron images of unexposed surfaces of siloxane coatings relatively high in added silica (top series) and relatively low in added silica (bottom series).

In addition, element maps were prepared from the same specimen surfaces as those examined in Fig. 35, and summary results are shown in Fig. 36. The results suggest that there are no features related to composition gradients or "partitioning" of the solids content that contribute to the cracking tendency previously noted and assigned to structure variation. In all cases among the siloxane coatings, the silicon-base nature of the material dominates the maps and renders discrimination among coatings based on the position of minor SiO_2 additions moot, although there may be a modest difference in the oxide particle distribution when the oxygen maps are compared (slightly more/larger particles in the high silica version). In particular, note that there are no obvious composition gradients in/around the cracks apparent in the high SHS material (which is in contrast to the results for SH additions to powder coats). Maps for all detectable elements were also prepared, but the elements shown in Fig. 36 represent the significant trend.

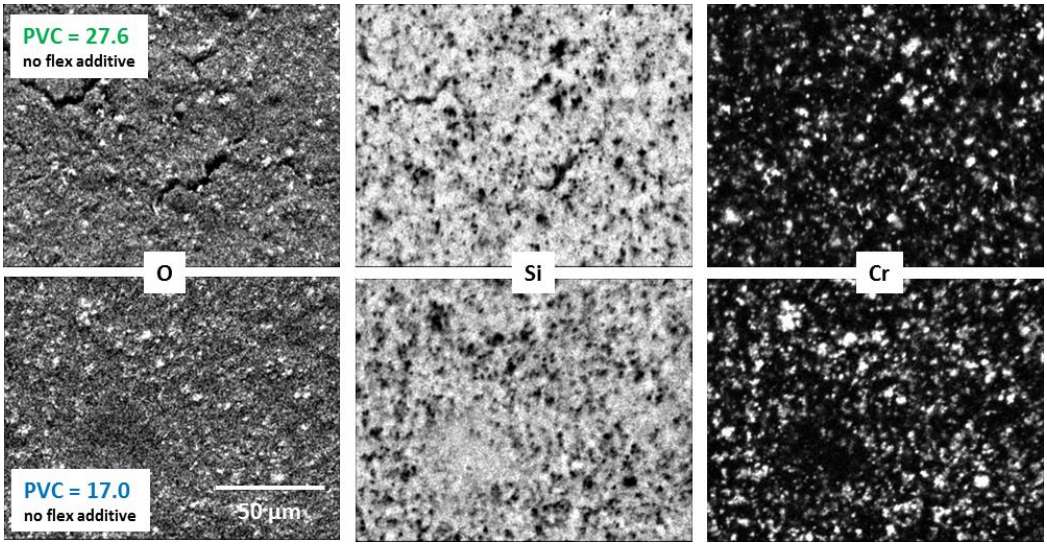

Fig. 36. Scanning electron microscope element maps for oxygen (O), silicon (Si), and chromium (Cr) from the surfaces of siloxane coatings relatively high in added silica (top series) and relatively low in added silica (bottom series).

Although apparently free from cracks and pores, the coating with no SHS addition was not observed to be completely smooth on the surface. Figure 37 shows a series of SEM images (same magnification series as in Fig. 35, but using secondary electrons to highlight surface relief) of a siloxane coating with color pigments only and no SHS addition. Some surface relief is indicated, with depth and area of the surface features not much different from the average water droplet size used to make roll-off measurements. This observation may explain the ~ 90° roll-off angles for all panels (independent of SHS addition), as cracks and dimples no doubt tend to "retain" beads of water. The only roll-off angles observed to be < 90° among the siloxanes evaluated were poorly reproducible values on the order of 30° for the most highly silica-loaded coatings.

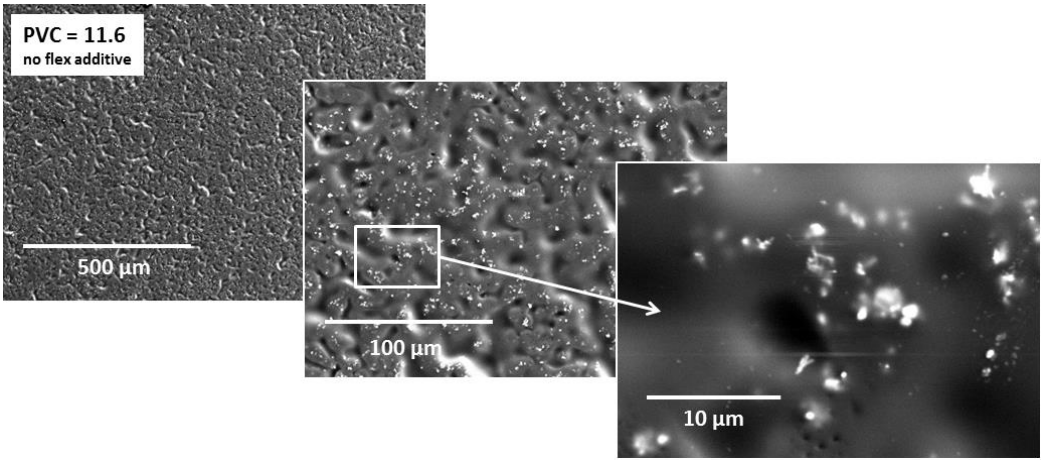

Fig. 37. Secondary electron images on an unexposed surface of a siloxane coating with no SHS addition and solids other than color pigments removed.

In addition to the trends already discussed, these results highlight the emergence of an important decision metric developed during this portion of the coating development effort; that is, striving for high or "best" water droplet contact angle is not necessarily the best goal for making coatings that are both structurally sound and capable of superhydrophobic behavior. The graph in Fig. 38 compares relative PVC value with water droplet contact angle and coating structure, and it suggests that contact angles on the order of 120° may be adequate for the combination of crack-free structure and water-shedding capability in the siloxane system. At a minimum, the data suggest that up to ~ 5 wt % SHS can be incorporated into this siloxane system with no negative structural implications, and this is perhaps a good starting point for continued coating development in this area. Further testing is required to establish the potential for improvement of moisture/corrosion resistance of siloxane coating systems via SHS additions.

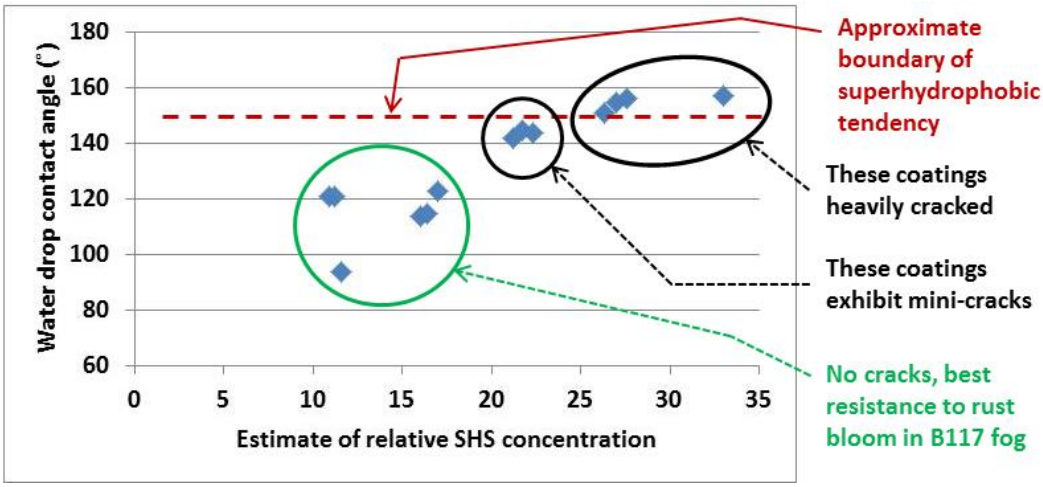

Fig. 38. Summary of relationship among SHS additions, coating structure, and water droplet contact angle for experimental siloxane coatings.

2.5.3 One-Component Solvent-Borne CARC

Additional collaborative efforts with NCP examined the utility of SHS additions to coatings in the "pre-formulation" stage (before the coating became an otherwise finished product). In one relatively successful case, about 8 wt % SHS (20% silane treated at ORNL) was added to a silica-flattened solvent-borne CARC material under evaluation at NCP. The SHS addition was accomplished early in the formulation process using low-shear mixing in an attempt to break up and disperse the SHS particles.

This experimental CARC material containing ~ 8% SHS was applied to bare steel panels (no primer or other surface preparation) at NCP using standard techniques resulting in an average dry film thickness of about 3.5 mils. For comparison, identical panels at average dry film thickness of 2.5 mils were prepared with the same coating without the SHS addition. Two panels representing each coating were exposed together in B117 salt fog conditions to compare relative corrosion protection of the substrate (resulting from structural features or wettability features or both). Figure 39 shows a representative result. Except for rust streams coming from the poorly coated edges of the panels, both the unmodified coating and the coating with an 8% SHS addition performed similarly in salt fog, with both being generally resistant to rust bloom and blisters. This is a positive result in that initial attempts to modify CARC coatings with SHS (added to a fully formulated coating system) were unsuccessful because the resulting coatings were

structurally flawed/cracked and thus unprotective in salt fog. The water droplet contact angles measured on the unmodified CARC averaged 122°—perhaps 20° higher than that observed on most other standard CARC coatings assessed in this program. However, the addition of 8% SHS positively influenced the contact angle, generating an increase to an average of 147° with no apparent structural distress to the coating. This experiment was terminated after about 30 d of exposure in B117 salt fog because all four panels essentially were completely covered with oxide stains generated from the top edge of the panel.

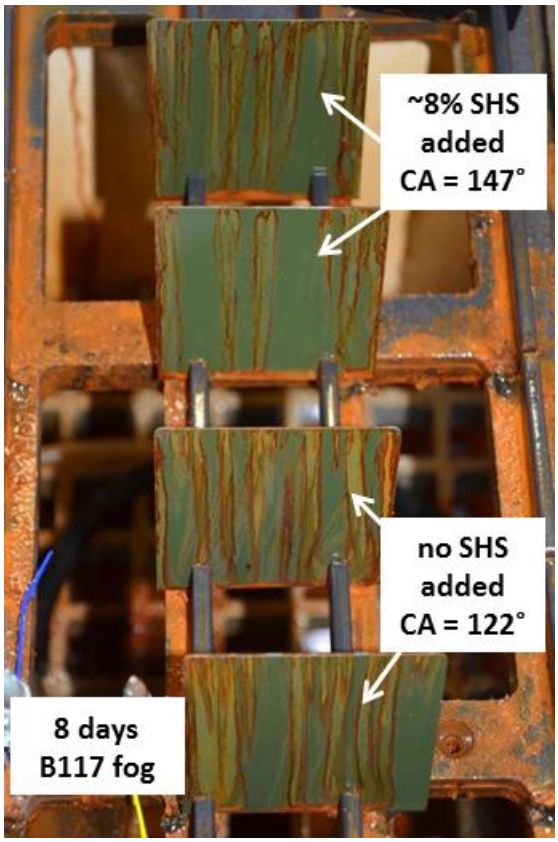

Fig. 39. Panels with 1K solvent-borne CARC and identical panels with 1K solvent-borne CARC modified with 8% SHS following 8 d of exposure in B117 salt fog.

In Fig. 40, the structure of each coating (examined on a piece cut from each panel before salt fog exposure) is compared. Both coatings exhibit modest surface relief, and both are similarly free of cracks and large pores, thus confirming the excellent protective qualities observed in the B117 exposure. That both films are free of cracks/pores on the surface indicates that the slightly greater dry film thicknesses of the modified version is likely not responsible for the perhaps better-than-expected performance of the 8% SHS coating. This positive result reinforces the utility of making SHS additions earlier in the formulation process rather than later. The project was terminated before additional experimentation and follow-up with this concept.

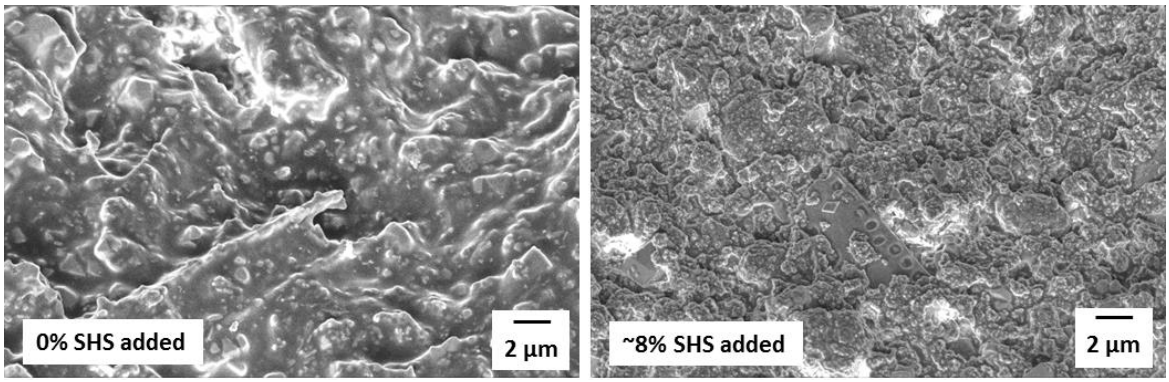

Fig. 40. Secondary electron images of the 1K solvent-borne CARC with and without modification to include 8% SHS.

2.5.4 Two-Component Urethane CARC

In another collaboration with NCP during the final month of the project, a two-component water-borne urethane (64159B type II) was modified with either 4% or 8% SHS additions to the otherwise fully formulated CARC system. The results are represented by the photograph in Fig. 41, which compares the performance of bare steel panels coated with urethane containing 0, 4, and 8% SHS additions (all 2–3 mils dry film thickness) after 10 d in standard salt fog exposure. After only 10 d in the B117 chamber, the unmodified coating system revealed extensive blistering of the coating (urethanes are known to be somewhat permeable to water and water vapor). Less blistering was observed for the coating system modified with 4% SHS, but clusters of blisters oriented in roughly vertical columns were observed in isolated locations. However, the coating modified with 8% SHS was found completely resistant to blistering and rust bloom (some stains resulted from uncoated edges on the panels) after 10 d in B117. This was the initial program demonstration that SHS could be added to a fully formulated CARC system with the advantage of superior corrosion protection qualities compared with the unmodified coating system. Also note that SH powders were added successfully to a water-borne formulation without apparent clumping or other incompatibilities associated with SHS in a water-rich matrix.

These coating surfaces were examined in SEM using small pieces cut from each panel before salt fog exposure. Representative information is depicted in Fig. 42, which compares the surface structure and surface silicon map for the 0% and 8% SHS versions of this experimental coating. Of significance is that although the 8% SHS loaded coating exhibits some cracking in the surface structure—confirmed by cross-sectional metallography and element maps showing carbon from the mounting epoxy irregularly penetrated to the substrate—the high surface concentration of silica in the modified version apparently compensates for the cracks and provides improved resistance to water penetration and blistering. Interestingly, the relatively high silica content is not simply concentrated in the coating surface but is roughly uniform throughout the coating thickness (see Fig. 43).

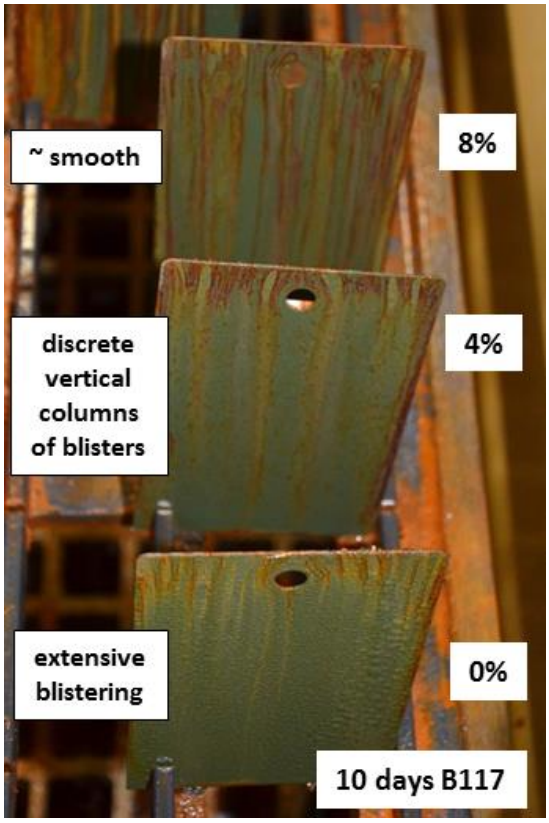

Fig. 41. Salt fog exposure comparison of urethane topcoats with 0, 4, and 8% SHS additions.

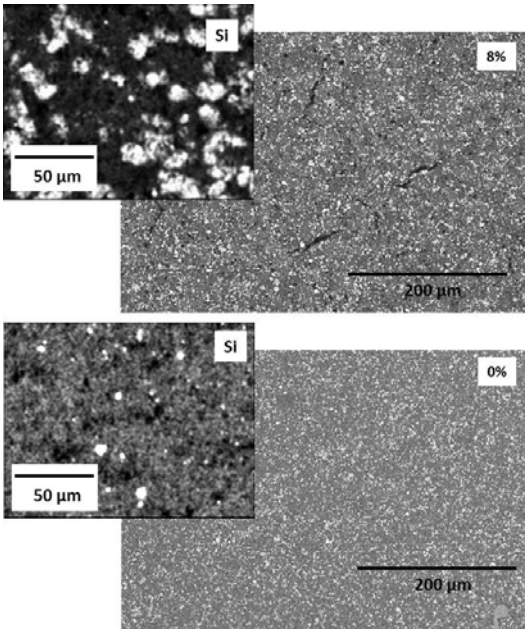

Fig. 42. Surface structure and silicon maps for the 0% and 8% SHS versions of the experimental urethane topcoat.

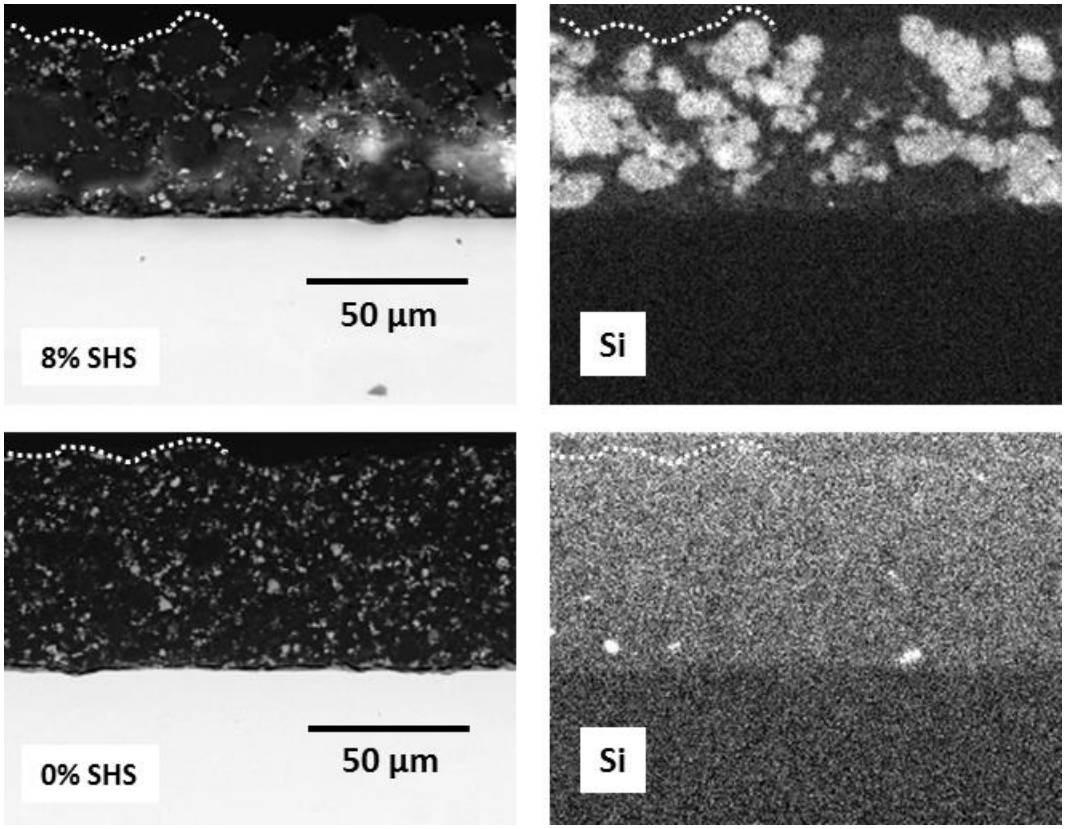

Fig. 43. Metallographic cross sections (left column) and element maps for silicon in the corresponding region (right column) for the 0% and 8% SHS versions of the experimental urethane coating. The surface of the coating is partially distinguished from the mounting epoxy by a dotted white line in each photograph. The steel substrate is distinct at the bottom half of each photograph.

In a related experiment, boundaries of the potential magnitude of the SHS addition to a two-component urethane system were explored. In this attempt, an experimental two-component urethane being developed at NCP was manipulated to remove all siliceous materials before adding back 15 and 30% SHS. Mixing was accomplished under low shear conditions to uniformly distribute the silica addition (and avoid clumps). Coating applications were made to bare steel panels at an average dry film thickness of just over 2 mils. Compared with the 8% SHS addition discussed above, both 15 and 30% SHS additions, even after all other siliceous material was removed, apparently exceed a "critical" volume or total surface area related to silica. Figure 44 summarizes the results of this experiment and shows that both coatings were cracked/faulted heavily and performed very poorly in salt fog. Before exposure in salt fog, the as-prepared coating surfaces exhibited superhydrophobic contact angles with water droplets in excess of 155° in all cases, yet clearly these very high contact angles do not correspond to a protective coating. Once again, this result points to the concept that maximum silica content and maximum contact angle are not necessarily the metrics of merit.

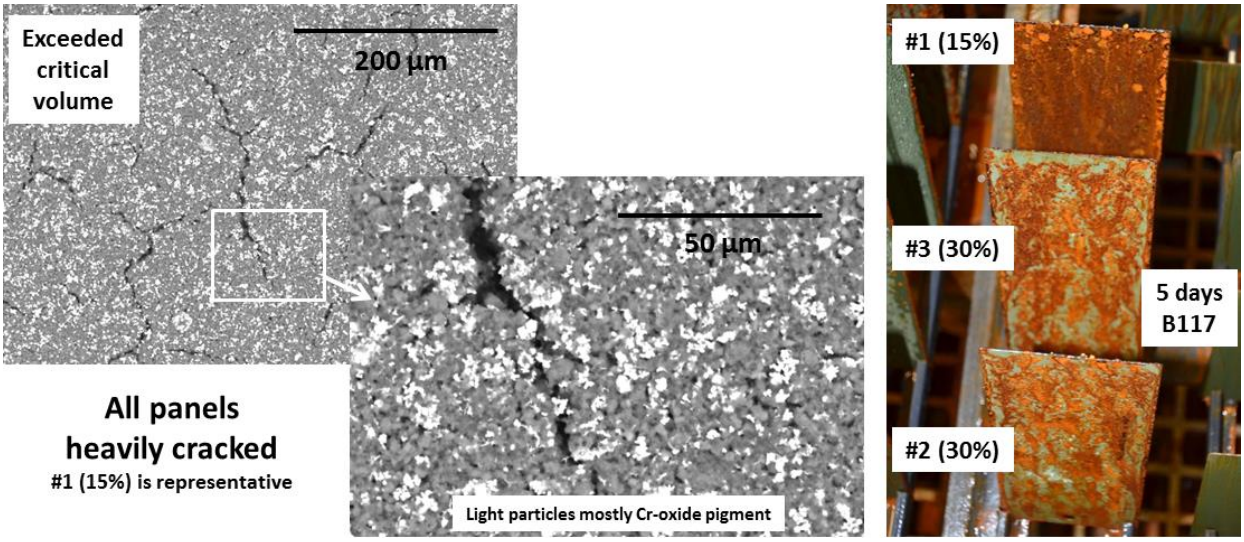

Fig. 44. Representative surface structure of an experimental 2K urethane topcoat with 15% SHS addition (all other siliceous material removed). At right, panels shown after five d in standard salt fog exposure.

2.5.5 NCP Model Coatings with Siliceous Materials Removed

In another collaborative effort with NCP in which the composition of the experimental coatings could be manipulated at the formulation stage, a developmental two-component urethane CARC (NCP N1433A) was modified by removal of all of the silica fillers normally incorporated into the coating. These fillers were then replaced with diatomaceous earth (Diafil 525) or nanosilica from ORNL, with the additional variable of having the silica additions receive (or not receive) the silane treatment to become superhydrophobic. Further, some coatings were prepared with mixtures of treated Diafil and treated nanosilica additions. Finally, the silica additions were incorporated into the coating via two low shear mixing and high shear mixing to compare relative results in dispersion of the silica. The resulting matrix of coatings for examination, all prepared and applied to bare steel panels at NCP, is shown in Table 6. In this case, the PVC for the base materials with the siliceous fillers removed was about 15%; after the silica additions, PVC was about 41%.

Similarly, Table 7 presents a related series of model coating compositions prepared using NCP N8066A/B/water (two component water borne urethane CARC, mixed 2:1:1) with siliceous fillers removed and various percentages of silane-treated diatomaceous earth or silane-treated nanosilica added back to the coating. In this case, the as-prepared base material had a PVC value of about 20.5, and the PVC varied with silica additions as indicated in Table 7. This set of coatings was also mixed and applied to bare steel panels at NCP and delivered to ORNL for testing and evaluation.

Table 6. Matrix of model coating compositions based on two-component solvent borne urethane CARC (NCP N1433A)

Sample ID	% Untreated Diafil 525	% Treated Diafil 525	% Untreated nanosilica	% Treated nanosilica	
72-B	100				low shear mixing
72-C		100			
72-D			100		
72-E				100	
72-F		30		70	
72-G		50		50	
72-H		70		30	
72-I	100				high shear bead mill
72-J		100			
72-K			100		
72-L				100	
72-M		30		70	
72-N		50		50	
72-O		70		30	

Table 7. Matrix of model coating compositions based on two-component water borne urethane CARC (NCP N8066A/B)

Sample ID	Wt % Treated Diafil 525	Wt % Treated nanosilica	Approximate PVC
80-A	0		20.5
80-B	2		23.2
80-C	4		25.7
80-D	8		30.5
80-E	12		34.6
80-F		2	23.2
80-G		4	25.7
80-H		8	30.2
80-I		12	34.2

Panels of each coating composition indicated in Tables 6 and 7 were exposed to B117 accelerated weathering conditions. Figure 45 shows the arrangement of the as-prepared panels in the salt fog chamber before testing. The different compositions result in a range of colors, with coatings loaded with Diafil 525 tending toward deeper green and coatings loaded with nanosilica tending toward pale green. In addition, all of the panel edges were coated with a thin layer of black epoxy to minimize edge effects (corrosion).

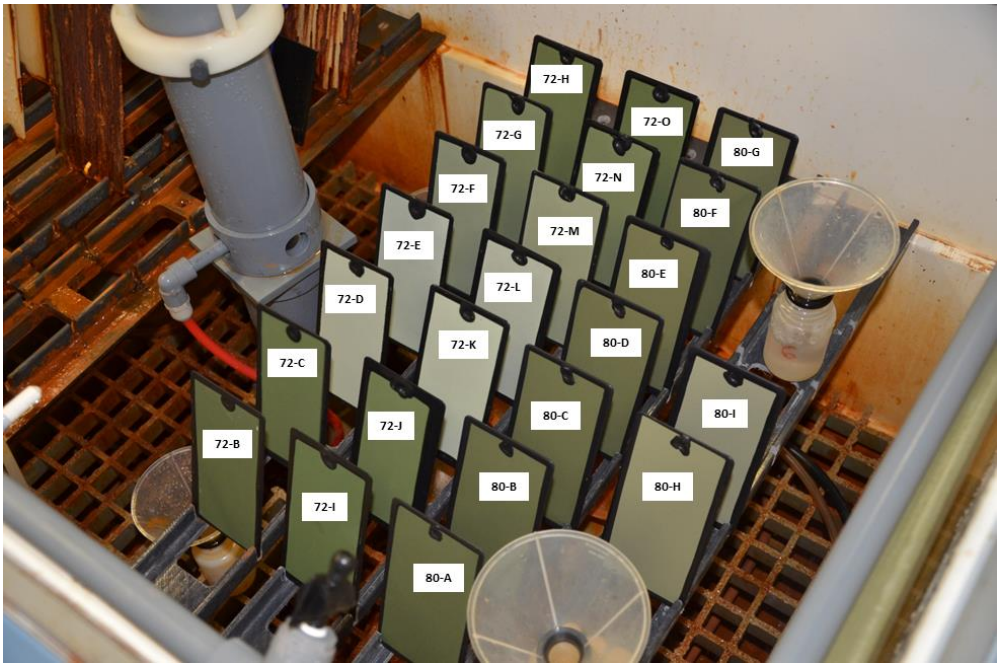

Fig. 45. Arrangement of NCP model coatings in the B117 salt fog chamber before exposure.

Figure 46 shows the appearance of the test panels following 7 d in the salt fog chamber; clearly, only a few coatings resisted rust bloom and blistering for more than a few days. The relatively best performers included 72-B and 72-I, both of which contain 100% untreated DE, and 72-E and 72-L, both of which contain 100% treated nanosilica. These results suggest that the mixing variable (low shear vs. high shear) was not significant in this comparison and that only the treated nanosilica was effective for repelling condensate. It was unexpected that the water-borne coatings (80-x series) would perform relatively poorly compared with the solvent-borne materials, but the two formulations (72-x and 80-x) are not equivalent in PVC and in other preparation and application factors. Following 2 weeks of exposure to condensing salt fog, all of the experimental coatings had completely failed because of heavy rust and/or blistering except for 72-B, E, and L.

Limited immersion testing (48 hours) in DI water revealed a similar pattern. That is, all panels experienced significant rust bloom at numerous discreet locations across the panel surface except for 72-E, F, and G (largest fractions of treated nanosilica additions in low shear mixing) and panels 72-L, M, and N (equivalent panels at high shear mixing), which were free of rust bloom or blisters following 48 hours of immersion. Because immersion testing tends to distinguish more readily the improvements associated with SH surfaces (the moisture arrives at the surface with surface tension), this is perhaps an expected result. Among the 80-x series coatings, only panel A (no silica additions) completely resisted rust bloom and blistering over the period of immersion, which suggests that the structure of the 80-x series coatings was sufficiently flawed by silica additions that wetting and penetration of water could not be prevented. Figure 47 shows representative results from immersion testing.

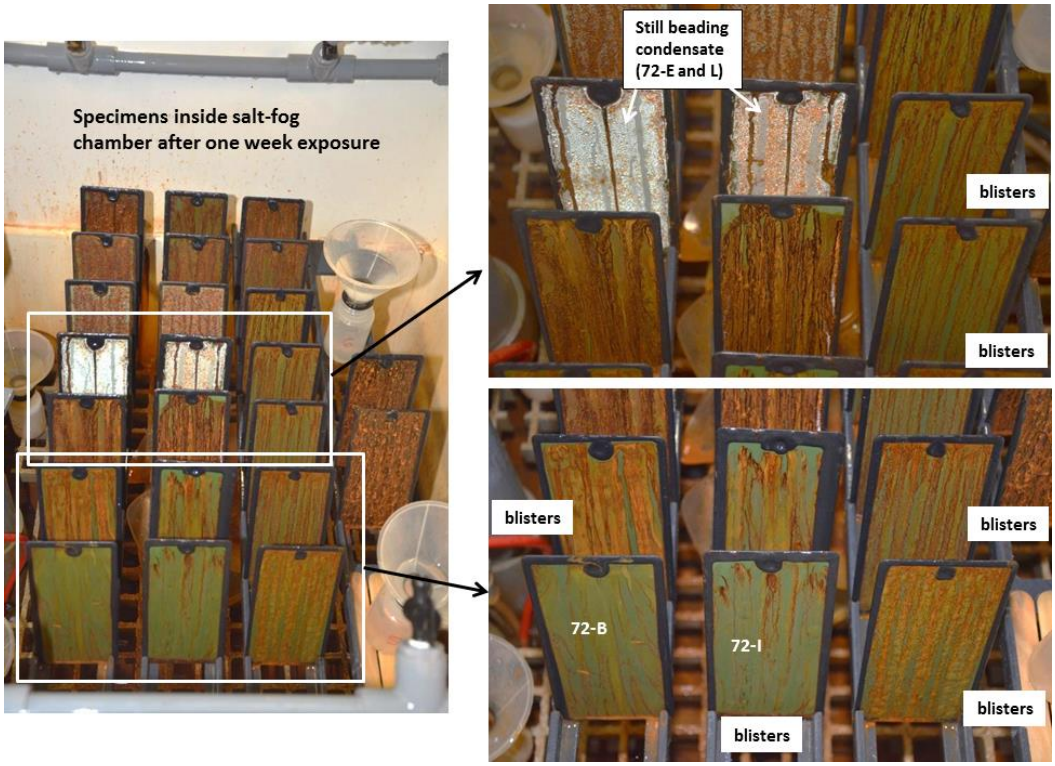

Fig. 46. NCP model coatings exposed y d in the B117 salt fog chamber. Most panels are extensively blistered or heavily rusted.

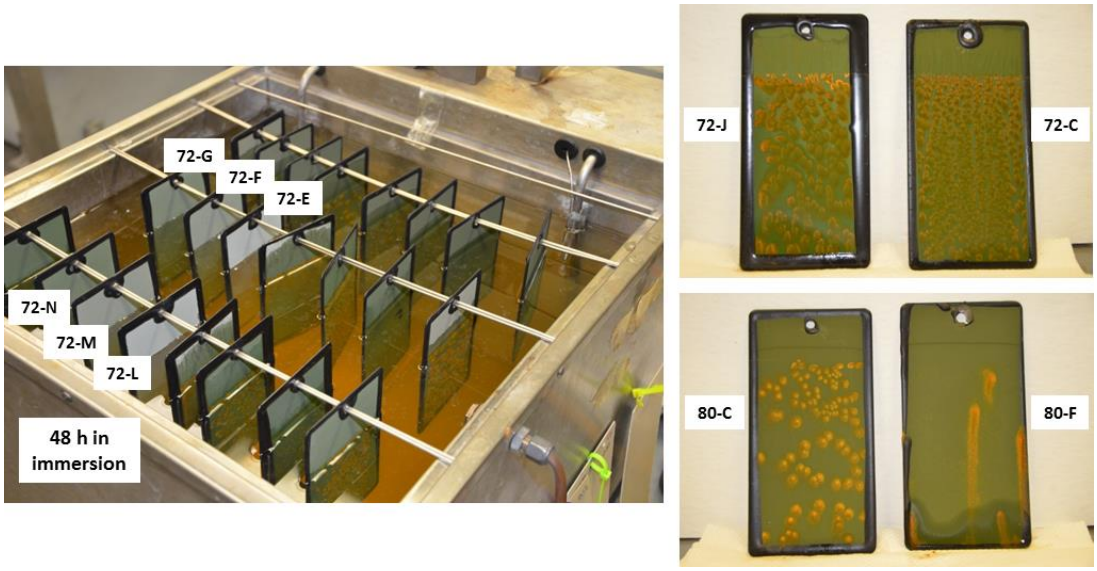

Fig. 47. Immersion testing arrangement and representative rust bloom results.

Given that most panels performed rather poorly in these accelerated exposure tests, few comparisons among the coating formulations may be useful to evaluate overall trends. One such potentially useful comparison is to consider coatings 72-D and E, both identically formulated with 100% nanosilica; the

superior performance of the latter is perhaps due to the silane treatment given to the silica to develop SH properties fully. Figure 48 shows similarly cracked structures for panels -D and -E, with identical distribution of Cr pigment and essentially complete coverage with Si on the exposed surface (including cracked areas). However, the E coating performed substantially better (no blisters or rust bloom, beading condensate) than the D coating, suggesting the efficacy of the silane treatment for the silica. In contrast, Fig. 49 shows that the surface silica distribution on the equivalent Diafil coating (here represented by untreated silica on panel 72-B) may not be sufficiently uniform (silica appears as larger, discrete particles) to facilitate beading of condensate or bridging/lining of cracks in the coating structure. Also note that, at least based on performance in B117, the low shear and high shear mixing variable did not produce discriminating results, and only the treated nanosilica was particularly effective for repelling condensate in all cases.

The surface structure of representative 80-x series coatings is shown in Fig. 50. Clearly, all of the structures exhibit cracks with variable size, including the coating bearing no siliceous material, so the variable performance in the test exposures among these coatings cannot be explained based solely on cracking tendency. (Note: sectioning of the coated panels for analysis involves cutting with a jeweler's saw, which might introduce some cracks or flaw. Similarly, when specimens are mounted in epoxy for cross-sectional metallography, a light vacuum is pulled on the mount to remove air bubbles that tend to adhere at the surfaces, which also might introduce flaws. However, the same processes were used for all sectioned coatings—not all were observed to crack—and maximum care was employed to cut slowly without heat generation and to polish some distance from disturbed surfaces in all cases.) Higher magnification SEM photographs (Fig. 51) readily resolve the Diafil addition to the baseline coating system as discrete particles. However, the matrix for the coating with no siliceous materials and the matrix for the nanosilica addition (individual particles difficult to resolve) appear quite similar, so this structural detail does not distinguish B117 or immersion testing results. Figure 52 shows that the pigment dispersion (represented here by chromium) is remarkably similar for each coating, but the silicon distribution varies widely among these coatings. It would be anticipated that best performance (B117 and/or water immersion) might be generated by the coatings with the most silicon, particularly if it is uniformly distributed on the surface. In this case, however, the coating with the least silicon performed best, suggesting that the silicon present in the model system is not distributed favorably for good hydrophobicity, contributing to physical stress within the matrix (cracking) or chemical stress resulting from hydrophobic particles within a water-borne matrix. Based on previous examinations of structures in similar coatings, it was unexpected that the water-borne materials (80-x series) would perform relatively poorly compared with the solvent-borne materials (72-x series). However, it should be noted that the 80-x series does not have PVC values/mixtures equivalent to those in the 72-x series, and the treatments and mixing fractions may require further optimization to achieve maximum performance within a water-borne system.

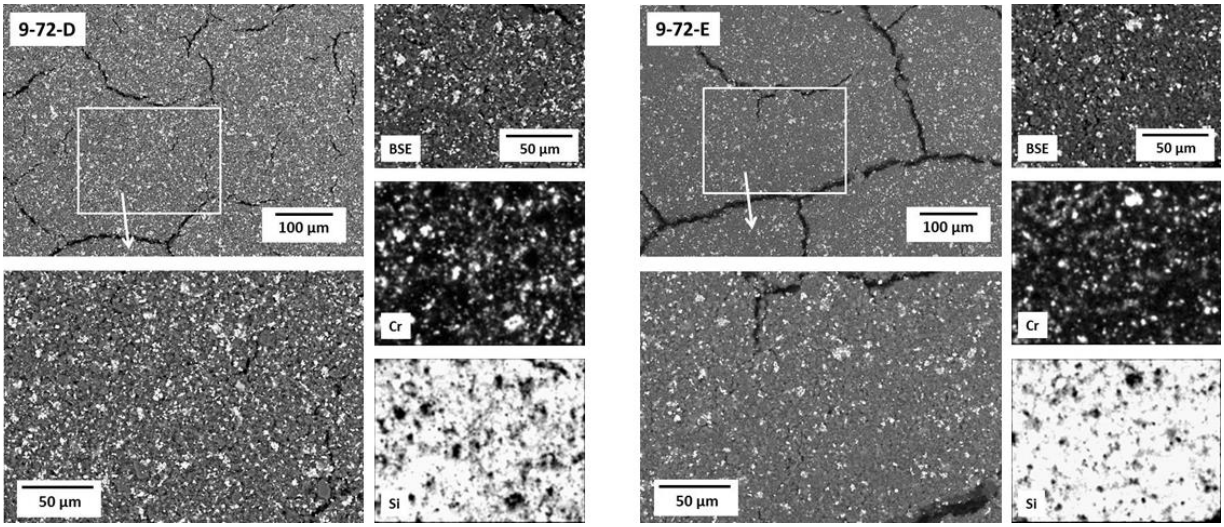

Fig. 48. Scanning electron microscopy (backscattered electrons) of the surface structure and distribution of chromium and silicon for panels 72-D (left) and 72-E (right).

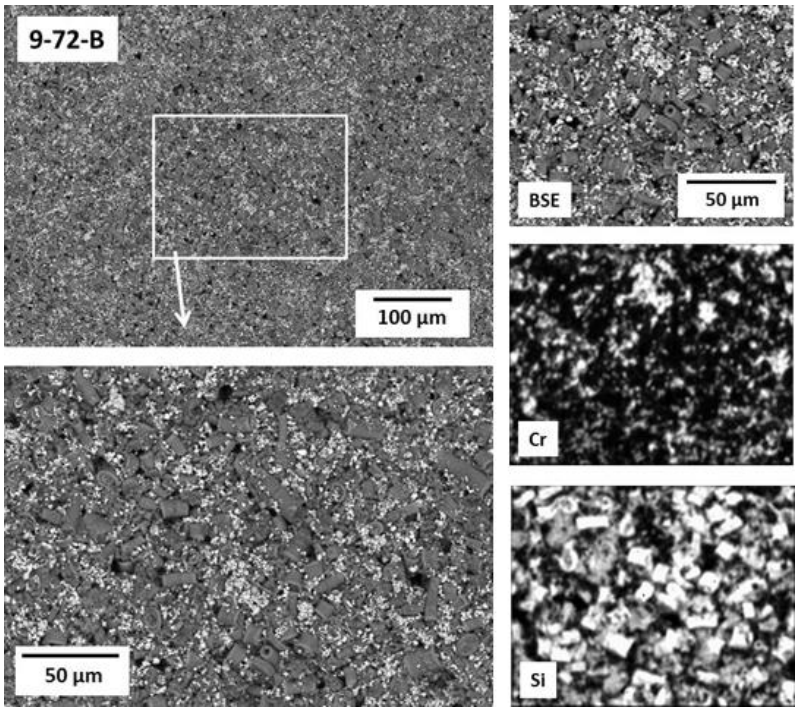

Fig. 49. Scanning electron microscopy (backscattered electrons) of the surface structure and distribution of chromium and silicon for panel 72-B.

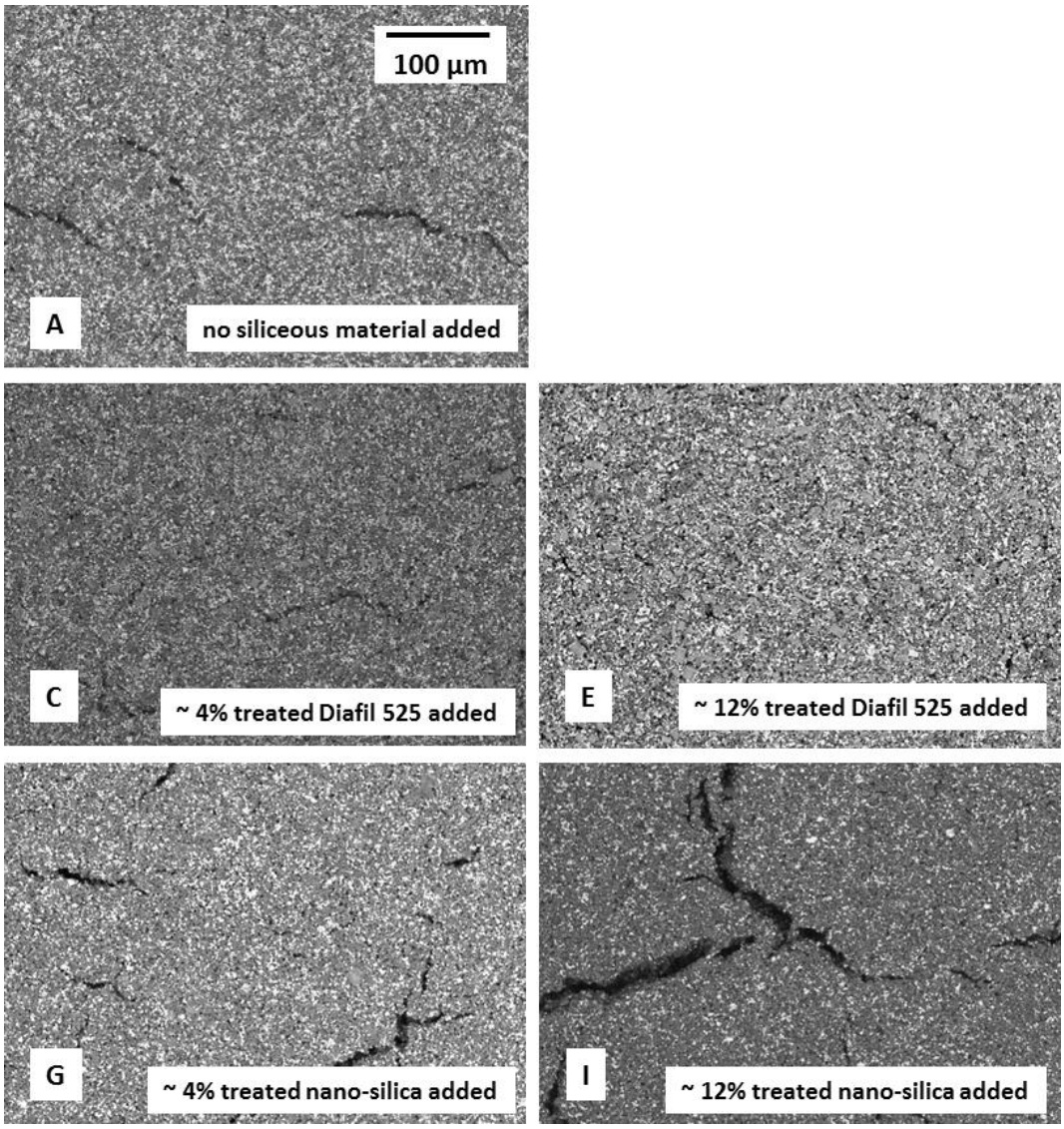

Fig. 50. Surface structures of representative 80-x series (water-borne CARC) coatings. Each photograph is a backscattered electron image at the same magnification.

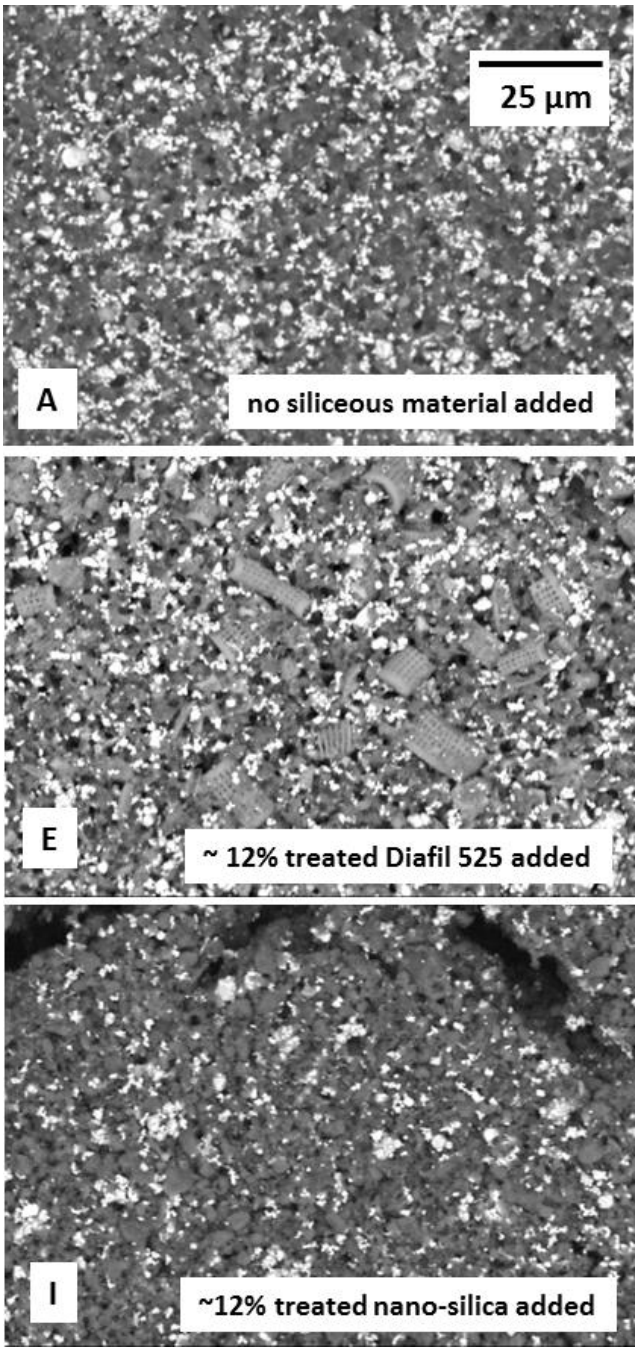

Fig. 51. SEM backscattered electron images comparing structural details within the coating matrix for no siliceous loading and the highest silicon loading for Diafil 525 and nanosilica forms.

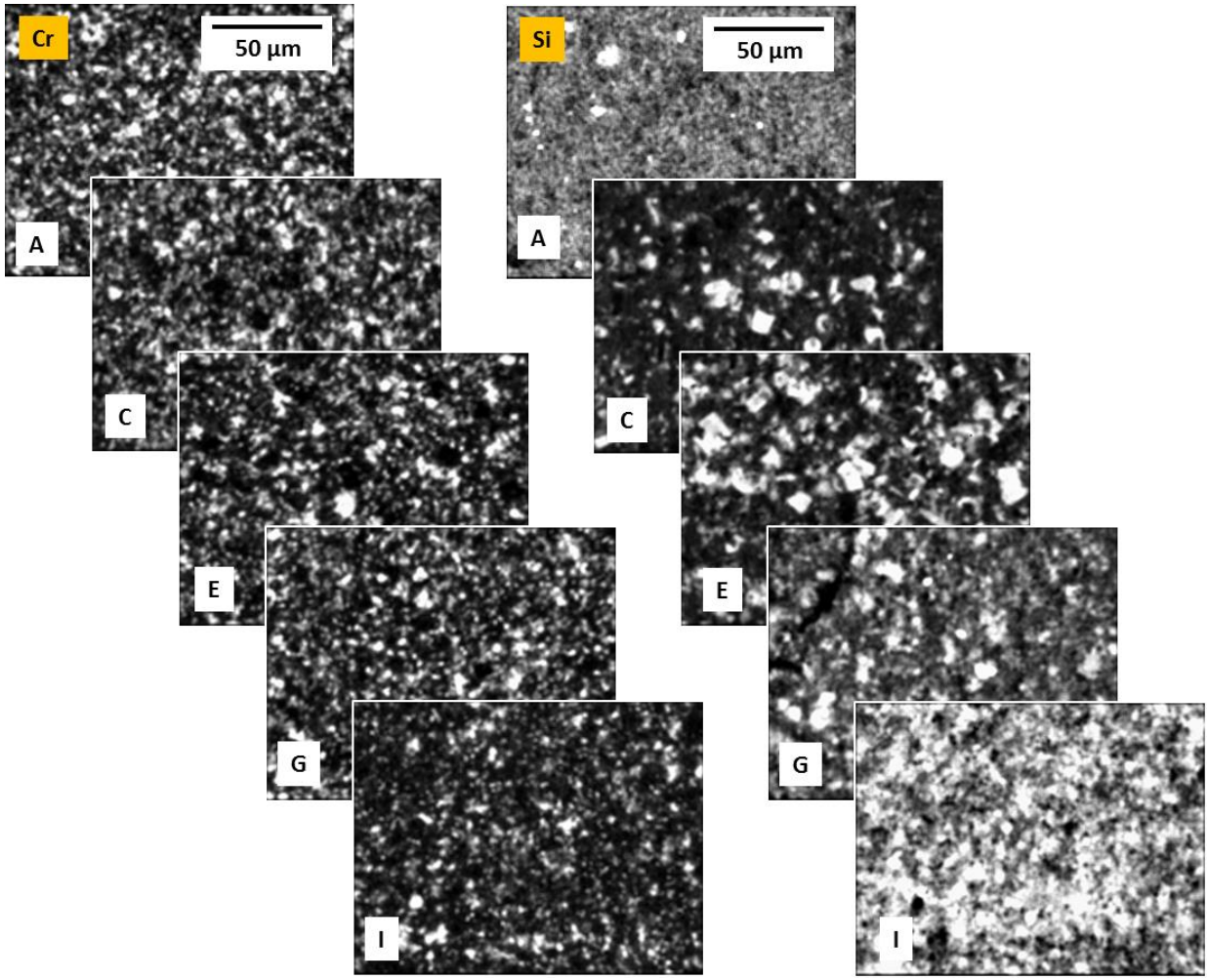

Fig. 52. Comparison of pigment distribution (chromium maps) and silica distribution (silicon maps) for representative coatings in the 80-x series of water-borne CARC. In each case, lighter-colored areas indicate high concentration of the element in question. Letters in the lower left of each photograph refer to the coating formulation given in Table 7.

Further structural analysis of these model coatings yields additional insights into the level of protective qualities of each formulation. Figure 53 shows a series of SEM images of the surface of representative 72-x series coatings as a function of silica addition. The absence of large, contiguous cracking in the coatings containing large fractions of Diafil suggests that stresses in the cured coating can be accommodated at least somewhat by the low packing efficiency (discontinuous surface porosity) of the relatively large/bulky Diafil. As the fraction of Diafil is decreased in favor of nanosilica, the coatings seem to develop more substantial cracking, both on a macro-level and a micro-level, within the structure. Whereas the nanosilica generally has been shown more effective in water repellency and related corrosion protection, this result may suggest that a mixture of treated nanosilica with some treated Diafil may develop a superior coating structure in terms of cracking and/or porosity.

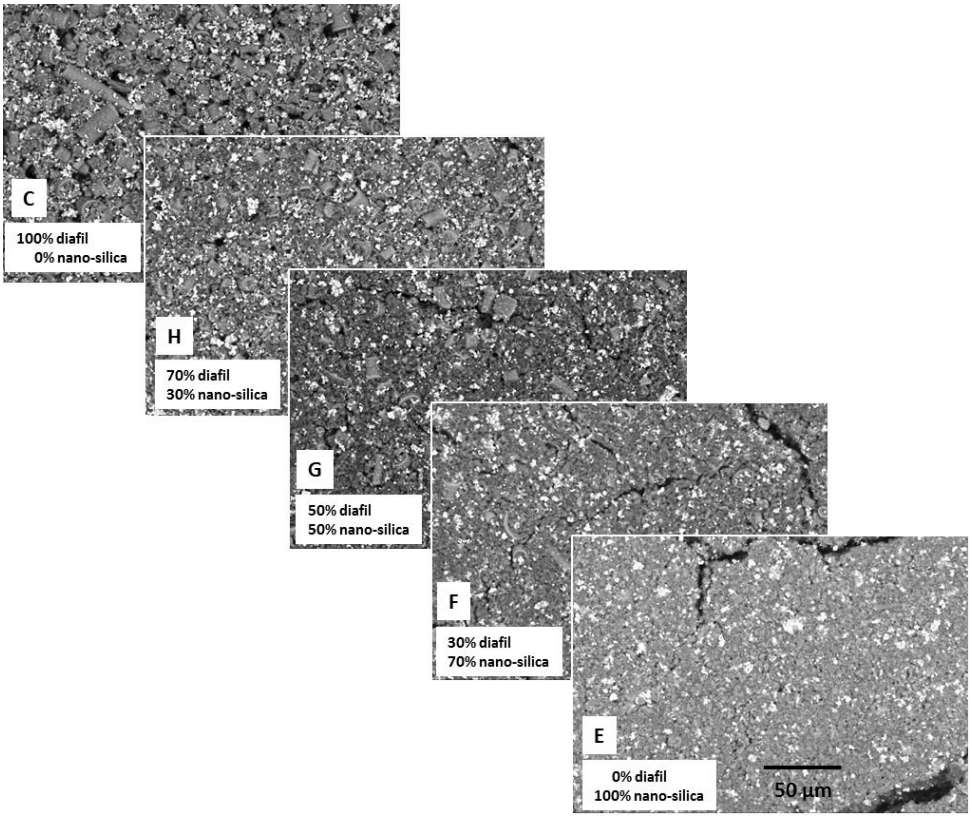

Fig. 53. Series of backscattered electron images of the surface of the NCP 72-x series coatings as a function of relative composition of silica type.

Figure 54 examines the cross section of the 72-B coating (100% untreated Diafil). The large and bulky Diafil constituent makes for a rather irregular density across the entire coating thickness, generating substantial porosity and inefficient "packing" of the silica components. This can be seen in particular in the element maps, which indicate that carbon (from the epoxy potting material used to prepare the metallographic mount) penetrated in potentially interconnected pockets all the way to the substrate steel. The silica and pigment (chromium oxide) generally were distributed evenly through the thickness despite the irregular shapes of silicon, but if the pockets of porosity are too large or numerous, such a coating will not contribute protective qualities and perhaps would retain chemical agents within the pores.

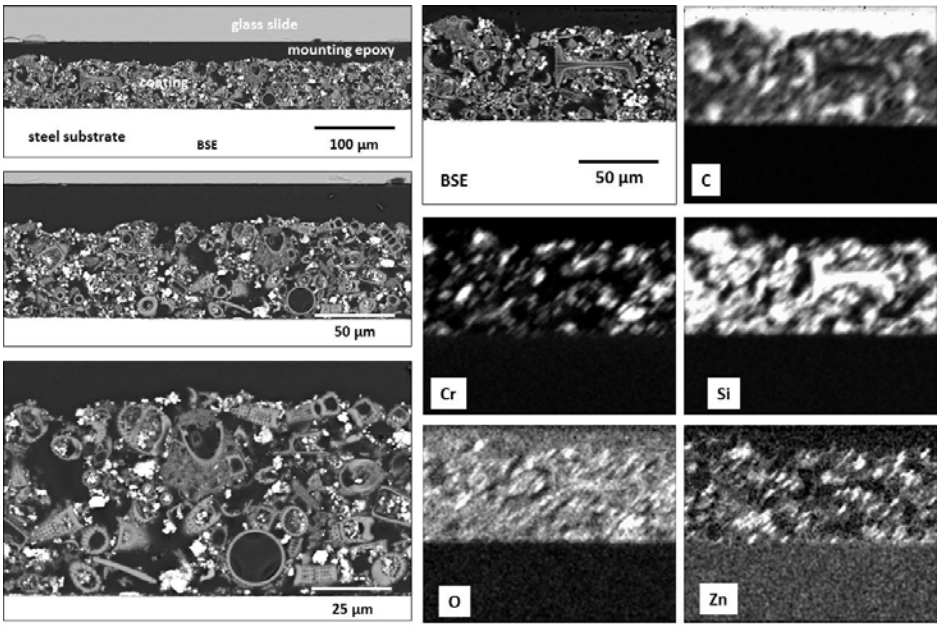

Fig. 54. Cross-sectional analysis of the 72-B coating (100% untreated Diafil addition). In the left column, backscattered electron images of the full coating thickness at increasing magnification are given. At right, element maps are presented for the analysis area (backscattered electron (BSE) image at top of center column).

Figure 55 offers a through-thickness comparison of coatings 72-D and E, both identically formulated with 100% nanosilica, but the superior performance of the latter is perhaps due to the silane treatment given to the silica to develop SH properties fully. Figure 55 shows similarly cracked structures for coatings D and E; cracks were observed routinely on both specimens that penetrate the entire coating thickness. The element maps indicate essentially identical distribution of chromium pigment and silicon across the coating thickness. However, the E coating performed substantially better (no blisters or rust bloom, beading condensate) than the D coating, suggesting the efficacy of the silane treatment for the silica. Although it is true that the E coating is approximately 35% thicker (average of 65 mils) than the D coating (average of 46 mils thick), cracks penetrate to the substrate in both cases so protection of the substrate is not directly related to the difference in thickness.

Figure 56 shows element maps in the immediate vicinity of a through-thickness crack in each coating (D and E). In both cases, the carbon map confirms that the cracks (or connected porosity) penetrate fully to the substrate steel, but the other maps represent the observation that the distribution of other constituents is the same in/around the crack as elsewhere in the coating. This is in contrast to previous observations made on powder coat cross sections (both urethane- and epoxy-based) suggesting that, in particular, silica tends to accumulate on the free surfaces of the coating (including cracks and pores).

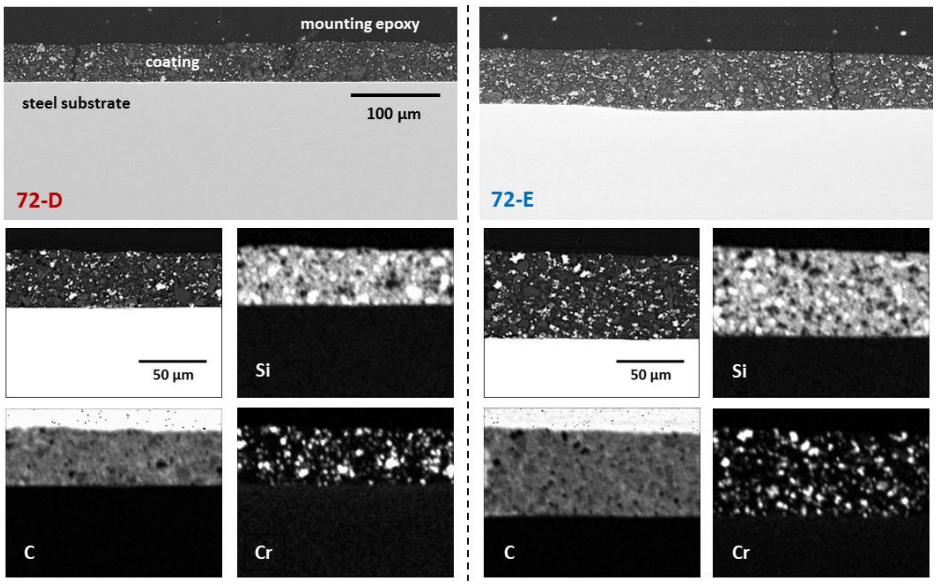

Fig. 55. Comparison of through-thickness metallographic sections (top image) and element mapping results for coatings 72-D (left) and 72-E (right).

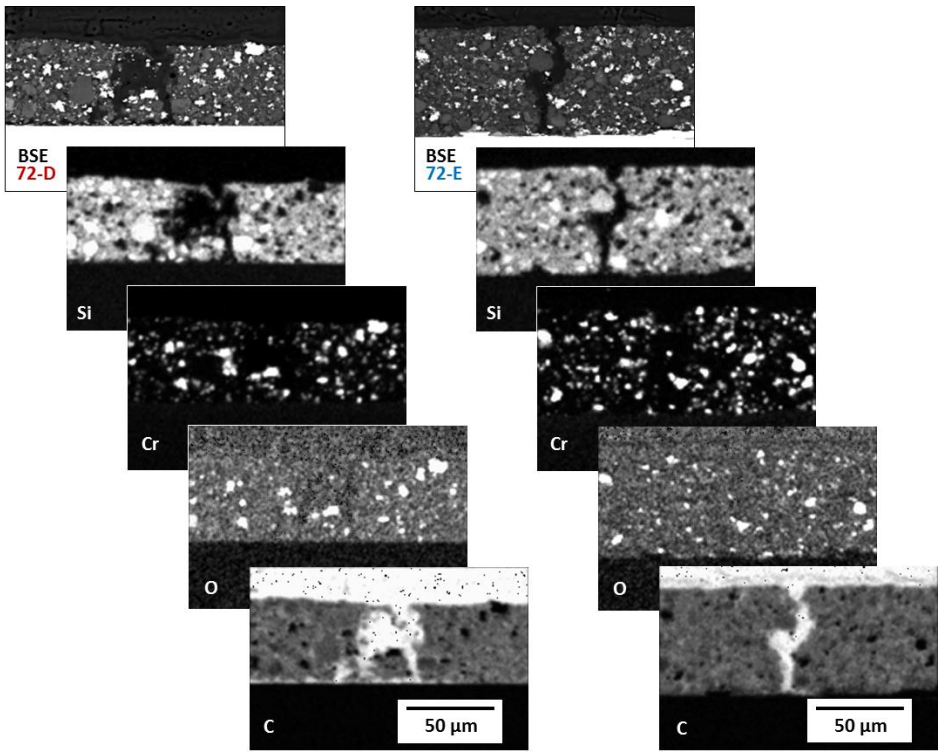

Fig. 56. Backscattered electron images with associated element maps for the immediate vicinity of through-thickness cracks in coating types D (left) and E (right).

Figure 57 compares cross sections of coatings 72-E, F, and H with features observed on the surface. Coating E performed relatively best of the three, being protective of the substrate in both salt fog and

water immersion. There are many micro-cracks in the E coating structure (in addition to through-cracks previously discussed), but apparently the overall density and relative abundance of silicon—as a fine dispersion as opposed to relatively large chunks—contributes to the protective qualities of the coating. The other two coating types both were less protective (type F offered some resistance to immersion conditions, but type H was poor in both immersion and fog conditions) but looked similar in surface structure to type E. Note, however, that the distribution of silicon is much different between type E (uniform) and that of types F and H (mainly large, discrete particles), and this may offer a key regarding development of protective qualities in these paint systems.

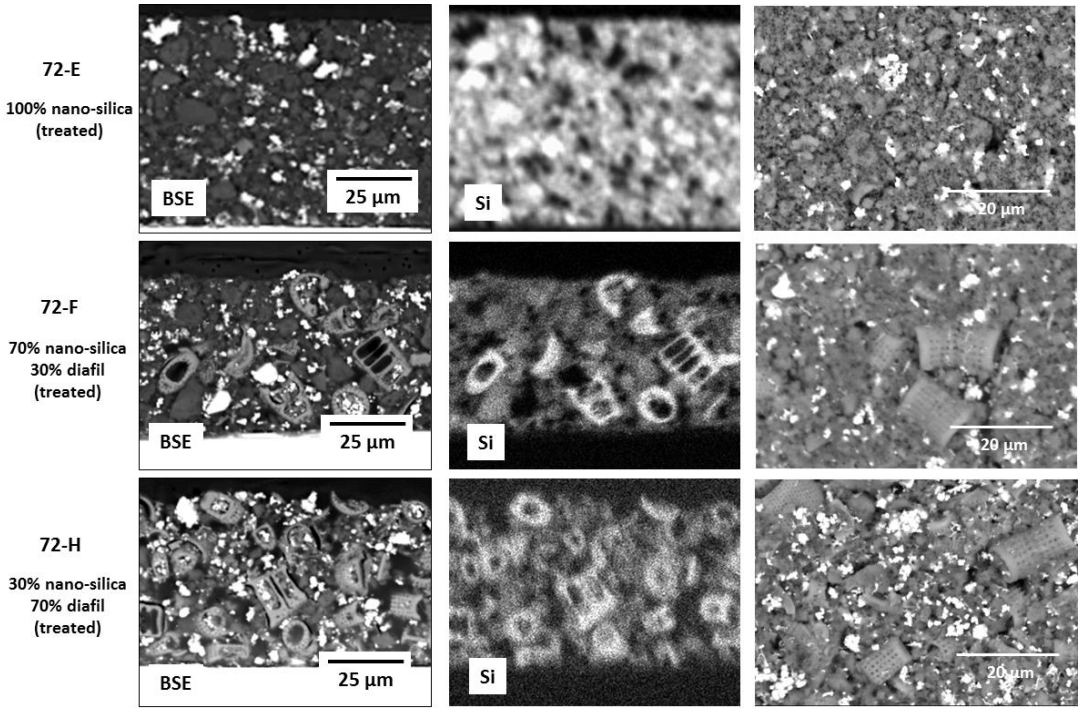

Fig. 57. Backscattered electron images (left column), associated silicon maps (center column), and surface topology comparison as a function of coating composition.

2.6 ARL MODEL COATINGS

As part of the on-going cooperation between ARL and the USMC/CPAC Program, ARL provided 11 different coated panels to ORNL for evaluation of the structure and composition (on the surface as well as through the thickness of the coating). Analysis techniques included water droplet contact and roll-off angles, SEM examination (images prepared using both secondary electrons and backscattered electrons) of the surface topography and element maps indicating the relative composition and composition gradients on the surface, cross-sectional metallography representing the through-thickness structure and composition gradients, and microprobe chemical analysis of individual pigment particles and other constituents. No salt fog or other performance testing was included in the evaluation for ARL. A full report was presented to ARL in August/September 2013 via conference call discussions with ARL staff and, finally, through electronic data transfer. Only key findings of that effort are reported here.

Table 8 records the general information provided by ARL for each coating specimen for evaluation. All coatings were provided in the as-prepared condition except for specimens 15 and 16, which had been weathered an equivalent amount (ultraviolet exposure designated "70 MJ" by ARL) at an outdoor test facility. The water drop contact angles included in the table (measurements at ORNL) indicate only one of the coatings (#10) exhibited a water contact angle notably above that observed for standard painted surfaces (order of 90–100°, SH character generally exhibits water contact angles ~ 150°). Also note that the corresponding roll-off angle for panel #10 was very high, further confirming the absence of SH character.

Table 8. Identity codes and information associated with coating specimens provided to ORNL from ARL. Contact and rolling angle measurements were collected at ORNL.

ARL ID	Designation	Type	Projected gloss (60°)	Contact angle (°)	Rolling angle (°)
1	MIL-DLT-64159	Water dispersible resin, polymeric beads flattening	1.0	40	
3	MIL-DLT-64159	Water dispersible resin, polymeric beads flattening	10.0	19	
4	MIL-DTL-53039	Solvent borne resin, polymeric beads flattening	1.0	102	>90
6	MIL-DTL-53039	Solvent borne resin, polymeric beads flattening	10.0	86	>90
7	MIL-DTL-64159	Water dispersible resin, silica flattening	1.0	73	
9	MIL-DTL-64159	Water dispersible resin, silica flattening	10.0	22	
10	MIL-DTL-53039	Solvent borne resin, silica flattening	1.0	122	>90
15	MIL-DTL-64159	Water dispersible resin, weathered 70MJ	1.0	82	
16	MIL-DTL-53039	Solvent borne resin, weathered 70MJ	1.0	97	
18	MIL-PRF-34328	Power topcoat thermal cure	1.0	103	>90
22	MIL-DTL-53022	Epoxy primer	30.0	83	

Figures 58 and 59 represent one key aspect of structural examination of these coating surfaces. The images in each set of photographs are of the identical area representing each coating, but the images in Fig. 58 were made with backscattered electrons whereas the images in Fig. 59 were made with secondary electrons. Both sets of images are intended to compare polymer bead and silica flattening for water dispersible coatings at two projected gloss levels. The backscattered electron images—which are relatively sensitive to general structure features (cracks and pores) and composition gradients (heavier elements backscatter electrons more efficiently than light ones)—reveal that at a fixed gloss, the surface structures are relatively independent of flattening agent and the chromium pigment (the small, almost white-appearing constituents in the images) is uniformly distributed. The secondary electron images, which are more sensitive to topology features than backscattered electrons, reveal that an increase in gloss for either flattening agent results in a substantially smoother, less "gravelly" structure, which potentially aids in the shedding of water or rinsing of chemical agents.

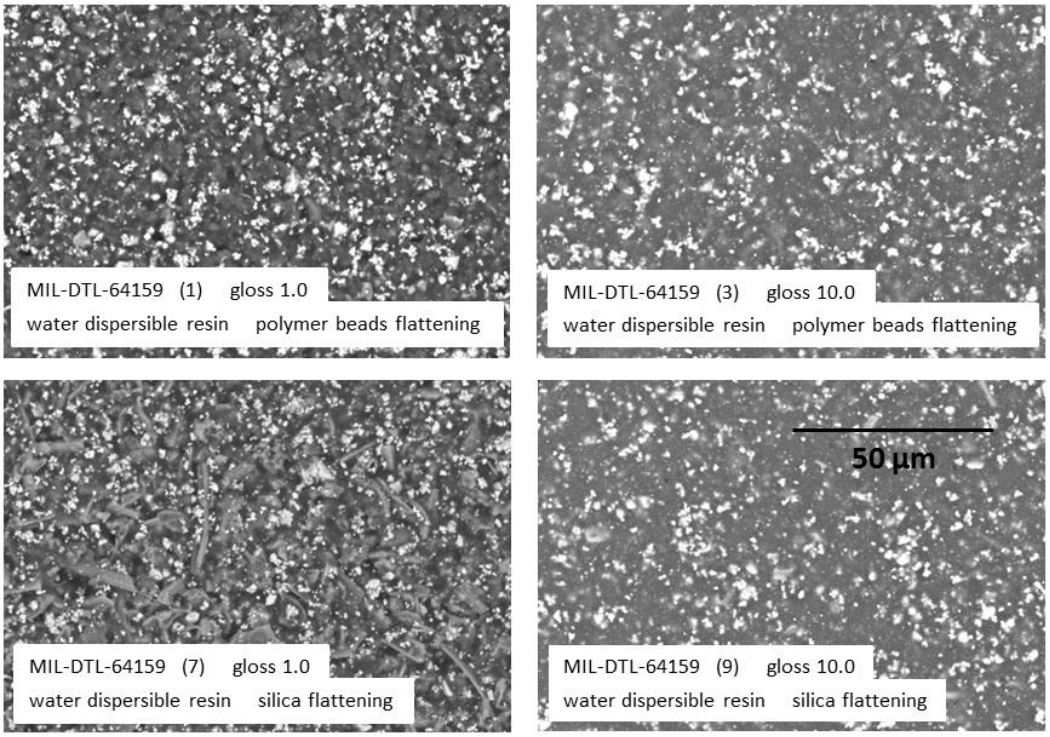

Fig. 58. Backscattered electron images of the surfaces of water dispersible coatings as a function of flattening agent and projected gloss. All images are shown at the same magnification.

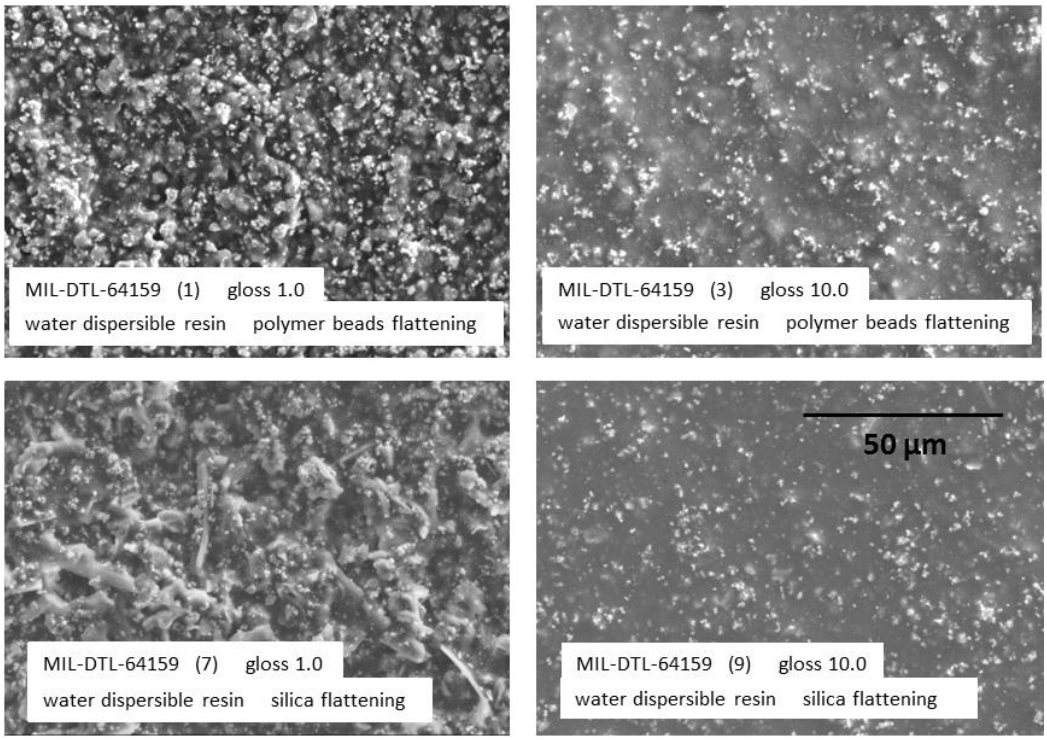

Fig. 59. Secondary electron images of the surfaces of water dispersible coatings as a function of flattening agent and projected gloss. All images are at the same magnification, and each image is of exactly the same area as the corresponding image in Fig. 58.

Similarly, Fig. 60 shows equivalent backscattered and secondary electron images of two of the solvent-borne coatings from ARL. In comparison to the water-dispersible coatings, the backscattered electron images here are representative of the observation that the solvent-borne coatings tend to have a number of cracks/pores visible on the surface that do not appear in the equivalent water-dispersible coating. However, the coating types are similar in that the high gloss surfaces exhibit much smoother and uniform surfaces than the low gloss equivalent.

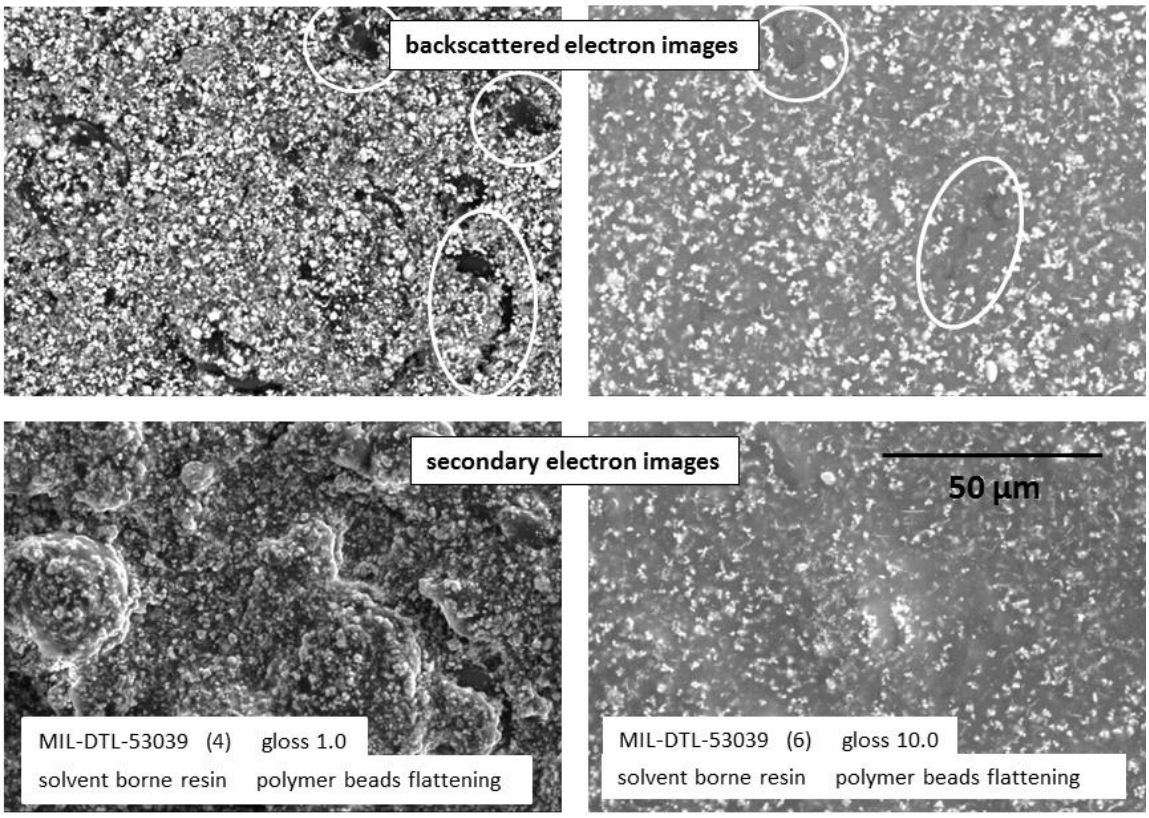

Fig. 60. Backscattered (top row) and secondary electron (bottom row) images of solvent-borne coating materials under evaluation for ARL. Representative cracks and pores are denoted in the backscattered images by white circles/ovals.

Among the most important features observed among the ARL coatings was that the solvent-borne versions tended to be susceptible to pores and cracks (as noted in the analysis of the coating surface), but metallographic examination confirmed that, in particular, porosity often extended throughout the coating thickness where the equivalent water-dispersible coatings were much closer to fully dense. An example of the porosity observed among the solvent-borne coatings is shown in the metallographic cross section of Fig. 61. In this case, the panel has been exposed to weathering, but as will be shown, weathering is not the cause of the observed porosity. In Fig. 61, the steel substrate is just barely visible at the bottom of the photograph. The primer, about 35 µm (1.4 mils) thick, appears as a mottled gray directly on top of the substrate. The topcoat, about 87 µm (3.4 mils) thick, is much darker but is filled with roughly circular and oval pores that are filled with the epoxy used for potting the sample as a metallographic mount.

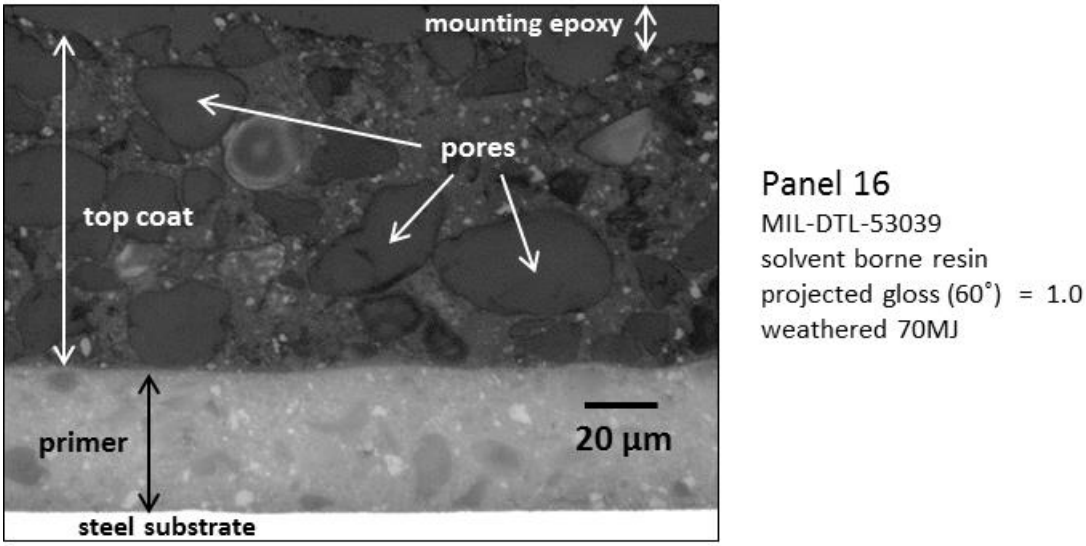

Fig. 61. Metallographic cross section of ARL panel 316, showing substrate steel, primer, and the full topcoat thickness.

The pores are filled with mounting epoxy, a fact discernible from Fig. 61 where the pores and the mounting epoxy are the same shade of dark gray with no other constituents present within the suspect area; this conclusion is confirmed via element mapping of the cross section. Figure 62 presents a collage of images; in the top left, the backscattered electron image of the analysis area is provided, and the other eight images are composition maps for the indicated element (all taken from the precise area shown at the top left). In the composition maps, the relative abundance of the element in question is revealed by the relative intensity of the light coloration (toward white), while relative absence is denoted as a darker color. Complete absence of the element (below detection levels, or masked by other components) is indicated by relative black. Thus, Fig. 62 reveals that the pore shapes exhibit very high carbon content, and the same relative signal is associated with the material known to be mounting epoxy appearing at the top of the image. Further, *only* carbon appears in the suspect pore shapes—no pigment (chromium or its oxides) or other constituent within the coating matrix is present, suggesting that the pore shapes are free of coating material. The images also clearly indicate the primer is predominantly magnesium, silicon, and titanium (and their oxides) that are also absent from the pores in the topcoat.

Of practical significance, the size/number of the pores suggest they form a nearly continuous network of potential penetration paths for moisture or chemical agents from the coating surface all the way to the coating system primer. Decontamination after penetration of an unwanted chemical to this depth/degree would pose a challenge for an actual coating with such properties.

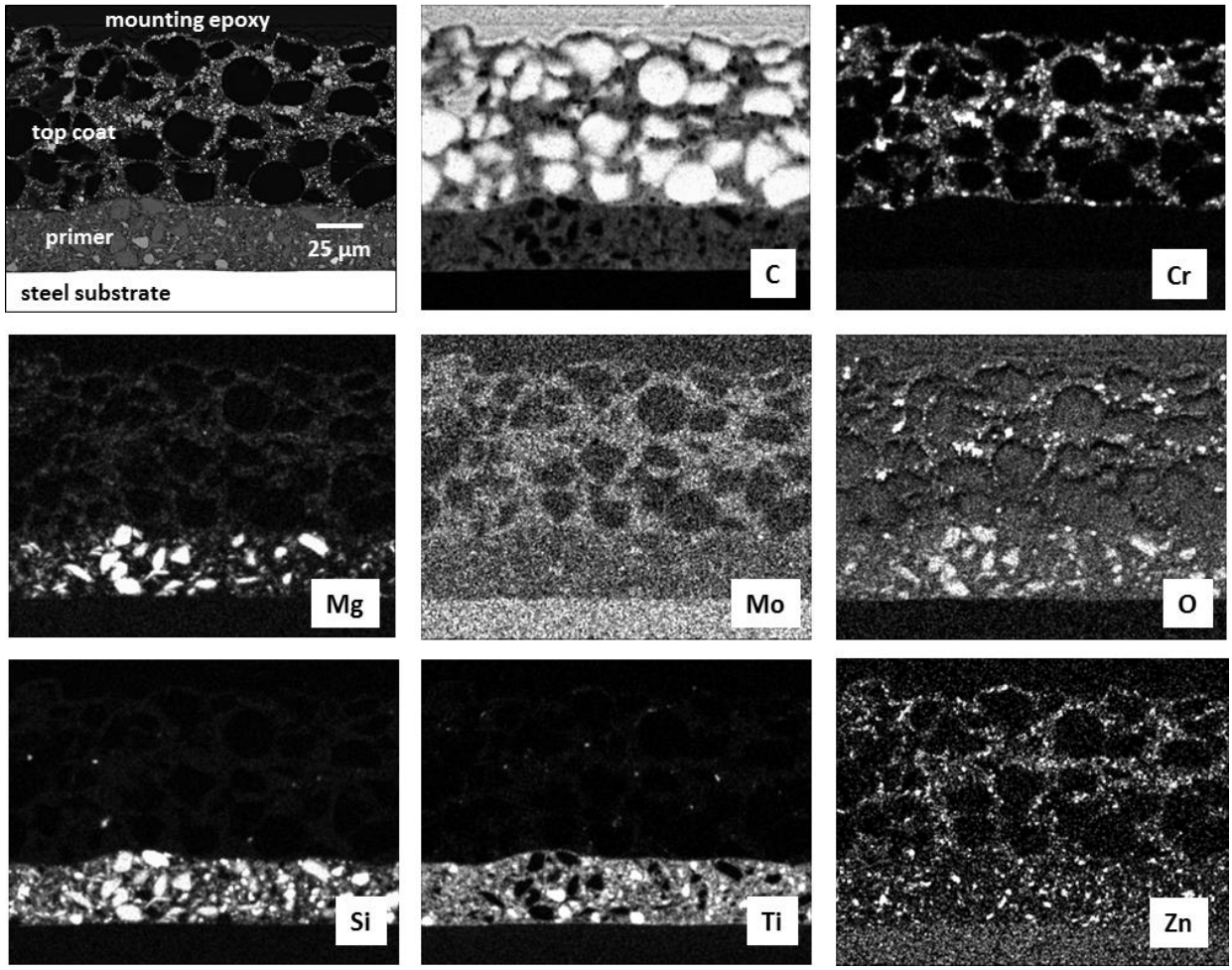

Fig. 62. Backscattered electron image of the analysis area (top left) along with corresponding element maps for the indicated constituents for ARL coating panel #16.

Similar composition maps were derived for ARL panels 4 and 10 (both solvent-borne coatings with polymer beads and silica flattening, respectively), but neither of these latter panels had been weathered, indicating the pores did not result from weathering/aging during exposure. Information equivalent to that shown in Fig. 62 is displayed in Fig. 63 for panel 4 (simplified to analysis area and maps for carbon, chromium, and molybdenum, as all the other information is essentially identical among ARL coatings), and the continuous pore network and its similarity to data in Fig. 62 is obvious. However, as a consistent trend, the equivalent water-dispersible coatings did not indicate a porous topcoat via penetration of the potting epoxy into the topcoat. Figure 64 contains the equivalent information to that in Fig. 63 for the water-dispersible coating with polymer bead flattening and a projected gloss of 1.0°. No pore network or uniform penetration of potting epoxy is evident, suggesting a more protective and more easily decontaminated water-dispersible topcoat, despite having a much lower water droplet contact angle. The latter observation once again suggests that water droplet contact angle is only a portion of the metrics necessary to develop a protective and water-shedding coating.

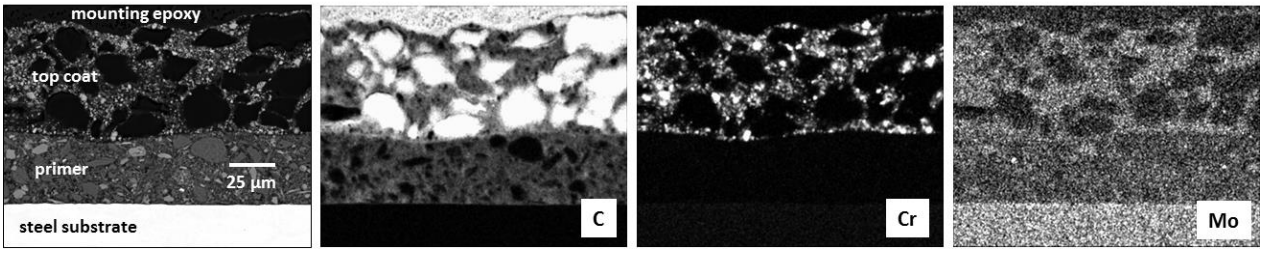

Fig. 63. Backscattered electron image of the analysis area (left) and element maps for carbon, chromium, and molybdenum for ARL panel coating #4 (solvent-borne, polymer bead flattened, gloss 1.0°).

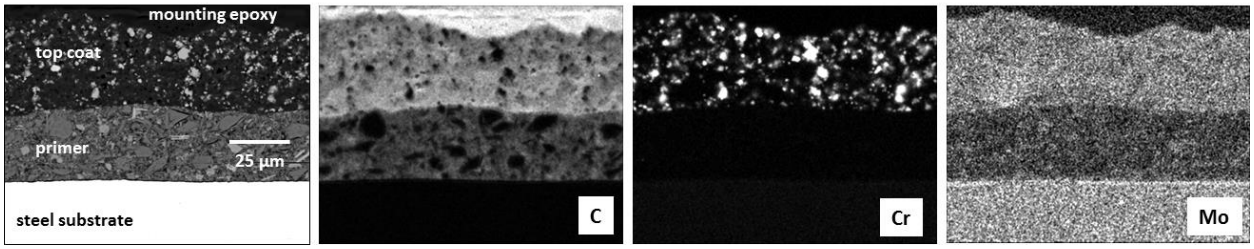

Fig. 64. Backscattered electron image of the analysis area (left) and element maps for carbon, chromium, and molybdenum for ARL panel coating #1 (water-dispersible, polymer bead flattened, gloss 1.0°).

2.7 TEMPORARY SURFACE MODIFICATIONS

Among the activities incorporated in Year 3 of this project was an attempt to evaluate and compare a number of temporary surface modifications that might have utility for improvement of water shedding capability on CARC coating systems. Conceptually, the idea was to evaluate commercially available products (or ORNL modifications to such projects, where liquid rather than spray versions were available) for water repellency and durability that might be used in a manner similar to CPCs—that is, something that could be sprayed/wiped onto a CARC surface periodically as a relatively inexpensive method to impart SH properties to a surface.

Specific details for particular products were conveyed to USMC/CPAC over the course of the experiments via oral presentations and written monthly reports. However, the potential audience for this particular ORNL/TM report summary is unknown, and therefore the authors have chosen not to name specific products. Commercially available products will be referred to Products A, B, and C, etc., for reporting in this format.

The general result of these experiments was that some of the available products examined can temporarily improve water repellency in immersion conditions, but none worked well in vapor (e.g., B117 exposures), and none proved to be durable at all. Further, a number of shortcomings were identified that compromise the potential utility of such products for widespread use. The following items are of potential interest to USMC/CPAC:

- There are concerns related to health and safety for both workers and the environment for many of these products. Several have extraordinarily high VOCs—on the order of 75% in a few cases and

upwards of 500 g VOC per liter of product in most cases. Generally associated with such high VOC content is an extreme flammability rating for the product. Among the products examined were one with a flash point of -150°F and another that recommended an air-supplied respirator for the workers using the product. Because of environmental and personal health concerns, at least one product has a strong warning from the state of California regarding potential carcinogens and birth defects resulting from exposure. Also associated with such high VOC content is very poor coverage per unit of product; the authors found an approximate cost of $\$3/ft^2$ per coat to be common based on publically available pricing, and most products claim the need for multiple coats to maximize effectiveness.

- Despite claims, many products do not provide a rapid "one-step" convenience necessary for field application for USMC/CPAC. For example, more than one of the evaluated coating systems recommended multiple coats with 30-minute cure cycles for each, and another system suggested making at least three coats (ideally more) to develop good water repellency. Several of the examined products recommend frequent re-application of the product (e.g., weekly or monthly) to ensure corrosion protection integrity. In addition, the authors found that several spray can products were difficult to use efficiently because of frequent plugging of spray nozzles with solids delivered in the solvent stream.

- While it is clear that *none* of the coating systems developed/examined in this program met all of the demanding USMC/CPAC performance goals, many of these temporary surface modifications were found to be extremely fragile or inappropriate for other reasons. Of particular note, any touching of prepared surfaces (finger oils) or even slight rubbing action during handling (abrasion) substantially reduced performance in terms of protective qualities (salt fog or immersion testing). Further, several of the products dried with a milky white haze, which potentially negatively influences requirements for gloss and color retention for military coating systems.

To support these observations and findings, a number of simple exposures were performed to compare performance of readily available commercial products. A few example results are presented here (with specific product names withheld).

In most experiments, steel panels were prepared in standard fashion—that is, degreasing and light grit blasting—before applying the temporary coatings directly to the bare steel (which is standard service duty for most of these products). In limited cases, a readily available commercial primer was applied to the steel before application of the temporary coating. However, it was found that the presence of a primer only slightly retarded rapid breakdown or penetration of the temporary coatings, and thus the performance of the temporary coatings was generally screened without the use of a primer. In the experiment depicted in Fig. 65, Product A (one coat and three coats) and Product B (one coat only) were applied to bare steel per the manufacturer's explicit directions. After full curing, light abrasion with a common kitchen scrub pad (one pass, light finger pressure) was used in an "x" pattern on the face of each prepared panel (8 ft × 4 in. × 0.25 in.). The panels then were exposed to accelerated weathering in a standard B117 salt fog chamber. In less than 24 hours, the protective qualities of the coating along the "x" marking were severely compromised, with immediate development of rust bloom. In less than a week of exposure, substantial substrate corrosion developed along the "x" mark of all panels in this test and, to a lesser degree, on the untouched surfaces of the panel as well. This result is representative of the trend that the

temporary coatings exhibit poor durability and marginal protective qualities in general for a vapor-phase exposure.

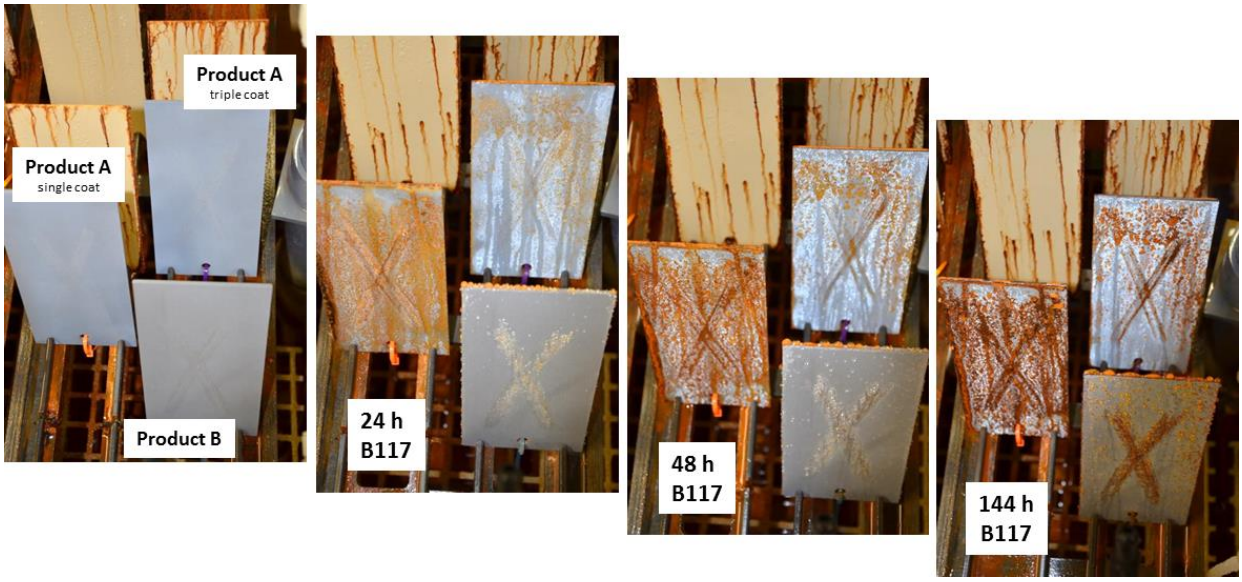

Fig. 65. Development of rust bloom and corrosion associated with an "x" scratch as a function of salt fog exposure time for Products A and B.

In a similar experiment, Products C and D were applied to bare (cleaned and lightly blasted) steel per manufacturers' directions and then exposed to B117 salt fog. In addition, liquid versions of each product were manipulated with an addition of ~ 10 wt % of silane-treated silica from ORNL. Subsequently, some treated panels were heated for 2 hours at 125°C in a furnace box (air exposure) to simulate exposure to "under-the-hood" engine temperatures, considered applicable service duty for these materials. A representative result is shown in Fig. 66. As was typical for both of these products (with or without heat treatment, with or without addition of silica), essentially full rust bloom over the panel surface developed within about 24 hours of salt fog exposure. In this particular experiment, the addition of 10% treated silica to the temporary coating may have had a slight positive effect on the salt fog panels—perhaps slightly less rust development in 24 hours—but this difference is not considered significant. In all cases, as panel surfaces dried after salt fog exposure, the temporary coating flaked and spalled as a dry powder from the surface.

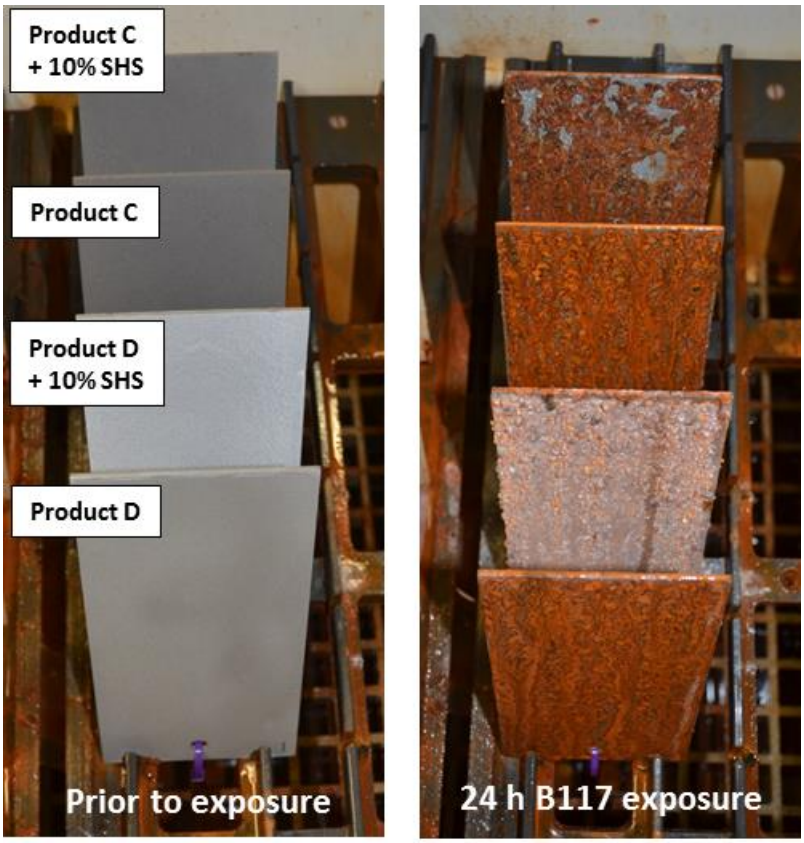

Fig. 66. Products C and D, with and without the addition of 15% treated silica, with brief salt fog exposure.

However, upon immersion of similar panels in deionized water for 48 hours, a slightly greater effect of silica addition was observed. A temporary surface coating designed to exhibit superhydrophobic character might be expected to perform better in immersion conditions than in vapor conditions (salt fog) because the arriving moisture has surface tension in the immersion case, which is combatted by superhydrophobic surfaces. Figure 67 shows a representative result, indicating only a few isolated spots of rust bloom in 48 hours of immersion for the baseline Product D immersed in water, but the addition of 10% treated silica completely prevented rust bloom over the same period. While Product D claims to contain silica in the formulation, this result suggests that additional silica or perhaps additional *treated* silica is the key to performance improvement. However, it was also observed that these temporary treatments (especially those bearing additional silica, but not uniquely so) adhered very poorly to the steel substrate. Figure 68 is a representative example, which shows the temporary coating lifting freely and nearly in a single sheet from the panel surface as it is withdrawn from the water bath after exposure, suggesting very poor durability for such a concept.

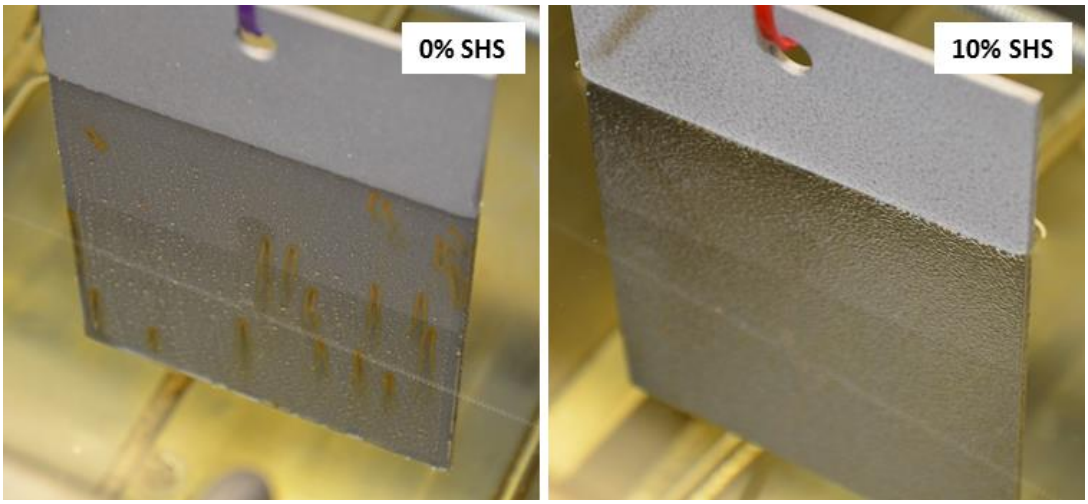

Fig. 67. Product D with and without 10% treated silica following immersion testing in deionized water for 48 hours.

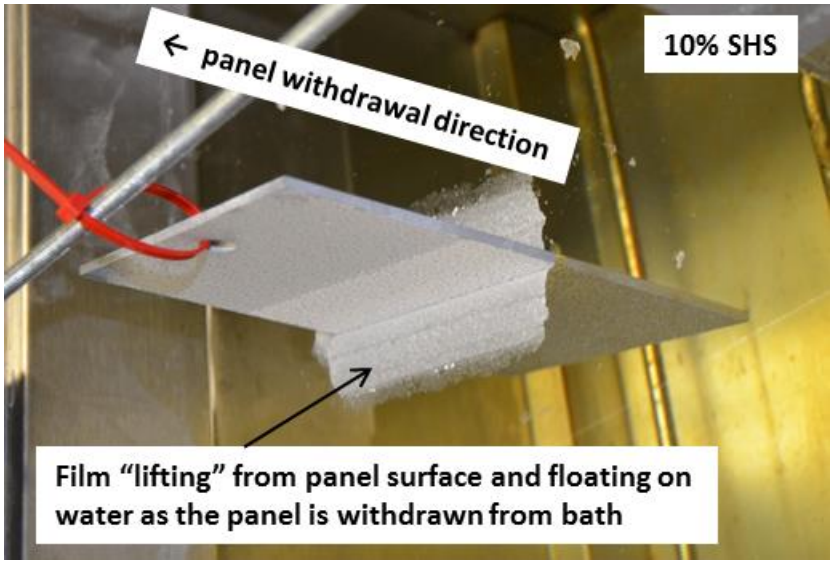

Fig. 68. Lifting a treated panel from the water immersion tank as portion of film subjected to immersion lifts from the panel surface.

A few products specifically intended for relatively higher temperature applications (e.g., engine components that reach several hundred degrees during service) were also examined. As with some other coatings in this series, these were examined with and without the addition of ~ 10% treated silica as a potential enhancement to the coating. Without exception, these materials performed very poorly in salt fog, exhibiting essentially complete rust coverage within a few days of exposure. Figure 69 shows a representative result. Interestingly, the surface structures observed for these "high temperature" materials tended to be smooth and crack-free without additions of silica but heavily cracked with additions of silica. The salt fog result was independent of the film integrity. Note that the high silica version tended to exhibit

superhydrophobic water contact angles, but this factor is perhaps not applicable to performance characteristics in a vapor.

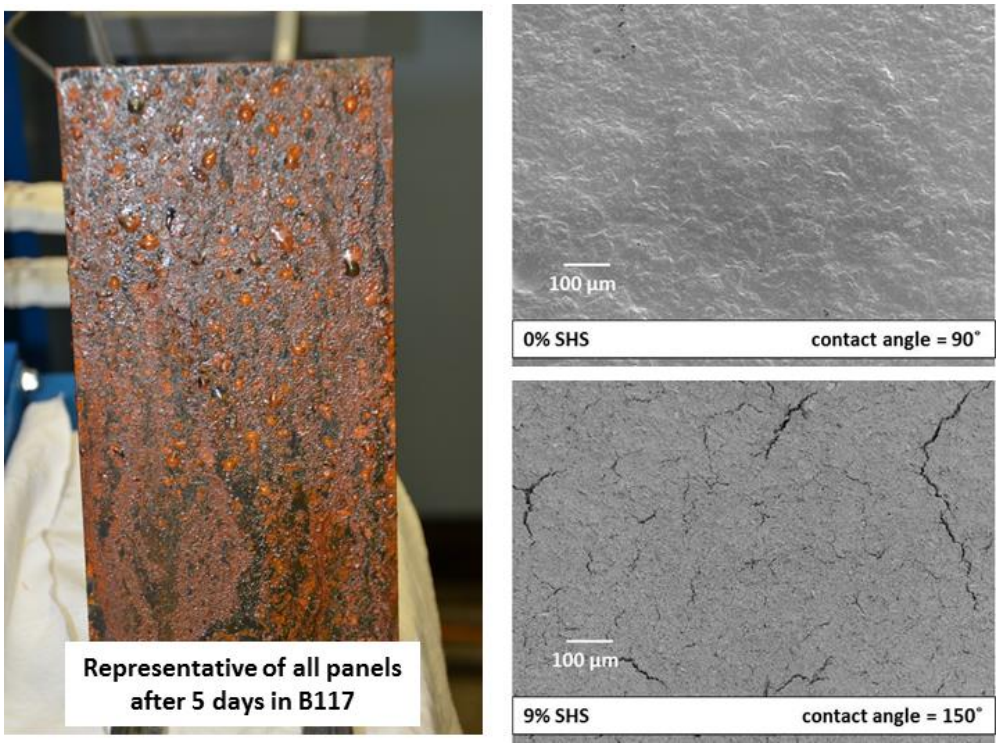

Fig. 69. Salt fog result (5 d) for baseline Product E (no silica additions) and surface structures showing 0 and 9% silica additions. Average water droplet contact angles are also reported for each structure.

In addition to salt fog and immersion testing, limited examination of temporary coatings was performed using Taber testing (ASTM D-4060). Water droplet contact angle was used as a metric to track changes in the surface as a function of number of abrasion cycles, and a typical result is shown in Fig. 70. Even for the "best" of the temporary coatings (in this case, modified with an addition of treated silica), only a few Taber cycles were required to reduce the water contact angle on the abraded surface to values below that typically associated with SH behavior (150°). The results were consistent with previous observations of poor durability associated with these temporary coatings.

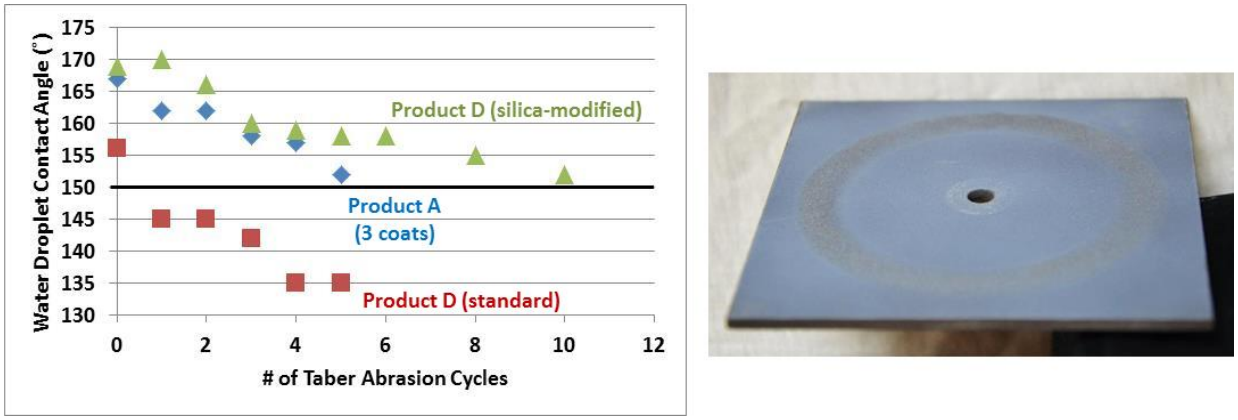

Fig. 70. Water droplet contact angle as a function of Taber test abrasion cycles for different temporary surface products. At right, a typical post-test panel is shown with the circular wear track.

3. KEY FINDINGS AND CONCLUSIONS

Over the course of this program (despite its termination before its natural conclusion), significant progress toward the goal of developing a bulk, single-step application SH topcoat system was demonstrated. Significant concepts and observations include the following:

1. Protocols for synthesis of a variety of high quality, consistent SH powder additives were developed and were progressively scaled up from gram-sized amounts to kilogram quantities.

2. Coating surfaces with SH water drop rolling angles (150–170°) can be achieved by adding silica-based powder additives to both liquid water-borne and liquid solvent-borne CARC.

3. Post-addition of SH powder additives (that is, additions to a coating system that is fully formulated) results in CARC with high contact and/or rolling angles but very poor corrosion resistance in salt fog testing because of microcracking of the coatings caused by resin overloading. The superior coating development effort incorporates SH powder additives at the coating formulation stage, so that total solids loading, dispersion, and related factors can be adjusted properly.

4. High contact angles are not a sufficient metric to ensure that SH coating will improve corrosion resistance. The structure of the coating surface is a key indicator of potential for protective capability. Examination of representative coatings revealed that existing CARC topcoat formulations also tend to be quite porous and cracked and provide little in the way of corrosion protection. Although CARC topcoats have primary objectives that do not include corrosion resistance, this program has indicated a path toward potentially improving the multifunction nature of CARC topcoats.

5. Durability of SH surfaces is a barrier that must be addressed. This study did not address that particular issue because of its premature conclusion, although strategies for improving durability were identified.

6. A variety of commercially available SH coatings were evaluated. All showed good initial behavior, but none were durable or protective beyond a few days of salt fog exposure, and they generally contain extreme levels of volatile organics or health hazards that prohibit use in large quantities.

7. Demonstrated SH powder coatings exhibited extremely high contact angles and exceptional corrosion resistance. One specimen surface remained dry after more than 2,000 hours of salt fog testing. SHS additions to powder coats showed particular potential for ease of incorporation into the parent material, and additions as low as ~ 1% were quite effective for improving corrosion protection qualities, although curing protocols and durability issues were not addressed fully. Researchers demonstrated commercial-scale processing of SH powder coatings at two separate facilities.

8. Salt fog testing is an effective screening tool, but a suite of characterization methods and tools is necessary to determine if a SH coating surface is protective and durable. There is also potential risk of false negatives with salt fog testing of SH surfaces because these surfaces are designed to repel liquid water, not water vapor.

9. Substantial progress in fabricating effective coatings was made in the last four months of the program, once a CARC manufacturer began partnering with the team; this partnership enabled experiments with reformulated CARC that accommodated the increased additive content. The final batches of coatings showed vastly improved corrosion resistance in salt fog testing compared with the earlier coatings made by post-addition of additives to off-the-shelf CARC.

4. REFERENCES

1. Aytug, T. *Atomically Bonded Clear Transparent Superhydrophobic Coatings*. ORNL/TM-2015/197, Oak Ridge National Laboratory, Oak Ridge, Tenn. (May 2015).

2. Hihara, L., and R. Sugamoto. *Final Report: Pacific Rim Corrosion Assessment and Mitigation Program (PacRimCAMP)*, prepared for the U.S. Marine Corps Corrosion Prevention and Control Program by the University of Hawaii at Manoa (January 8, 2015).

3. ASTM. *ASTM B117: Standard Practice for Operating Salt Spray (Fog) Apparatus*. American Society for Testing and Materials International, West Conshohocken, Pa. (2009).

4. Yan, N., et al. "Measurement of Contact Angles for Fumed Silica Nanospheres Using Enthalpy of Immersion Data." *J. Colloid and Interfacial Science* 228 (2000): 1–6.